

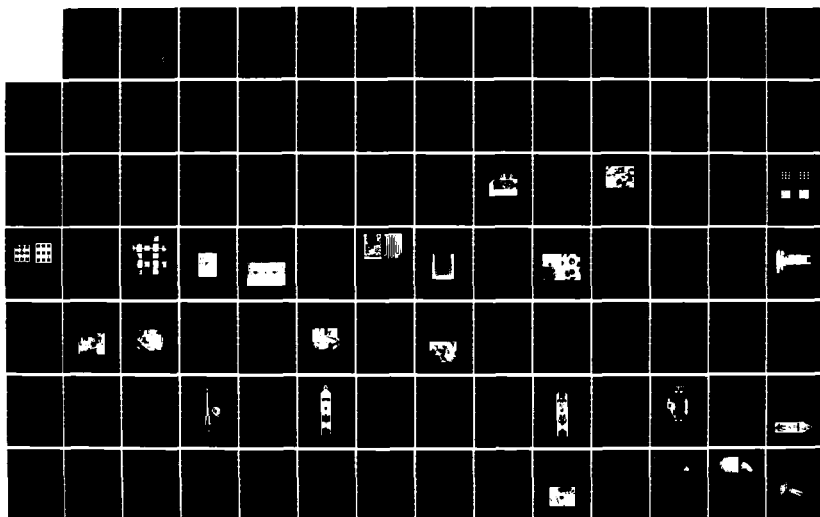
AD-A164 187

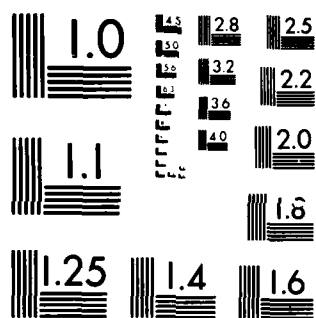
ELECTRON MICROSCOPY OBSERVATION OF ELECTROTRANSPORT(U)
AIR FORCE INST OF TECH WRIGHT-PATTERSON AFB OH SCHOOL
OF ENGINEERING J V MASKOWITZ ET AL. DEC 85
UNCLASSIFIED AFIT/GE/ENG/85D-25

1/2

F/G 28/3

NL





MICROCOPY RESOLUTION TEST CHART
 NATIONAL BUREAU OF STANDARDS-1963-A

AD-A164 107



ELECTRON MICROSCOPY OBSERVATION
OF ELECTROTRANSPORT

THESIS

James V. Maskowitz William E. Rhoden
Captain, USAF Captain, USAF

AFIT/GE/ENG/85D-25

DTIC FILE COPY

DTIC
ELEC
FEB 13 1986
S
E

DEPARTMENT OF THE AIR FORCE
AIR UNIVERSITY

AIR FORCE INSTITUTE OF TECHNOLOGY

Wright-Patterson Air Force Base, Ohio

This document is approved for	release
-------------------------------	---------

86 2 12 1986

AFIT/GE/ENG/85D-25

ELECTRON MICROSCOPY OBSERVATION
OF ELECTROTRANSPORT

THESIS

James V. Maskowitz William E. Rhoden
Captain, USAF Captain, USAF

AFIT/GE/ENG/85D-25

DTIC
E

Approved for public release; distribution unlimited
AFIT/GE/ENG/85D-25

ELECTRON MICROSCOPY OBSERVATION
OF ELECTROTRANSPORT

THESIS

Presented to the Faculty of the School of Engineering
of the Air Force Institute of Technology
Air University
In Partial Fulfillment of the
Requirements for the Degree of
Master of Science in Electrical Engineering

James V. Maskowitz, B.S.
Captain, USAF

William E. Rhoden, B.S.
Captain, USAF

December 1985

Preface

The purpose of this study, was to design and fabricate test apparatus and test vehicles for conducting electromigration analysis in both the scanning and transmission electron microscopes (SEM and TEM) respectively. The apparatus fabricated for the SEM maintains a constant temperature of 86 K while electromigration studies are conducted in the SEM. The TEM apparatus fabricated allows crystalline analysis through TEM generated diffraction patterns and bright field micrographs. Prior to this thesis the temperature variable had not been adequately controlled and no TEM electromigration work had been conducted in situ.

We would like to thank several individuals, for their valuable help and guidance. Our sincere thanks goes to our thesis committee, Major Donald R. Kitchen who gave timely guidance and the right amount of latitude, and Dr Theodore E. Luke for his assistance in writing this document. We would like to thank to Mr. Ralph Omlor, Dr. Dave Mattie, and Mr. Don Smith for their technical support in working with the microscopes. We extend our appreciation to Ms. Cheryl Heidenreich for her photographic support of the thesis. We are grateful to Lt. Joseph Grzyb and Mr. Larry Callahan for their support with the fabrication and packaging of several test vehicles used in our research. We would like to thank the AFIT Fabrication Shop, headed by Mr. Carl Shortt, which built the hardware required for this effort.

Finally, special thanks goes to our wives, Rita Maskowitz and Vikki Rhoden, and children, Katie and J.J. Maskowitz, for all their patience and support during our AFIT experience.

Accession For
NHL GRA&I
FIR
[Handwritten marks and stamps follow]

Table of Contents

	Page
Preface	ii
List of Figures	v
List of Tables	viii
List of Equations	ix
Abstract	x
Introduction	I-1
Background	II-1
Experimental Setup and Procedure	III-1
III-1 Test Vehicles	III-1
III-2 SEM Cold Stage Design	III-14
III-3 Setup and Procedure for SEM Coldstage ...	III-26
III-4 MARK II Holder Design	III-34
III-5 Setup and Procedure for TEM MARK II	III-44
Results and Discussion	IV-1
IV-1 SEM Technique	IV-1
SEM	IV-1
Prototype Refrigerator	IV-4
Nitrogen Gas Supply	IV-12
Constant Current Density Failure Data	IV-12
Constant Temperature Failure Data ...	IV-16
Additional Data Points	IV-20
Gradient T and Structure	IV-22
IV-2 TEM Technique	IV-24
Design of the MARK II Holder	IV-24
Aluminum Bridge Test Vehicle	IV-32
Electromigration Diffraction Patterns	IV-36
Conclusions and Recommendations	V-1
Appendix A: Aluminum Bridge Test Vehicle	A-1
Appendix B: Microminiature Refrigerator System	B-1
Appendix D: Elapsed Minute Timer	C-1
Bibliography	BIB-1
Vitae	VITA-1

List of Figures

Figure	Page
1. Integrated Circuit Industry Trends	II-2
2. Saddle Point	II-4
3. Thin Film Forces	II-6
4. Atomic Redistribution vs Mobility	II-9
5. Temperature Gradient of a Thin Film	II-11
6. Grain Boundaries	II-12
7. Triple Point	II-13
8. Flux Divergence at a Triple Point	II-14
9. Abrupt Grain Size Changes	II-15
10. Hillocks and Holes On an Aluminum Stripe	II-16
11. Closeup of Electromigration Damage	II-18
12. MOSIS NMOS Test Vehicle	III-3
13. MOSIS Pattern Designations	III-4
14. Complex Test Vehicle With Diodes	III-6
15. CTV TP-23 Pattern	III-7
16. Patterns of Interest on CTV	III-8
17. AFIT Test Vehicle	III-10
18. Bell Labs Test Pattern	III-11
19. Bridge Test Vehicle	III-13
20. SEM Modification Block Diagram	III-15
21. Cold Stage	III-16
22. Input Current Wiring	III-17
23. Alumina Bonding Block	III-18
24. SEM Chamber With Cold Stage Inside	III-19

25. Cold Stage Position In SEM	III-20
26. Interface Flange	III-22
27. Electrical Port With Cold Stage	III-23
28. Vacuum Chamber	III-24
29. Cold Stage Mount With Door Spacer	III-25
30. Jeol EM-SHH Heating Holder	III-35
31. Jeol EM-SHH Heating Holder Tip	III-37
32. MARK II Holder Stage	III-39
33. MARK II Holder Tip	III-41
34. Transport and Holding Box	III-43
35. TEM Field of View on MARK II Holder	III-45
36. Banana Plug/Bonding Block Relationship	III-46
37. SEM Micrograph of In Situ Electromigration	IV-2
38. Sample Mount	IV-4
39. Quartz Refrigerator Slide	IV-5
40. Modified Wiring on Cold Stage	IV-6
41. Refrigerator Support Set Screws	IV-7
42. Operating Envelope at Maximum Power	IV-9
43. Constant Current Density ($4 \times 10^6 \text{ A/cm}^2$) vs Temperature	IV-14
44. Constant Temperature (223 K vs Current Density)	IV-18
45. Test Stripe at 135 K	IV-21
46. Test Stripe at 100 K	IV-22
47. First Attempt at Holder Design	IV-25
48. MOSIS Test Vehicle Mounted on MARK II Holder ...	IV-27
49. Electromigration Effects on Test Vehicle	IV-31
50. STEM Photograph of Bridge Test Vehicle	IV-35

51. Diffraction Pattern of Underlying SiO ₂	IV-36
52. Diffraction Pattern of Aluminum Stripe	IV-37
53. STEM Photo of BTV in place on MARK II Holder....	IV-38
54. Bright Field STEM of Etched Holes in BTV	IV-39
55. Mosaic Mapping of BTV Stripe	IV-40
56. Post Stress Mosaic of BTV Stripe	IV-43
57. Crystallographic Micrograph of Voided Stripe ...	IV-44
58. BTV Mounted in MARK II Holder	IV-45
59. Dual Etched Holes in BTV of Experiment #3	IV-46
60. Bright Field TEM of Failure Point	IV-48
61. Bright Field TEM of Linestripe	IV-49
62. Diffraction Patterns of BTV Experiment #3	IV-50
63. Diffraction Patterns of Oxide Window	IV-51
64. Standard Refrigerator	B-3
65. K-77 Controller Diagram	B-5
66. Electromigration Circuit With Timer Interface ..	C-3
67. Timer Schematic Diagram	C-5
68. Timer Rear Panel Diagram	C-8
69. Modified Timer Setup for External Resistor	C-9
70. Modified Timer Setup for External Power Supply .	C-10

List of Tables

Table	Page
1. Constant Current Density vs Temperature	IV-13
2. Constant Temperature vs Current Density	IV-17
3. Additional Data Points	IV-20
4. Effects of Etching Time on Bridge Test Vehicle ..	IV-34
5. Timer Parts and Description	C-6

List of Equations

Equation	Page
1. Temperature Gradient Force	II-5
2. Einstein Relation	II-6
3. Atomic Flux	II-7
4. Atomic Flux vs Mobility	II-9
5. Flux Divergence	II-10
6. One Dimension Flux Divergence	II-10
7. Derivative of Flux Divergence	II-10
8. Triple Point Divergence	II-13
9. Resistance Relation	IV-8
10. Diffusion Coefficient	IV-16
11. Mobility vs Temperature	IV-16
12. Atomic Flux vs Mobility	IV-16
13. Atomic Flux	IV-20
14. Atomic Concentration	IV-23
15. Derivative of Flux Divergence	IV-23

Abstract

This investigation has resulted in the development of apparatus and test vehicles for use in conducting electromigration research in situ both in the scanning and transmission electron microscopes (SEM and TEM) respectively. The unique design of test vehicles and modification of equipment allows for the experimental use of a prototype Joule-Thompson microminiature refrigerator. The refrigerator inside the SEM allows for the direct observation of electromigration experiments while controlling the temperature of the test vehicle. Research was performed in a temperature range lower than any previous effort, (93 K to 373 K).

The patent-pending design and fabrication of the TEM specimen probe and its associated test vehicles provides the means for conducting in situ research into the crystalline structures and crystallographic changes associated with electromigration. The design provides the previously unattainable ability to monitor structure changes during the electromigration process in a non-contaminating environment which exists in the TEM.

Finally, the research of this thesis has established the foundation for ongoing reliability studies at AFIT.

ELECTRON MICROSCOPY OBSERVATION OF ELECTROTRANSPORT

I. INTRODUCTION

Problem Statement

With the maturing of Very Large Scale Integrated (VLSI) technology, decreasing feature size and increasing gate densities are resulting in higher current densities which are exceeding 10^6 A/cm^2 and linestripes which are reaching into the submicron range. In this environment, electromigration can cause unwanted open or short circuits in thin films. Thus electromigration in thin film conductors has serious implications on the reliability of any integrated circuit.

Although enormous amounts of research effort has been put into the study of electromigration, (1-3; 5-14; 16-20; 21; 22; 30-35; 38-43; 46; 48; 50-55; 57; 58; 68-71; 74-92; 99-103; 107-110), most research has been conducted at high temperatures and the exact method of void nucleation and hillock growth is as yet not understood (16; 22; 30; 39; 48; 52; 86; 98). The effects of low temperature (T below one half the melting point temperature) and the crystalline structures involved in electromigration have not as yet been researched thoroughly (5; 14; 27; 28; 38; 54; 58; 84; 87; 94; 107; 109). Even with the large volume of published material, these areas have not been addressed sufficiently, and are awaiting further research.

The objective of this thesis was to advance electro-migration research capabilities in the areas of low temperature environment and crystalline morphology through the design and fabrication of test equipment and thin film test vehicles for use in scanning and transmission electron microscope research.

Specifically, the design, fabrication, and testing of equipment and test samples, were accomplished to conduct both low temperature electromigration experiments in the SEM and crystalline structure research in the TEM. Both designs allowed electromigration experiments to be conducted in situ, or within the vacuum environment of the microscope. The exercise of this equipment led to numerous important achievements.

Major Results

This thesis research resulted in the successful design, fabrication, and testing of apparatus and associated test vehicles which permit viable research and observation of electro-migration in both the SEM and TEM. Specifically, test vehicles were designed and constructed to take advantage of simple geometries and control of dimensions. The MOSIS test vehicle was successfully used on the cold stage for the in-situ observation of electromigration at cryogenic temperatures. The unique Bridge Test Vehicle was constructed by combining a number of techniques. The process yielded the first successful suspended linestripe available for research at the institute. The bridge test vehicle, utilizing the patent pending MARK II TEM Holder, enabled the unique observation of crystallographic

changes in the morphology of a powered linestripe.

A cold stage for the in-situ viewing of a powered line-stripe at cryogenic temperatures was designed. The prototype refrigerators passed vacuum testing down to a pressure of 10^{-6} torr. This represents a breakthrough in the technology of high vacuum glues which were used to hold the refrigerator together. The prototype microminiature refrigerator system incorporated into the SEM allows electromigration testing to be accomplished in situ while isolating a critical variable in electromigration studies, the temperature. With the temperature of a linestripe suppressed, the effects of high current density ($> 3 \times 10^6 \text{ A/cm}^2$), on the stripe structure were observed. Electromigration damage was sustained by a linestripe at cryogenic temperatures (93 K).

The patent pending design of the MARK II Holder used in conjunction with the Bridge Test Vehicle and its suspended Aluminum linestripe, devoid of an interfering substrate, yields excellent data and observation of electromigration and the study of its crystallographic composition through bright field and dark field photomicrographs and diffraction patterns. The data obtained showed that the morphology of a linestripe under stress will change due to a high current density ($> 10^6 \text{ A/cm}^2$). These results were obtained on the basis of simplifying assumptions which allowed for a concentrated effort in specific areas.

Assumptions

The following assumption apply:

1. A key element for the existence of electromigration is a current density above 10^6 A/cm^2 .
2. Increased temperatures due to joule heating enhance and accelerate electromigration in thin film conductors.
3. The primary force in the transport of metal atoms is the electron wind or the momentum transfer from the electron current to the conductor ions.
4. The presence of temperature gradients, electric forces, and structural factors all lead to the possibility of electromigration. These multiple causes make the contribution of any one factor difficult to calculate.

Scope

The scope of this research is limited to samples composed of aluminum films deposited by evaporation on Silicon wafers.

Design and fabrication of equipment and test samples are limited to modifications of both existing equipment and procedures for the sake of simplicity and ease of implementation and duplication. Testing of the prototype micro-miniature refrigerator is limited to vacuum testing of the quartz cold stage down to 10^{-6} torr. Cold temperature studies are limited to temperatures between 88 K and 373 K. Finally, all current densities were maintained at or above 10^6 A/cm^2 .

General Approach

The study consisted of two parallel research efforts with five major variations. The first part was the design and fabrication of aluminum thin film test vehicles utilizing photolithography techniques and existing metalization masks. These results are included in chapter III.

The second step was to design and construct two digital timers which would measure the elapsed time in minutes of applied current to the test vehicle. This device is discussed in Appendix C.

The third step is the point in which the study branches into two research efforts. One path is the design, fabrication, and testing of an instrument which maintains the test stripe at a constant low temperature while conducting SEM electromigration studies in situ. The second branch of the third step is the design, fabrication, and testing of a sample probe and associated thin film test vehicle for use during in situ TEM electromigration studies. This apparatus is also discussed in chapter III.

The final step in this research was to document the findings of the investigation and draw conclusions concerning the feasibility of in situ electromigration research. Recommendations for further study were then made.

Major Equipment Used

The equipment used for this study includes the Nanometrics CWIC Scan 104 Scanning Electron Microscope (SEM) and

the Jeol 100CX Transmission Electron Microscope (TEM). The temperature research conducted in the SEM was accomplished using a prototype MMR Technology Microminiature Refrigerator, while the TEM studies utilized a redesigned Jeol EM-SHH sample insertion probe. During the photolithographic processing of the thin film test vehicles the aluminum was applied by evaporative deposition using a CVC Vacuum System and mask alignment and wafer exposure was accomplished using a Cobilt Mask Aligner, Model Ca 200.

Sequence of Presentation

This thesis is presented in the following chronological order. There are four main sections, the background, the test vehicle and instrument fabrication and testing, the discussion of the results, and the conclusions.

Chapter II provides background information for this thesis. It discusses the theories used in this research which were extracted from the literature. It includes a short discussion on the cause and effect of electromigration in thin film conductors.

A description of how the test vehicles used were designed and fabricated and what modifications to existing microscope equipment were made to conduct electromigration in situ is presented in chapter III. Section III-1 discusses the test vehicle fabrication. Section III-2 presents the design, fabrication, and testing of the cold stage adaptation used in the SEM. Section III-3 describes the

experimental setup and procedure used for the SEM. Section III-4 describes the design, modification, and testing of the patent pending MARK II Holder used in the TEM. Section III-5 describe the experimental setup and procedure used for the TEM.

Chapter IV presents the results of the in situ electro-migration testing. Section IV-1 discusses the SEM results while section IV-2 details the TEM results.

Chapter V presents the conclusions drawn from the design and testing results in Chapter IV, and offers recommendations for further study.

Finally, the appendices contain supplemental information detailing the unique equipment and procedures utilized. Appendix A details the fabrication procedure for the aluminum Bridge Test Vehicle. Appendix B shows the design and fabrication of the production microminiature refrigerator. Appendix C depicts the timer which was designed and fabricated to measure elapsed time in minutes.

II. BACKGROUND

The existence of electromigration in thin films has been acknowledged since the early sixties. Initial interest had been of a theoretical nature as electromigration had little impact on circuit reliability. With the maturing of VLSI technology, gate densities are exceeding 10000 gates per square centimeter. Current densities are exceeding 10^6 A/cm^2 while linestripes are reaching into the submicron range. In this environment, electromigration can cause unwanted open or short circuits in thin films. This has serious implications on the reliability of any integrated circuit (33:113; 57:208).

The earliest integrated circuits experienced little in the way of poor reliability due to electromigration. Gate densities in the late sixties were very low. A typical metal line width exceeded 10 microns and carried a current density that was well below 10^4 A/cm^2 . Cracks and holes in the metal stripes were of little consequence due to the width of the stripe and its spacing with any neighboring stripes.

As the integrated circuit industry entered the eighties, the emphasis was on gate density (61:v). The general trend is illustrated in Figure 1.

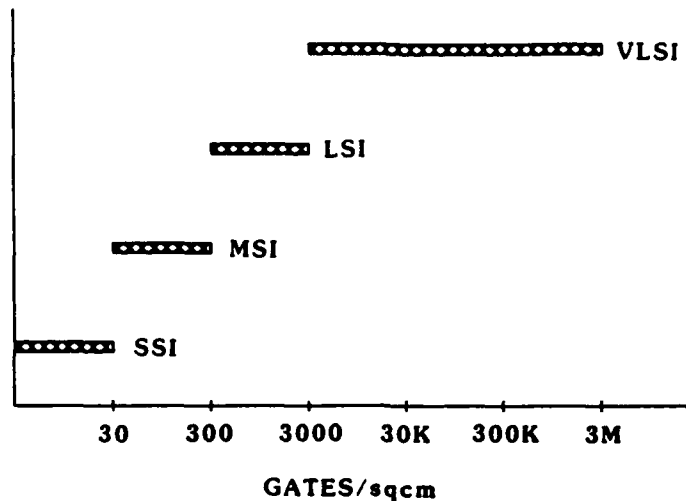


Figure 1. Integrated Circuit Industry Trends
Source: (72:772)

Small Scale Integration (SSI) of less than 10 gates on a chip were to be replaced by denser Medium Scale Integration (MSI). SSI chips were yielding to both MSI technology of densities from 10 to 100 gates per chip, and LSI technology of gate densities from 100 to 1000. Very Large Scale Integration (VLSI) is promised to yield chips with device densities that range from 1000 to 10,000 gates per square centimeter (60:31; 72:772). By 1990, millions of transistors may be fabricated on a chip with feature sizes smaller than the wavelength of visible light (61:v).

Decreased feature size and increased gate density results in higher current densities for the circuit components. The higher current densities pose new problems of

temperature control on the chip and an increase in the probability of electromigration, both of which have serious implications for chip reliability (13:215; 33:114; 57:208).

Electromigration Theories

Electromigration is identified as the mass transport of atoms in a conductor under a current stress (2:2381; 9:339; 12:485; 25:244; 34:51; 35:69; 36:751; 42:76; 50:25; 87:309; 91:937; 103:2; 105:114). Numerous theories have been proposed, with most relating electromigration to temperature and the current density of the conductor. An atom in a lattice is usually represented using the potential well model (8:143; 26:1410). Early theories relate the effects of thermal and electric forces on an atom in the crystal lattice (42; 81). Later theories introduce the concept of an atomic flux and the effect of varying structure and mobilities on it (5; 8; 9; 26). These theories represent a basis for the current understanding of electromigration.

Potential Well Model. In a conductor at a uniform temperature above absolute zero, an atom in the lattice can be viewed as being in the bottom of a potential well (8:142; 9:339; 26:1410). Energy is required to excite the atom out of the well where it is unrestrained by neighboring atoms in the lattice structure. Thermal excitation will excite a small percentage of atoms at any given temperature out of the well to what is known as the saddle point shown in Figure 2a.

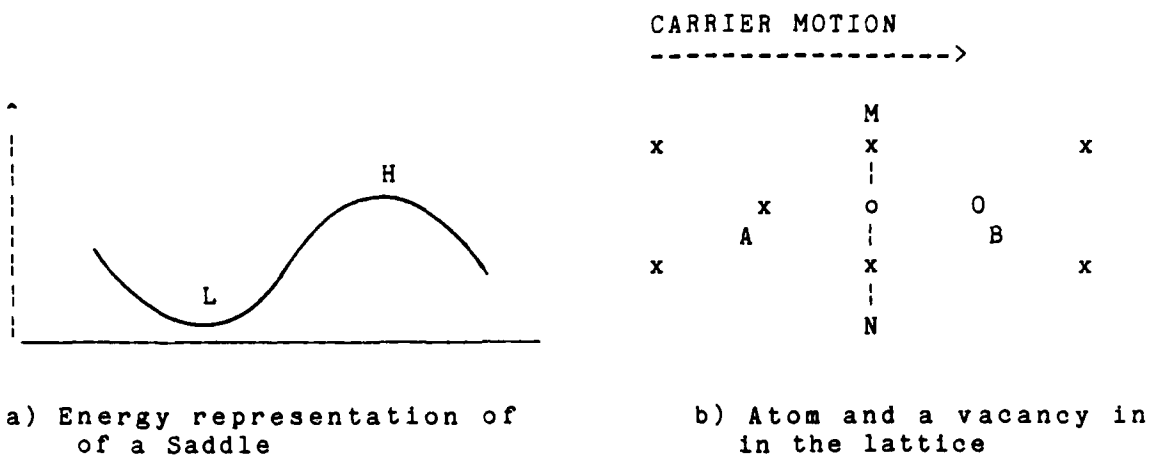


Figure 2. Saddle Point
Source:(26:1410)

Assume that an atom is excited from its normal position A to saddle point O as shown in Figure 2b. At the saddle point, the displaced atom is squeezed between two neighboring atoms and must eventually return to a lower energy state.

Assuming a vacancy or hole in position B, the atom at the saddle will have an equal probability of moving back to A or going on to B (9:339; 26:1411). Under an external bias such as a temperature gradient, the probability of movement toward any particular available direction will be influenced by the bias. An increasing mobility going from A to B would increase the probability of an atom at the saddle point moving toward B and decrease the probability of movement toward A.

Temperature Forces. In a thin film conductor that is carrying a current, the potential presence of a temperature gradient can be shown (9:343; 32:15; 109:1777). Typically, the center of a thin stripe will be hotter than either end, due to the heat sink effects of the end contacts and the less than ideal heat sinking characteristics of the substrate (25:254; 109:1777). In a region of a high temperature gradient, (10^4 K/cm), an atom in the lattice is subject to a force

$$\bar{F} = (Q^*/T)\bar{\nabla}T \quad (1)$$

where Q^* is the energy flow per unit mass transported (18:12; 43:268; 88:15). While an atom in the potential well may not move, an atom at a saddle point may experience movement in the direction of F toward a nearby vacancy in the lattice. An atom that jumps to a vacancy may increase or diminish the value of Q^* by interaction with phonons. A jump to a vacancy may add or subtract energy to the local system dependent on the energy of the atom relative to the energy required to make the transition to the vacancy. Atomic mobility is related to temperature and is affected by the existence of a temperature gradient. The thermal migration of matter due to a temperature gradient is known as the Soret Effect or simply thermomigration (18:12; 23:1410; 43:268; 88:15). Thermomigration is often found in current carrying conductors.

Electric Forces. The structure of a conductor that is carrying a current is subject to an electric field which extends from the cathode to the anode (87:309; 88:4). The individual metal ions feel a force from this field which tries to move them from their present position toward the cathode, as shown in Figure 3.

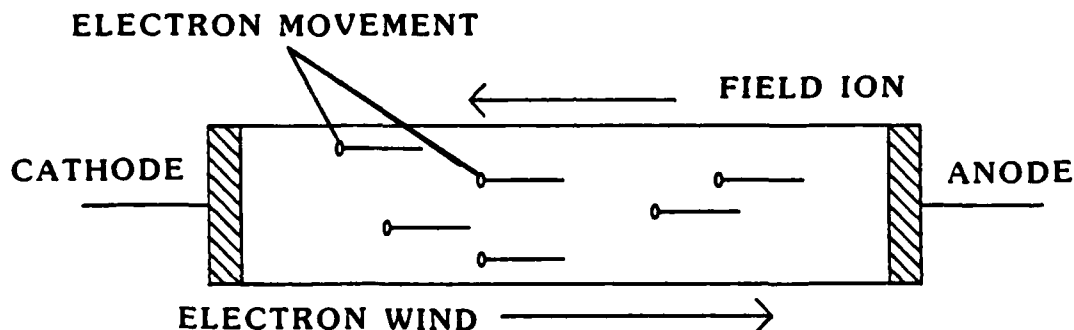


Figure 3. Thin Film Forces

The effect of this electrostatic interaction is dependent on the magnitude of the field and on the diffusivity of the ions. The ion diffusivity is related to the conductor temperature by the Einstein relation

$$D = \mu kT / Z^* e \quad (2)$$

where $Z^* e$ is the effective charge of the ion, k is the Boltzmann constant, and T is the temperature in Kelvin

(23:1410; 62:324). The mobility μ , of an ion within the conductor structure is typically low. With this low mobility, high activation energy is necessary to initiate mass transport. The activation energy required to account for the atomic flux observed during electromigration would place the temperature above the melting point of the conductor. Additionally, the flow of atoms has been observed to move in the direction toward the anode, which is not explained by the field ion effect (8:142; 9:339; 12:485; 18:7). The volume of mass transported is not explained by the field ion effect either. It is apparent that other mechanisms are at work besides electrostatic interaction.

The mass flux of conductor atoms has been observed to move from the cathode to the anode (12:485; 23:1410; 46:969; 77:201). This movement is opposite the direction of movement attributed to the field ion effect, and is caused by a dominant force, the electron wind. The conductor ions experience a momentum transfer from the electron current that is travelling down the stripe. The ions experience a force that is analogous to the force felt by a leaf on a tree that is being blown by the wind. The magnitude of the force is dependent on the current density. The effect of the "electron wind" on an individual ion depends on the mobility of the ion. An expression for the atomic flux J_a is

$$J_a = (ND/kT)Z^+eP_j \quad (3)$$

with j being the current density, N is the concentration of ions, and D is the atomic diffusion coefficient. Z^*e is the effective charge of the ion, which is a function of the electron wind relative to the electrostatic force interaction. ρ is the resistivity of the conductor (1:3954; 12:485; 85:2533).

In a thin film conductor, all three of the effects, thermal, field ion, and electron wind are at work, making the impact of any one hard to distinguish. Besides the electric and temperature effects, the very structure of the thin film has an effect on the probability of electromigration damage.

Structural Effects. A thin film that is carrying a current will experience a stress that is a result of that current. Joule heating effects will cause thermal gradients within the film which can lead to the Soret effect. The field ion effect and the presence of the "electron wind" will also be felt by the film lattice structure. These forces can give rise to an atomic flux that travels down the conductor. A flux alone cannot cause damage to the line-stripe. The structural interaction with the atomic flux has a significant role in the damage to the stripe. If an atomic flux is established by a combination of thermal and electrical effects, there will be a net flow of atoms through any unit volume. The flux in should equal the flux out. Should the flux per unit volume out be different from the flux per unit volume in, then a redistribution of the

atoms in the lattice will occur. From the equation

$$\bar{J}_a = \mu \bar{F} \quad (4)$$

The atomic flux is related to the applied force \bar{F} and the atomic mobility μ (7:24; 23:1410; 42:76). The divergence of the flux, \bar{J}_a will be zero if the total concentration of metal ions remains constant for a given volume (18:8). At locations along the film where there is a discontinuity in the atomic flux, there will be either a buildup or a depletion of material, as shown in Figure 4 (8:145; 11:264; 33:114; 68:116).

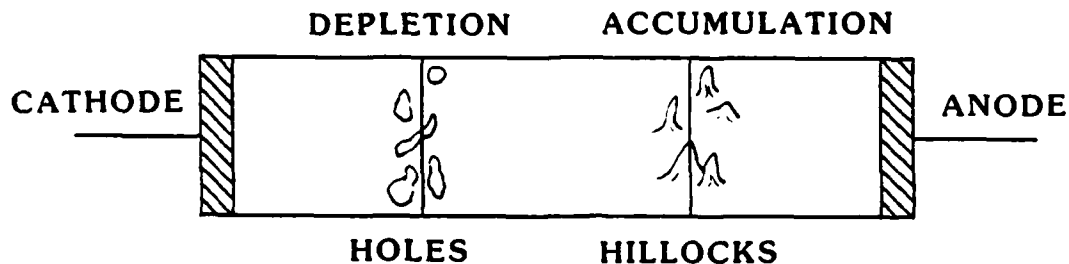


Figure 4. Atomic Redistribution vs Mobility
Source: (34:52)

A change in the ion concentration over time for a given volume means that dC/dt is non zero. Then the divergence of the flux, $\text{del} \cdot (\bar{J}_a)$, is also non zero (11:264; 18:8). If the applied force is assumed to remain constant along the

film, a non zero flux divergence can be caused by changing the mobility of the metal ion. Assume that the ion flux divergence is the time rate of change of the ion concentration for a given volume.

$$dC/dt = -\text{div}(\bar{J}_a) \quad (5)$$

For one dimension,

$$dC/dt = -dJ_a/dx \quad (6)$$

Assuming that J_a is a function of both structure and temperature, then

$$dC_x/dt = -[(dJ_a/ds)(ds/dx) + (dJ_a/dT)(dT/dx)] \quad (7)$$

Thus, the mobility of the lattice atoms can be affected by temperature and structural discontinuities in the film (5:881; 11:264; 18:9; 101:159). The mobility is related to the diffusivity and the temperature through the Einstein relation. A typical thin film under current stress will exhibit a temperature profile with a hot center section and cool ends as shown in Figure 5 (25:256; 109:1777).

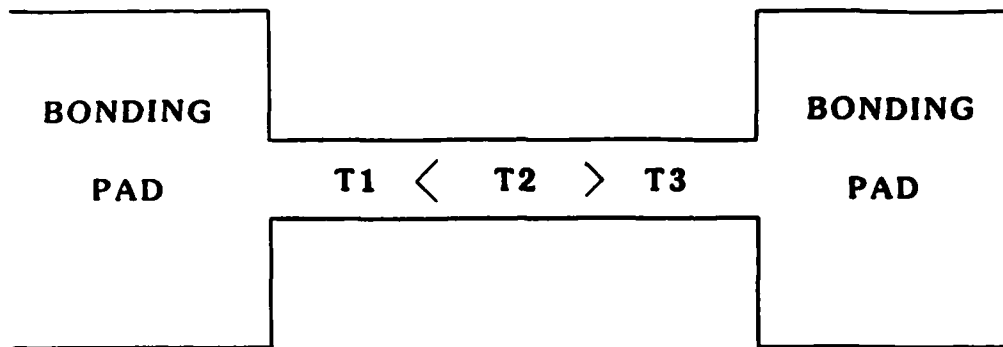


Figure 5. Temperature Gradient of a Thin Film
Source: (25:256)

In the area of positive temperature gradient, where T_2 is greater than T_1 , experimental evidence has shown that mass depletion can occur, due to a decrease in the atomic mobility, causing the flux in to be less than the flux out per unit volume (8:143; 12:487; 23:1411). In the area of negative temperature gradient, where T_2 is larger than T_3 , a mass accumulation can occur since the flux out is less than the flux in (9:346; 12:487; 23:1411). A typical temperature for activation of lattice diffusion would be between 150°C and 450°C with a temperature gradient of 10^4 $^\circ\text{C}/\text{cm}$ (12:488; 75:264). Flux divergences can arise from other factors besides temperature gradients.

Structural defects play an important role in flux divergence. Assuming that a thin film is composed of crystal grains with random orientations, lattice diffusion can occur in three locations; either within the crystal

grain, on the surface, or on the grain boundary. Within the crystal grain, the lattice organization is regular with few vacancy sites available for lattice diffusion by substitution (8:142; 27:81). At the grain boundary however, the regularity of the lattice is disrupted, yielding many vacancies which lend themselves to substitutional diffusion as shown in Figure 6.

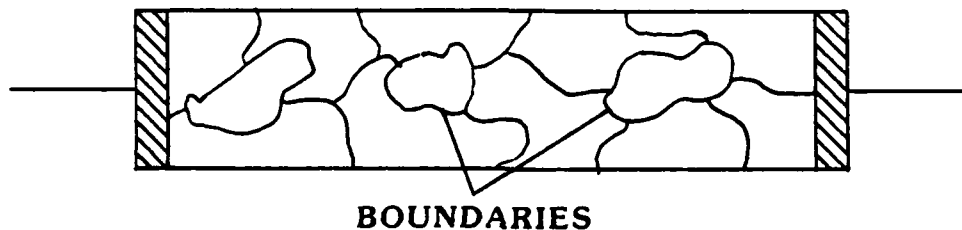


Figure 6. Grain Boundaries

Experimental evidence suggests that the activation energy for lattice diffusion within the crystal grain is much higher than the energy required to initiate diffusion along grain boundaries (75:264). The prevailing view is that the primary location for damage is along grain boundaries (5:880; 12:488; 46:968; 75:263; 80:513; 99:481).

Three damage mechanisms are attributable to structural discontinuities. Mixed grain size, crystal orientation, and boundary properties will have an effect on the mobility of

migrating atoms. Of these, flux divergence or convergence has been shown to be most likely to occur at boundaries where the periodicity of the lattice is severely disrupted (5:880; 23:1415). The most severe disruption and the highest candidate for electromigration damage is the triple point. A triple point is the point of intersection of three grain boundaries as shown in Figure 7 (5; 34:52; 77:201).

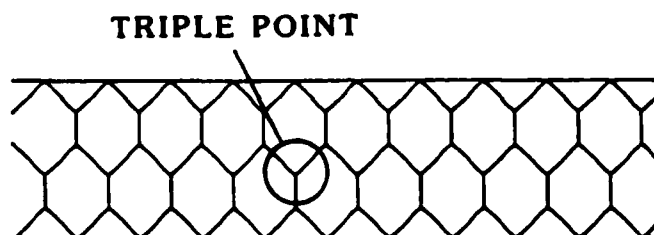


Figure 7. Triple Point
Source: (34:51)

An atom at the triple point will experience a change of mobility if it tries to diffuse through the lattice of the grain in its path. The more likely event will be a change in direction of the atom to proceed down the grain boundary. The mobility will remain constant, but the force on the charge will decrease by

$$F(ab) = F(\cos(b)) \quad (8)$$

where b is the angle of the grain boundary relative to the electron flow force down the film (5:881; 23:1415; 24:272). Migration has been shown to occur along the grain boundary most aligned with the force down the film as shown in Figure 8 (24:272).

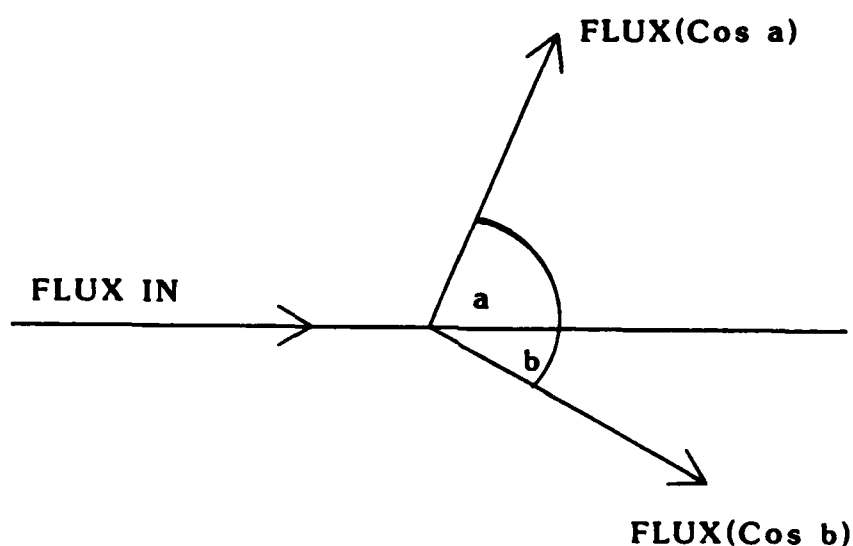


Figure 8. Flux Divergence at a Triple Point
Source: (5:881)

Besides the boundary effects on mobility, the size of the grain and the crystallographic orientation have an effect. Current that flows through a region of small sized grains into a region of larger grains will experience a change in mobility due to flux divergence (2:2383; 23:1413; 24:275). Abrupt grain size changes in the film that can cause the

flux divergence necessary to effect electromigration damage are shown in Figure 9.

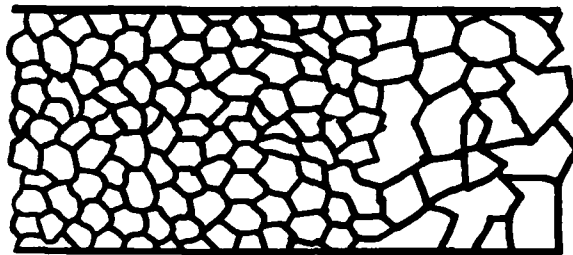


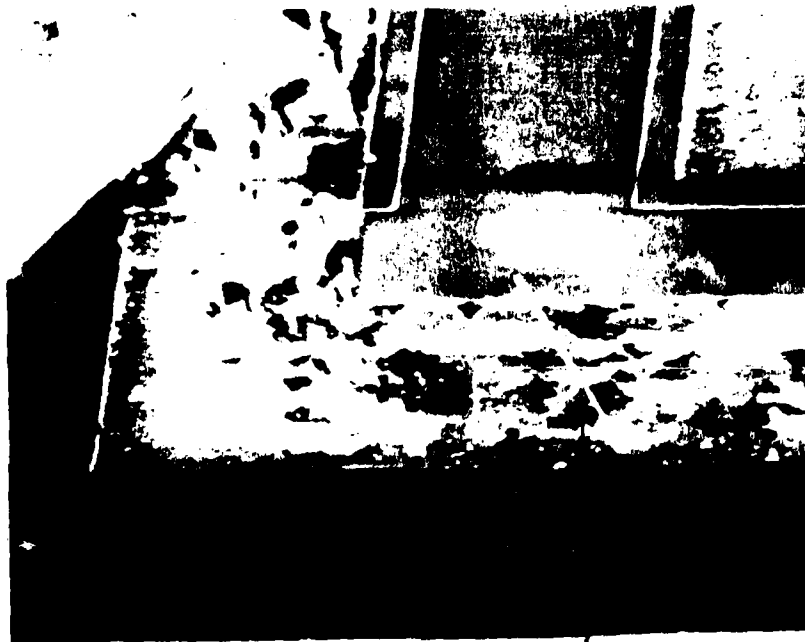
Figure 9. Abrupt Grain Size Changes
Source: (76:2383)

Analysis of the Brillouin zone for various crystallographic directions will show direction dependent mobilities for a particular substance (62:237). Attardo noted the variation in grains related to the conditions existent during film deposition,

"The Al films deposited at 600°C were found to have a predominately $\langle 111 \rangle$ orientation (98%), while those deposited at 200°C had a mixed $\langle 111 \rangle$ and $\langle 110 \rangle$ orientation. Transmission electron micrographs of the two films... revealed a near grain size of 1.2 and 7.8 microns for the 200°C and 500°C Al films respectively." (2:2382)

The presence of temperature gradients, electric forces, and structural factors all lead to the possibility of damage due to electromigration. The multiple causes make the con-

tribution of any one factor difficult to calculate. Figure 10 shows the result of these forces being exerted on a conductor over the course of time (96).



WHISKER

Figure 10. Hillocks And Holes on an Aluminum Stripe, 600x
Source: (96)

The aluminum stripe experienced a current density of 10^6 A/cm^2 at a temperature of approximately 140°C . After about 25 hours of run time, the stripe exhibits the signs of electromigration. Numerous holes in the conductor structure

are visible. The displaced matter appears in the lightly colored deposits as an accumulation or hillock. The cross sectional area of some portions of the stripe have decreased, which increases the current density on those areas of metal that remain. Eventually, a number of holes will combine and bridge all the way across the stripe, causing failure by open circuit. The long thin protrusion from the stripe is known as a whisker. It is a growth from the metal which can have serious consequences. Should it grow out away from the stripe, it could possibly reach a neighboring stripe and cause a short circuit between the two. The exact nature of whiskers is not known.

Figure 11 shows a closer view of migration damage sustained by a conducting stripe.

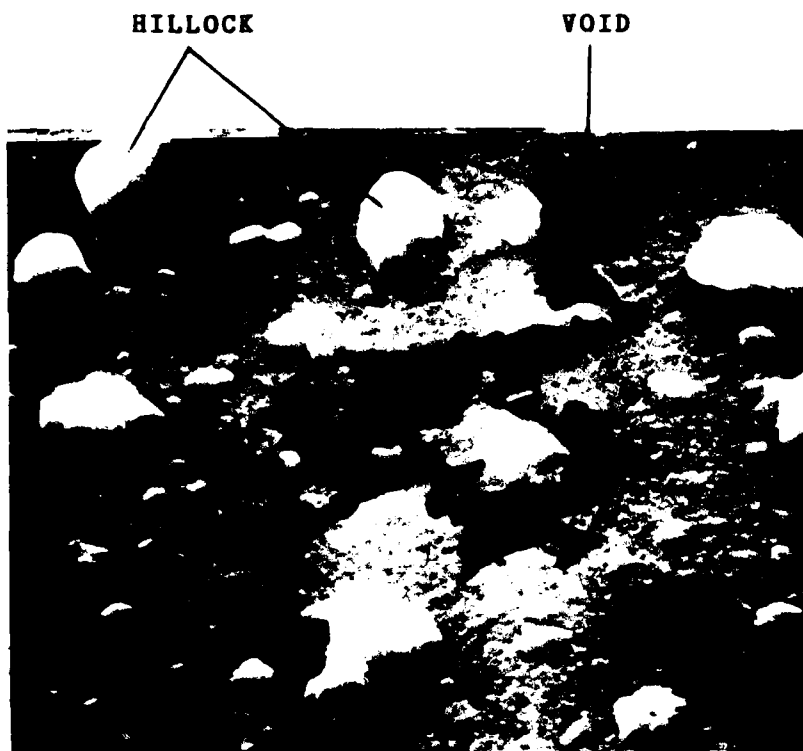


Figure 11. Closeup of Electromigration Damage, 3000x
Source: (96)

The actual walls of the individual grains can be seen in the hole. Matter from the hole migrates down the stripe and then accumulates at a point where the flux converges, causing hillocks to form on the surface. The mechanism by which matter is transported and deposited in the stripe is still the subject of research.

III. Experimental Setup and Procedure

The experimental effort of this thesis required special equipment. The in situ viewing of electromigration is not new in itself, but the control of variables while observing electromigration is a new frontier. To control variables such as current density and temperature, the experimental setup must start from the beginning with known parameters. Test vehicles were acquired through various sources, with known electrical, material, and geometric properties. The SEM and the TEM were modified to accept prototype support equipment and yield the desired data. Finally, experimental procedure are established, for the conduct of in situ electromigration studies in both the SEM and the TEM.

III-1. Test Vehicles

Electromigration testing of actual integrated circuits can become rather involved with questionable results. A researcher typically has little or no control over the manufacture of the integrated circuit. Therefore, little is known about the internal or crystalline structure of the metal line stripes. There is usually no information on the localized internal operating temperature of a given line stripe. Tests utilizing controlled test patterns where the researcher has a degree of control over the line stripes would simplify the job of data analysis. Results should be

easier to interpret do to the elimination of many variables that are not a factor in the study at hand. The opportunity for control makes the specialized test vehicle ideal for use in the lab environment (78:126).

Four test vehicles were available for use. One vehicle was produced commercially by vendors through the MOS Implementation Service (MOSIS). A second vehicle mask was produced at Bell Labs for electromigration experiments by Shela Vaidya (100:165). The remaining two patterns were produced in on base laboratories. All four vehicles offer a simple geometry with a constant stripe cross sectional area. Large bonding pads allow for the introduction of current to the linestripe. All four vehicles were produced with no over-glass layer, unbonded, and unmounted.

MOSIS Test Vehicle. The MOSIS test vehicle is shown in Figure 12.

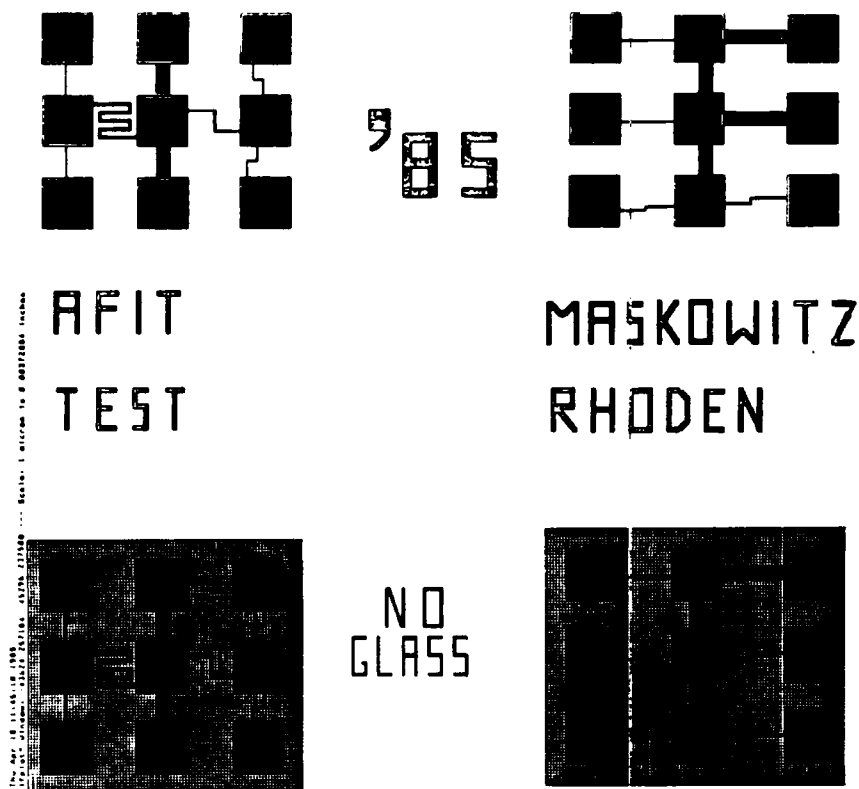


Figure 12. MOSIS NMOS Test Vehicle

The basic cell consists of two separate blocks of nine bonding pads, shown in the upper half of Figure 12. Each block of nine bonding pads are interconnected to each other with one of five different metal or polysilicon patterns. Each pattern is referenced with respect to the letters on

the bonding pads for each test stripe, as shown in Figure 13.

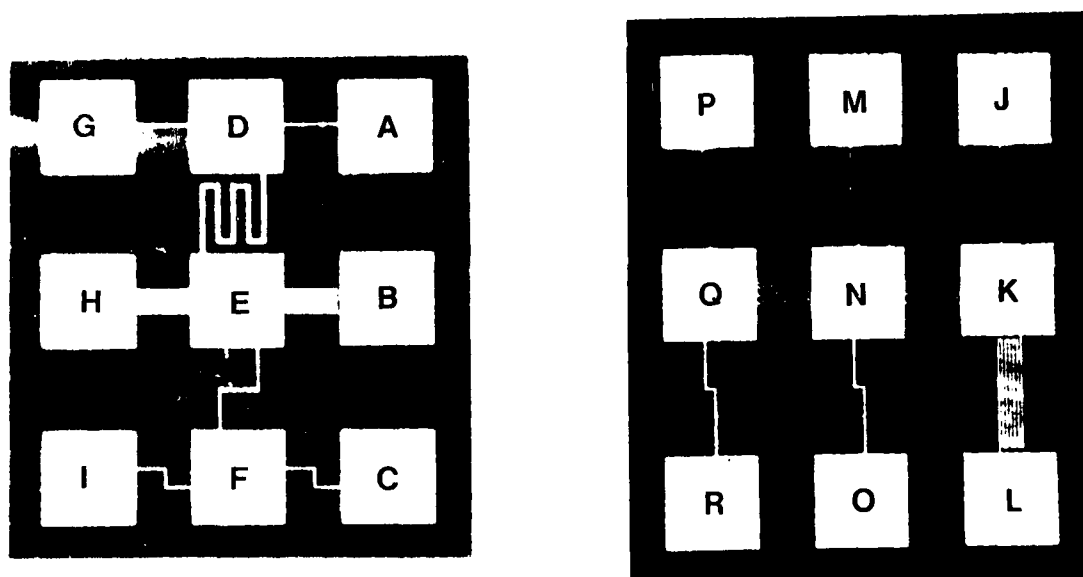


Figure 13. MOSIS Pattern Designations

Using 1.2 micron NMOS technology, the thinnest stripe width is 2.5 microns with a height of 1 micron. The pad size allows thick bonding wires or ribbon bonding interface with the test pattern without electromigration occurring outside of the test pattern itself. Fabrication information provided by MOSIS is as follows:

Metal Line Composition - 99% Aluminum, 1% Silicon

Method of Deposition - D.C. Sputtered

Temperature - Ambient

Vacuum - 1×10^{-6} torr

Annealed (Alloyed)

Temperature - 450°C

Time - 30 Minutes

Environment - N_2H_2

The metal stripes were deposited by evaporation onto the first metal layer, with no glass overlay. Four versions of the vehicle are available. Besides the basic cell, the same patterns are available with glass overlaid (the bottom half of Figure 12). A more complex version contains the test patterns in second metal, plus three different polysilicon stripes for future testing. The last version is the basic cell with the inclusion of a planar diode underneath the test pattern as shown in Figure 14.

Comprehensive Test Vehicle. The Comprehensive Test Vehicle, (CTV), is produced by the Avionics Lab, WPAFB in support of their ongoing Gallium Arsenide research (15:27). The test pattern of primary interest is TP23, located in test area A2, as shown in Figure 15.

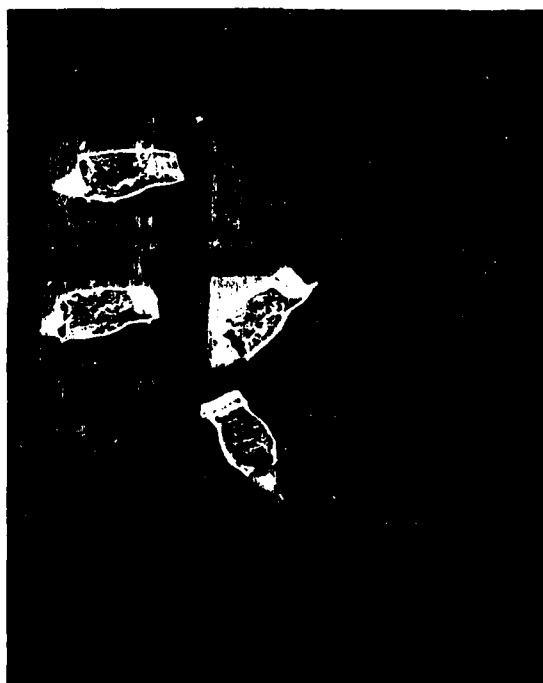


Figure 15. CTV TP23 Pattern

The CTV test vehicle was modified during manufacture by using only the #5 gate mask to produce flat stripes instead of the original stripes that cross step grades. The line width is 0.8 microns with a height that can be controlled during the aluminum evaporation deposition as desired. The pattern length is 4000 microns long with tap points at the 1000 and 2000 micron points (15:117). Other useful patterns for preliminary work include TP29 and TP30, both located in area A3. Shown in Figure 16, TP29 and TP30 possess a line width of 12.4 um with a length of 797.8um.

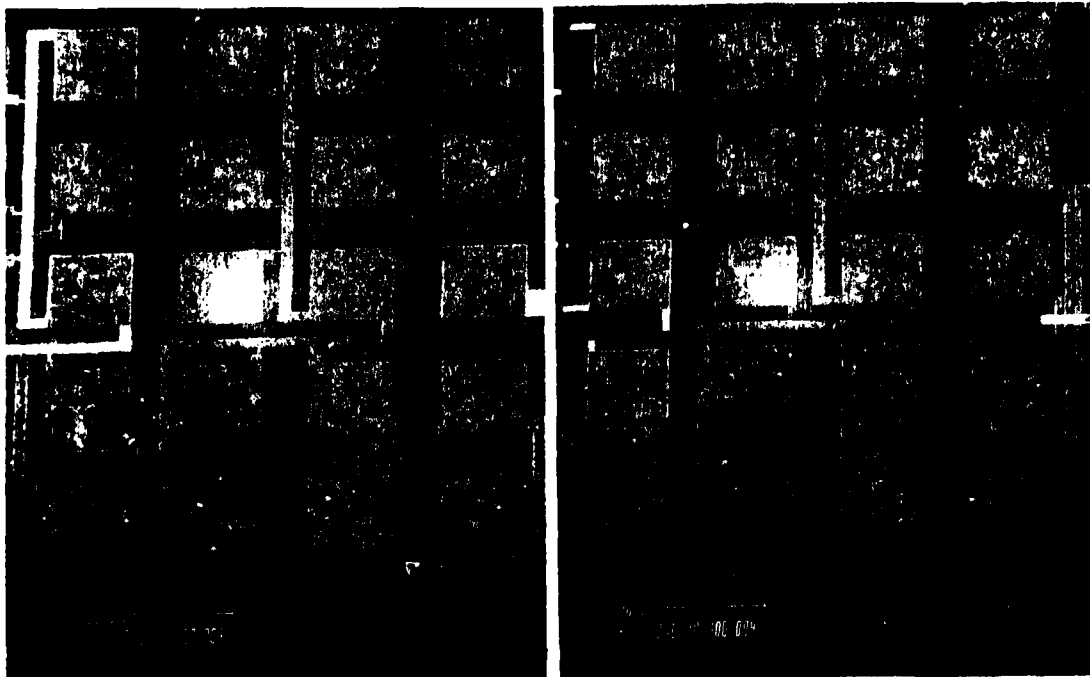
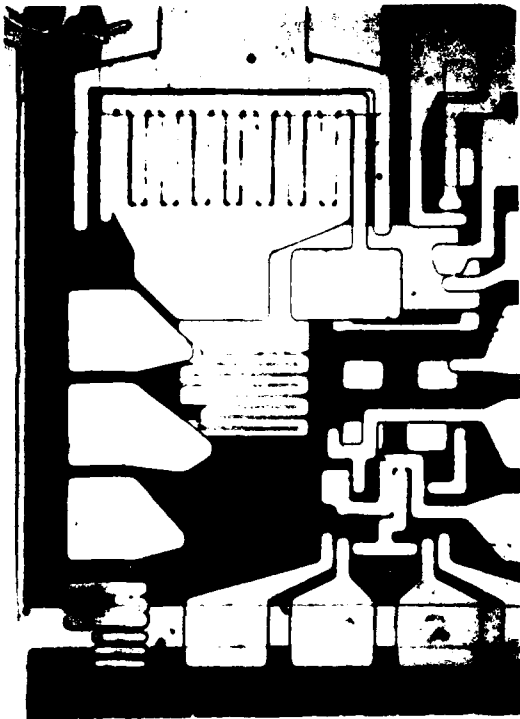


Figure 16. Patterns of Interest on CTV

Metal that is deposited on the wafer by evaporation is patterned by a positive lift-off technique. The finished product can be left unmounted and unbonded. All test vehicles are made of aluminum deposited on a silicon substrate which is insulated with a thermally grown 2000-3000 angstrom layer of silicon dioxide.

AFIT Test Vehicle. The AFIT test vehicle was designed at the Institute. The circuit is built from a double photolithography process in which two mask steps are used. The photolithography process utilizes two separate masks. The first mask is the bonding pad mask. The bonding pads are evaporated onto a Boron doped Silicon wafer which is covered with 2000 angstroms of Silicon dioxide for insulation. After etching, a second photolithography step with a separate pattern mask is used. The second line pattern is evaporated onto the wafer with line ends in contact with the bonding pads. After a second etching, the result is the test vehicle shown in Figure 17 which can be manufactured in large quantities.



a) Magnification 60x



b) Magnification 300x

Figure 17. AFIT Test Vehicle

The line width is 8 microns wide with a typical height of 2000 angstroms. The pattern length is 800 microns long. Although this structure provides the most flexibility, the process also takes a long time and the yield of usable patterns per wafer is low. For initial testing and experimental setup, this pattern represents the most expendable vehicle.

Bell Labs Test Vehicle. The Bell Labs test vehicle was constructed at the institute, using a pattern mask acquired from Bell Labs in Murray Hill, New Jersey. This pattern was utilized during previous research by Shela Vaidya in 1970 (100:165). Figure 18 shows the four patterns that comprise the pattern.

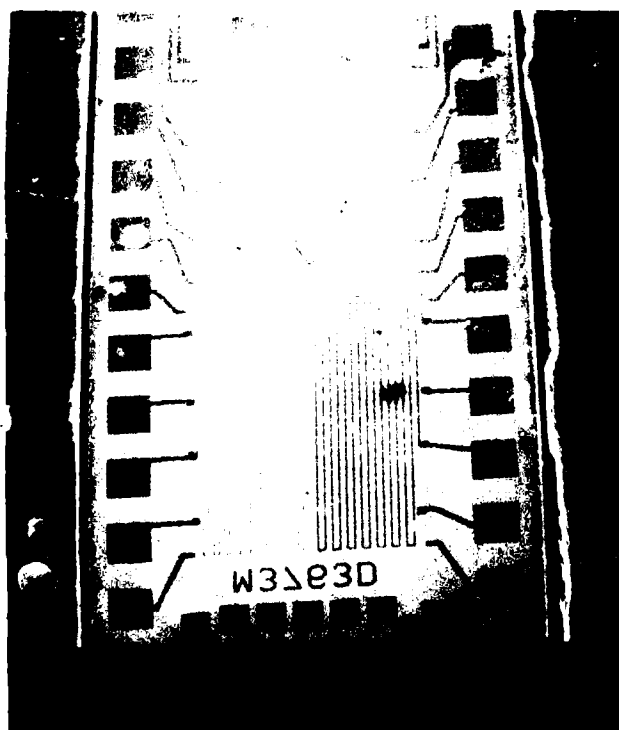


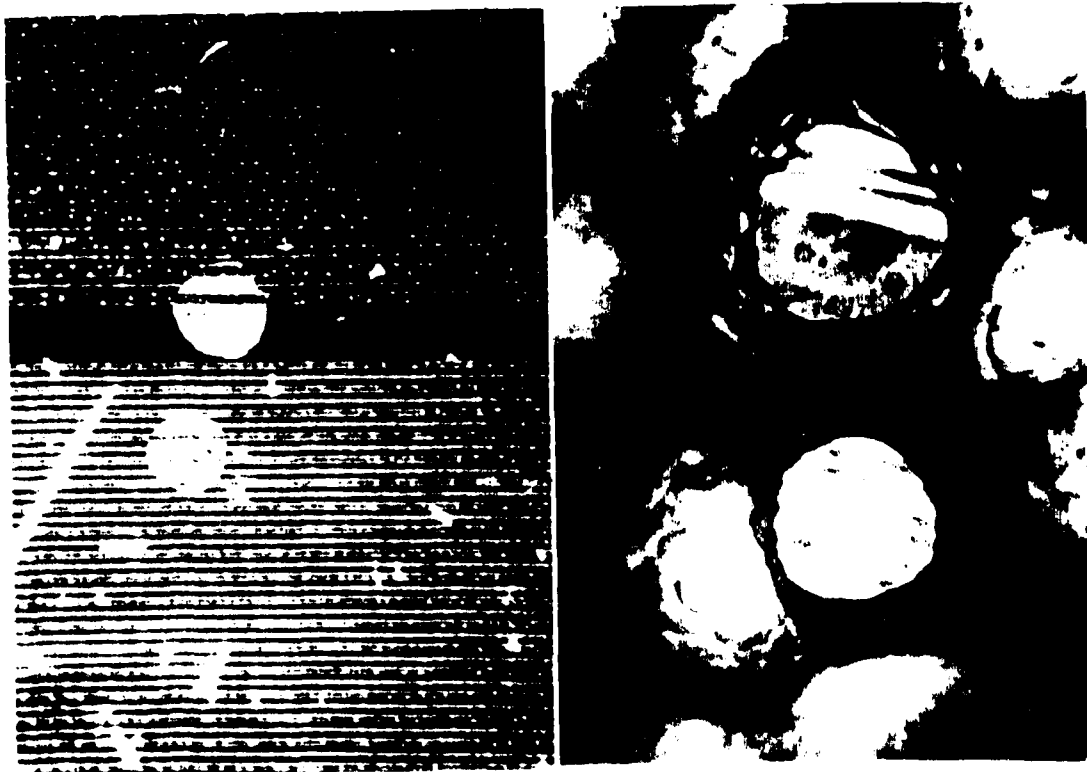
Figure 18. Bell Labs Test Pattern

Each linestripe measures 4000 angstroms long with a widths of 3.58, 5.7, 6.75, and 9.24 microns. The thickness of the stripe is controlled during fabrication. An interdigital comb structure separates the linestripes from each other. This structure is connected to a contact pad and can be used to detect a stripe failure caused by a shortcircuiting of the linestripe pattern with the comb structure.

Aluminum was evaporated on the surface of a Boron doped wafer that had 3800 angstroms of wet grown SiO_2 on the surface. The pattern was formed through a single photolithography process. The excess metal was then etched away, leaving only the test patterns. The patterns were annealed at 500°C for 10 minutes to adhere the aluminum to the substrate. Two thicknesses of aluminum were deposited, 1900 angstroms and 6000 angstroms.

Bridge Test Vehicle. The Bridge Test Vehicle (BTV) is an offshoot of the Bell Labs pattern previously described. The 1900 angstrom thick patterns were further processed to produce the bridge pattern. The test pattern is pressed into melted wax on the surface of a sapphire disk. Wax is melted around the edges of the pattern to seal the pattern, leaving holes on the back side of the test vehicle exposed. With the test vehicle sealed in wax, the disk is immersed in an etchant solution. The etching is periodically checked for progress. When the etchant has eaten through the substrate, the stripe pattern is initially protected from the etchant by the oxide layer between the test pattern and the sub-

strate. The test vehicle is then removed from the acid, rinsed and dried. The oxide layer may remain or be removed by a second etchant bath. Figure 19 depicts the stripes over the etched hole from the test vehicle side and also a view from the back of the test pattern visible through holes in the substrate layer.



a) Pattern Side of BTV, 100X

b) Etched Side of BTV, 200X

Figure 19. Bridge Test Vehicle

These holes allow for the passage of an electron beam through the suspended linestripe, enabling detailed structural TEM observation of the sample. Detailed Fabrication procedures for the BTV are presented in Appendix A.

The AFIT test vehicle and the CTV patterns were utilized primarily in the early stages of experimental setup. Many patterns were stressed to exercise and prove the electromigration test circuit design, which includes the timer and the isolation circuitry required for non-interference with the set current density. The MOSIS and Bell Labs test vehicles were reserved for actual experimental setup runs on both the SEM and TEM. The Bridge Test Vehicle was used primarily for the in situ observation of electromigration in the TEM. Both microscopes required modification to accept a power-on linestripe at test conditions.

III-2. Sem Coldstage Design

The unique capacity to observe electromigration in a SEM while controlling the operating temperature requires modification to the SEM specimen chamber. To accomplish this, a cold stage capable of maintaining a powered circuit at a temperature of 93K was designed. The core of the design involves the mounting of a test vehicle on the cold stage of a prototype MMR microminiature refrigerator, (see Appendix B). The refrigerator was modified to allow for the introduction of power to a device located on the cold stage. The high vacuum requirements for operation of the SEM and the

refrigerator led to the design of an interface flange which allowed for electrical and thermal access to the test vehicle. The cold stage was designed, constructed, and then inserted into the SEM, where a vacuum of better than 5×10^{-6} torr must be maintained (64:64). Figure 20 shows the block diagram of the equipment.

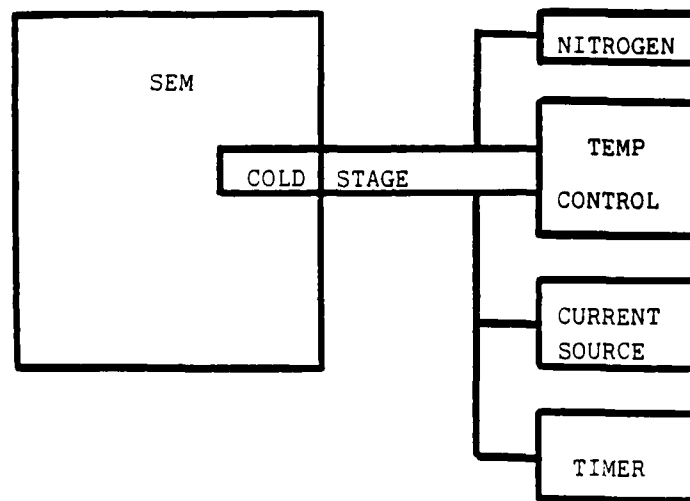


Figure 20. SEM Modification Block Diagram

Prototype Refrigerator. The prototype cold stage is manufactured by MMR Technologies Inc.. Four quartz cold stages were provided by MMR Technologies for testing. The Quartz stage is a flat plane with a capillary tube system running from the flange end to specimen end, as shown in Figure 21.

Wiring to the Alumina bonding block on the cold stage is depicted in Figure 22.

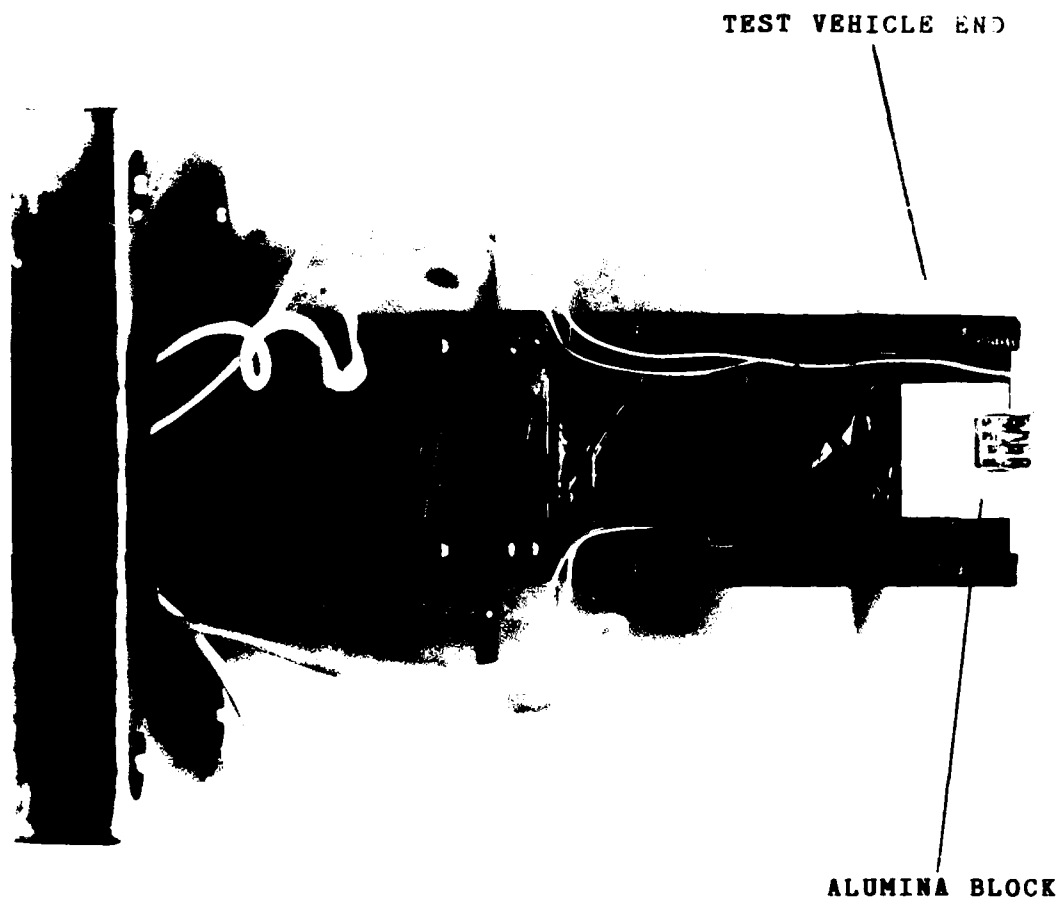
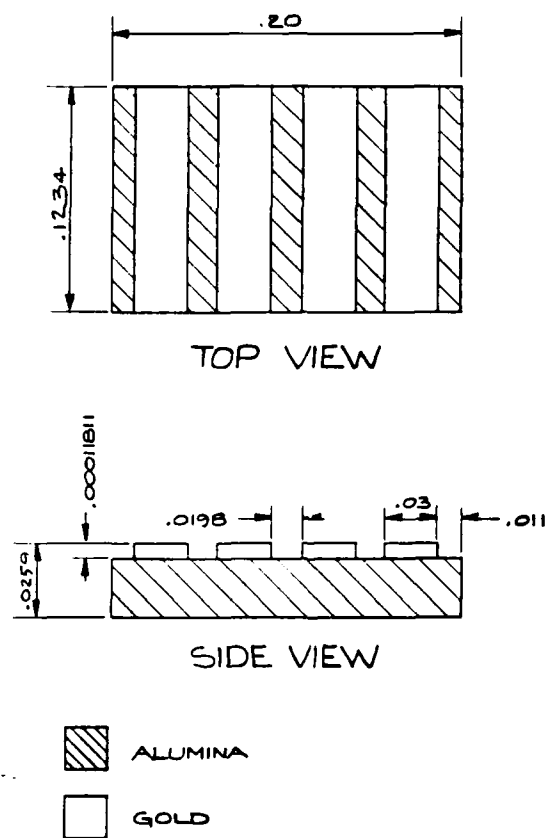


Figure 22. Input Current Wiring

Silver Paint (SPI #5001), was used to secure the test vehicle to the cold stage just left of the bonding block. The high thermal conductivity of the paint was required to

keep from thermally insulating the test vehicle from the refrigerator. As shown in Figure 23, a square of Alumina with four gold contact stripes was mounted on the stage close to the test vehicle for use as a bonding post.



NOTE -
ALL DIMENSIONS ARE IN INCHES

Figure 23. Alumina Bonding Block
Source: (4)

Electrical connections to the test vehicle can be made with relative ease, allowing the introduction of current to the test pattern. From the gold stripes, wiring could then be run to an outside source. The routing of the electric and gas connections were determined by the orientation of the cold stage in the SEM specimen chamber.

SEM Modifications. Figure 24 depicts the size of the SEM specimen chamber.

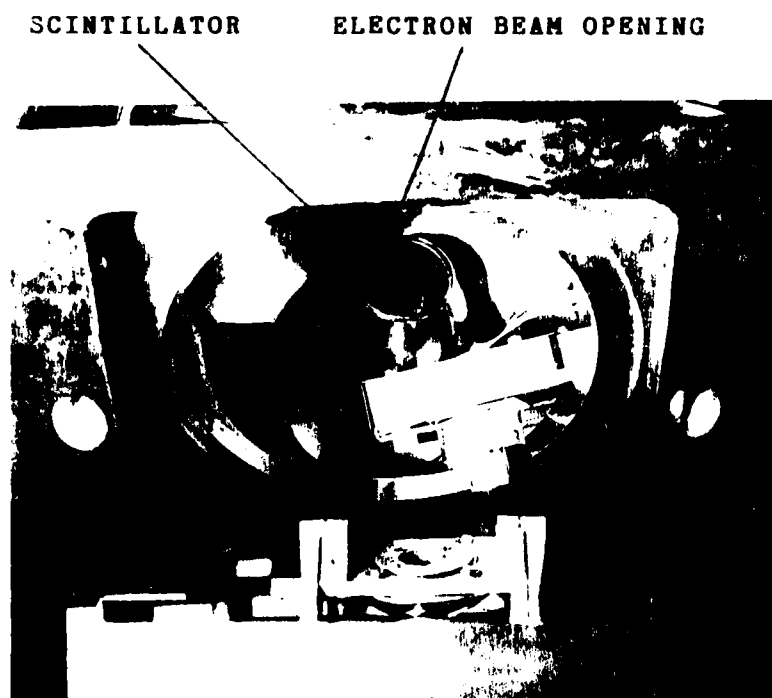


Figure 24. SEM Chamber with Cold Stage Inside

The scintillator is in the center rear of the chamber, while one of two access ports is visible in the upper right hand corner. The largest diameter hole is for the specimen door. This hole measures 8.9cm in diameter compared to the cold stage length of 6.35cm. To avoid contacting the scintillator with the cold stage, the stage required positioning as shown in Figure 25.

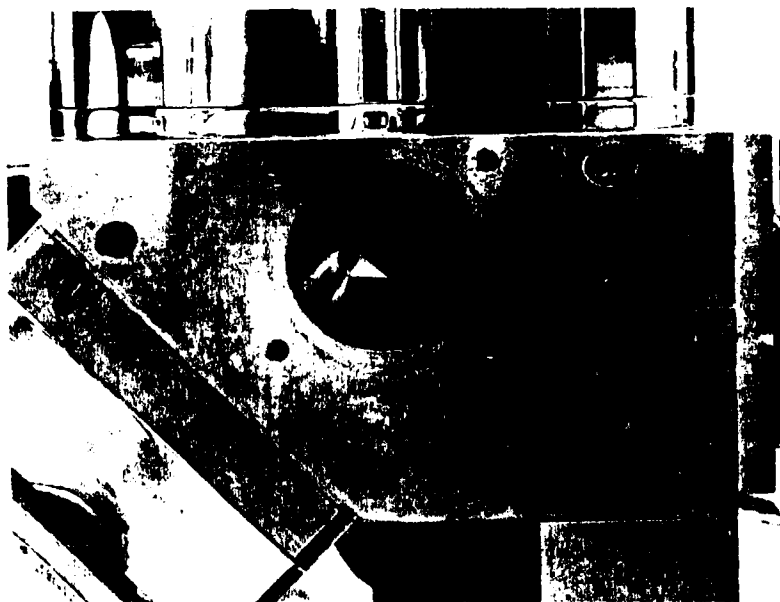


Figure 25. Cold Stage Position in SEM

With the test vehicle mounted on one end of the cold stage, the stage has to be positioned at an offset from the center of the chamber. This offset is required to place the

test vehicle underneath the electron beam opening from the gun chamber. The opening is located just above the scintillator in Figure 25. This positioning limits the movement of the cold stage inside the specimen chamber. The flange end of the stage actually extends into the electrical port located on the side of the SEM specimen chamber. The diameter of this port is the limiting factor in the available movement of the cold stage. This orientation does however, provide a convenient port for both electric and gas connections to enter.

To accommodate the required connections, an interface flange shown in Figure 26, was constructed and mated to the SEM port shown in Figure 25.

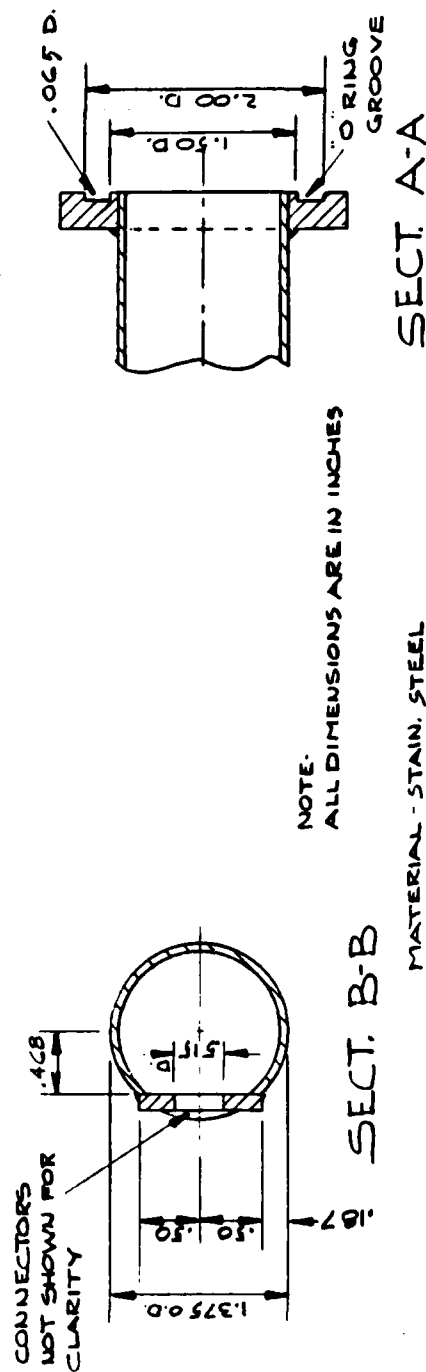
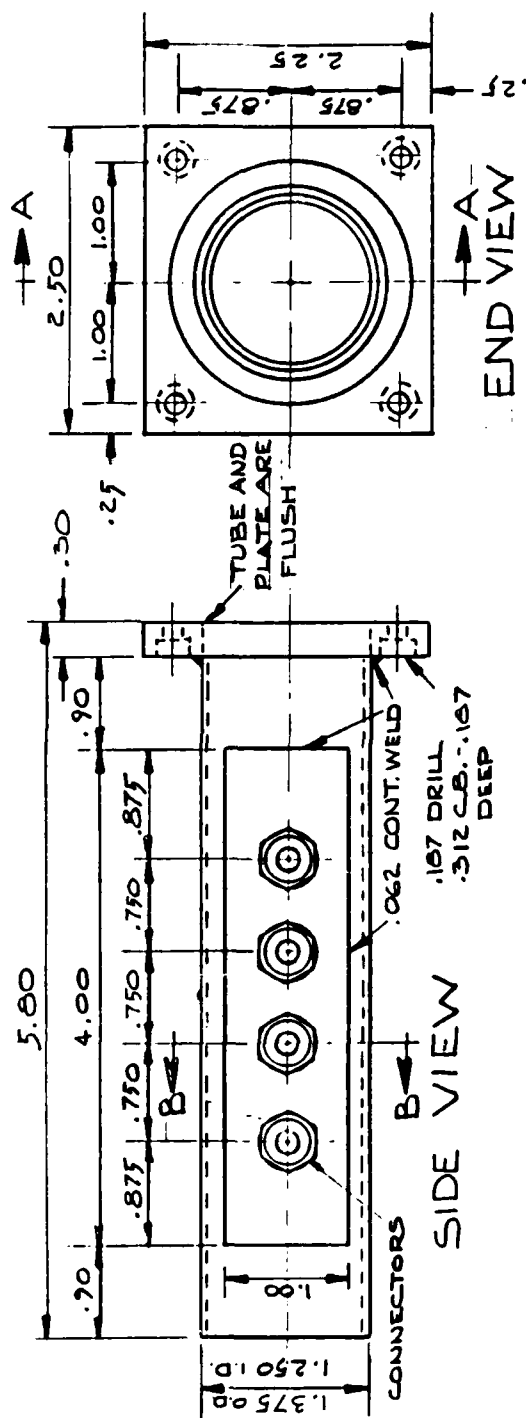


Figure 26. Interface Flange
Source: (4)

This provided room for the cold stage in the port corridor and for the wiring and plumbing to reach from the stage to the interface. Flex tubing and wiring allowed for limited movement of the stage through the range limited by the chamber dimensions. Figure 27 shows the interface flange in position mated with the SEM electrical port.

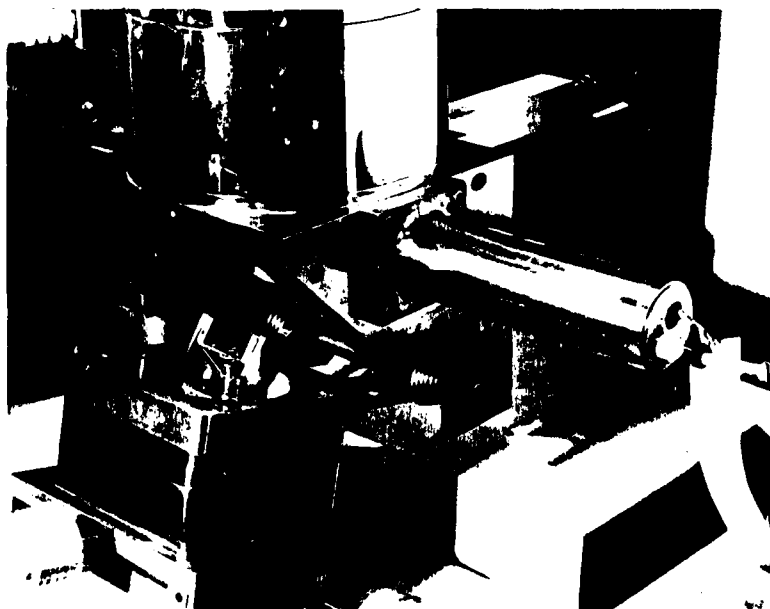
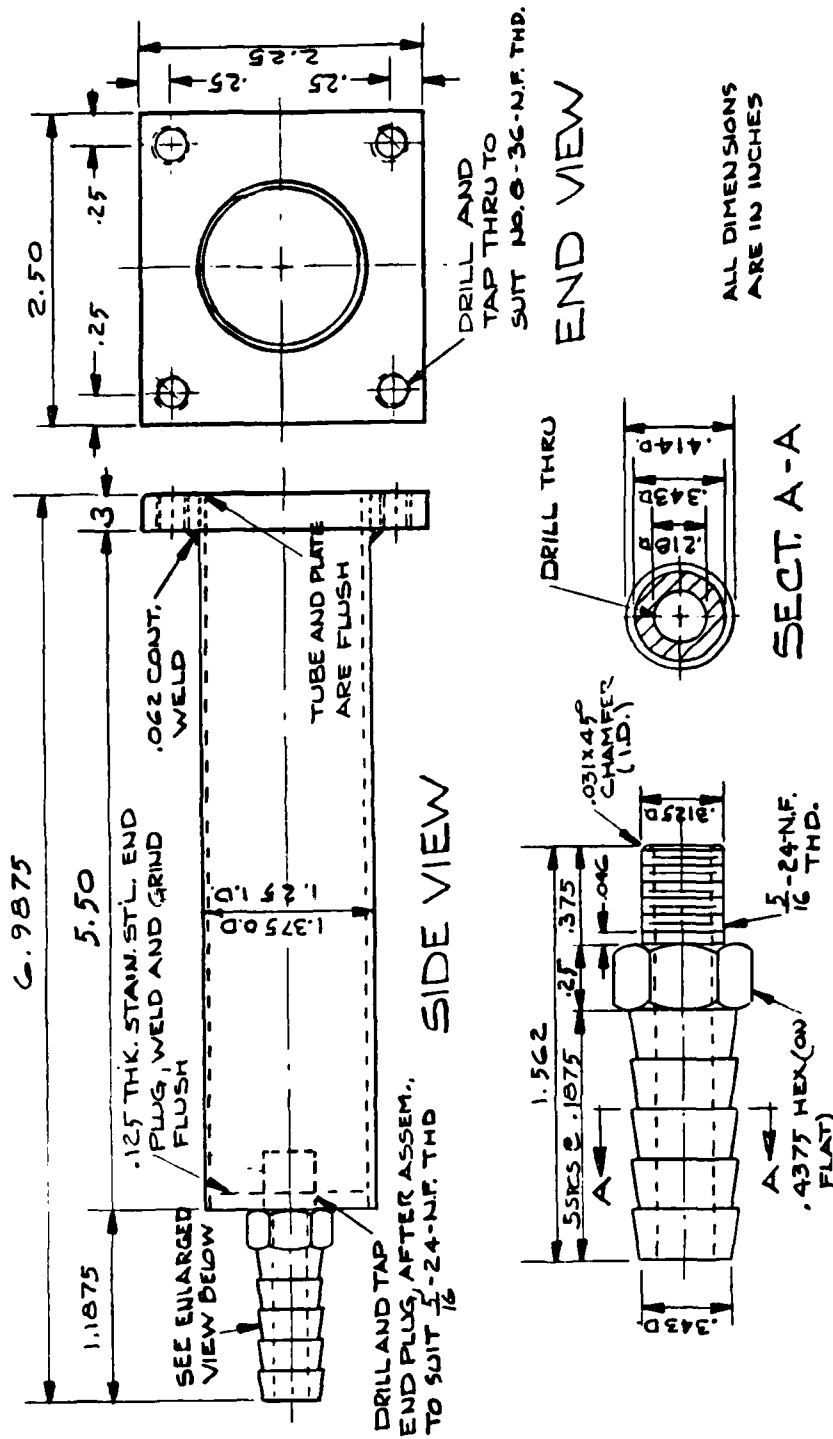


Figure 27. Electrical Port with Cold Stage

An additional flange was constructed and matched to the interface flange. This flange, shown in Figure 28, provides a separate vacuum chamber which can be pumped down independent of the SEM.



NOTE:
MATERIAL IS STAINLESS
STEEL, EXCEPT AS SHOWN

Figure 28. Vacuum Chamber
Source: (4)

This setup allows for leak checking of the system before mating the refrigerator and flange assembly to the SEM. The additional flange also provides a method for introducing a controlled atmosphere to the cold stage during an experiment.

To provide for precise movement control, the SEM stage controls were used. A modified version of the SEM specimen chamber door was constructed to position the cold stage and provide precise control of stage movement. A spacer plate was fabricated for the door to correctly position the cold stage and allow for stage control. The mount with the door spacer plate is shown in Figure 29.

SPACER PLATE

COLD STAGE MOUNT

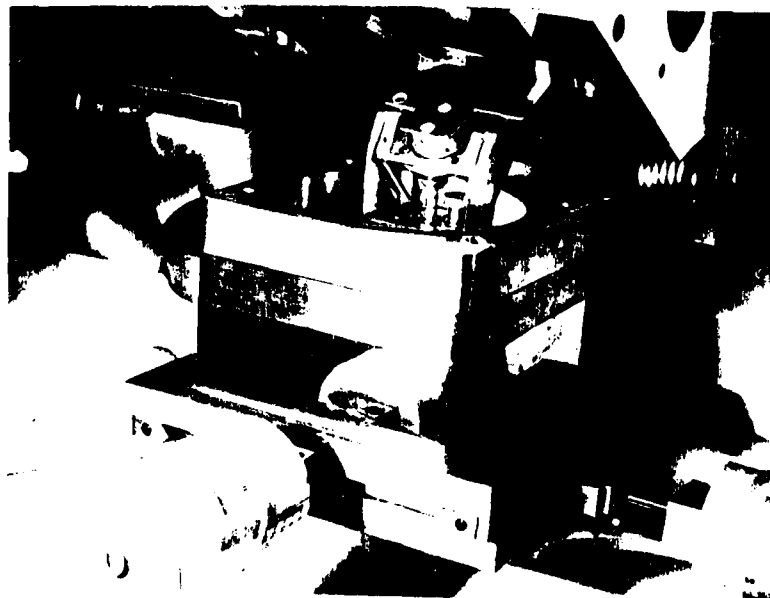


Figure 29. Cold Stage Mount With Door Spacer

Specimen stage travel had to be limited to preclude cold stage damage by exceeding the travel limits imposed by the modifications. The modified stage and cold stage mount positions the cold stage at the axis of symmetry inside the electrical port. This position allows full scale translation in the x and y direction by moving the SEM specimen stage controls. The port walls limit rotation about z to a maximum of 5°. Rotation about y is unrestricted by the modifications and is limited only by the SEM control itself. Rotation from 0° to 80° is available. The modifications coupled with the tight space within the chamber requires careful handling of equipment to avoid damage.

Once assembled, the SEM is pumped down to operating pressure. The refrigerator is then activated, providing temperature control of the test vehicle. Current is applied to the vehicle and monitored by a timing circuit and ammeter. The timing circuit monitors time to failure by detecting an open circuit (See Appendix C). Electromigration can be observed as it progresses toward a failure mode. With the proper equipment setup and procedure, excellent observations of linestripe damage can be recorded.

III-3. Experimental Setup and Procedure for SEM Coldstage

The setup of equipment for use in the SEM experiments can be accomplished in a matter of hours. Two types of experiments can be accomplished with the same equipment configuration by selecting one of two interfaces to the SEM

specimen chamber. Numerous steps must be taken prior to the running of an experiment to insure the outcome of usable data. Once the experiment is ready to commence, strict adherence to the experimental procedure is required to preclude personal harm and/or property damage.

Setup. Preliminary work starts with the selection of a suitable test circuit that has been diced and cleaned. The circuit should be probed for good continuity and examined in a SEM for structural anomalies, non-adhesion to the substrate, variable linewidth or thickness, and other irregularities which may affect the outcome of the experiment. Photographic documentation of the linestripe to be tested will simplify the job of comparing the before and after stress states. After documentation, the circuit is mounted and bonded.

The test vehicle can be mounted directly on the refrigerator stage or on a standard 24 pin Dual In-Line Package (DIP). In either case, the test vehicle is secured with silver paint. The 24 pin DIP allows for bonding wire contact with a maximum of 24 bonding pads on the test vehicle. The refrigerator cold stage is limited to a maximum of four wire bonds due to the limited number of external leads. The wire bonds connect the bonding pads on the circuit to the gold stripes set on the alumina bonding block on the cold stage (see Figure 23). A photograph should be taken, depicting the wire bonds and their contacts. This will aid in determining the correct pin numbers for the desired circuit.

Once the connections have been established, electrical continuity of the test pattern should be verified with a voltage-ohm meter. With the test vehicle documented, mounted and bonded, the package can be connected to the power source, the monitoring equipment and to gas, if required, as follows;

1) Mount the test vehicle package inside the SEM. This requires a two step process;

a) Feed the DIP package or the refrigerator through the specimen chamber port and secure the flange.

b) Position the package via the specimen chamber door so that the mounting post engages the movable holder.

2) Close the chamber door once the package is properly positioned.

3) Connect the active plugs to the EM connectors on the rear of the timer box as shown in Figures 55 and 57, Appendix C. Note the polarity of the wires. For the ambient test, use the feed-thru leads. For the cold stage, use the BNC connections.

4) Turn off the EM switch and the VOM switch on the timer. Turn both potentiometers fully counterclockwise on the timer rear panel.

5) Confirm voltage source settings (+5 v and ± 22 v) with a volt meter.

NOTE

If increased voltage is required to attain the proper current density, an alternate power supply may be incorporated as per Figure 70, Appendix C.

6) Connect the timer to the voltage source. See Figure 66 and Figure 68 in Appendix C. The led seven segment displays should illuminate.

CAUTION

Improper voltage or polarity may damage the timer circuit or test vehicle.

7) Cold Stage experiment only: Connect the high pressure gas line to the cold stage vacuum chamber intake port. Insure that no restrictions are present in the gas line. Refer to The MMR model 2205 users manual for the connection procedure (20).

8) Cold Stage Experiment Only: Configure the gas source by closing the regulator flow control valve and opening the cylinder valve until full tank pressure is registered on the tank gauge.

WARNING

High pressure gas can be harmful if mishandled. For complete information on the proper operation of gas regulators, see the Matheson Gas Regulator Users Manual (63).

9) Adjust the regulator on the gas supply to register a maximum regulated delivery pressure of 1800 psig.

10) Connect the ammeter to the timer while noting the polarity. Turn the ammeter on and set it to the proper scale.

Procedure. The successful running of an electromigration experiment requires the execution of several steps in the proper sequence. The vacuum environment must be obtained and if necessary, the temperature must be set. All monitors must be initialized and the current stress must be applied at the proper time. Proceed as follows;

- 1) Determine the desired temperature and current density for the experiment.
- 2) Evacuate the atmosphere from the SEM specimen chamber. Follow the procedures outlined in the SEM Users Manual. The vacuum for operation in the Cwixscan 100 should be 5×10^{-6} torr or better. The MMR refrigerator is not compatible with vacuum pressures less than 10^{-6} torr due to limitations imposed by the high vacuum glues used to construct the refrigerator body.
- 3) Cold stage experiment only: Adjust the regulator delivery pressure to 500 psig. Open the flow control valve on the gas regulator to allow 500 psig nitrogen to flow through the refrigerator for a minimum of 30 seconds. This purges the system of moisture and contaminants. Close the flow control valve and adjust the delivery pressure to 1800 psig.
- 4) Cold stage experiment only: Open the flow control valve to allow 1800 psig nitrogen to pass through the refrigerator. Set the desired temperature on the K-77 Temperature Controller. Instructions for operating the K-77 are found in the K-77 Users Manual (44). Allow the temperature

to stabilize. (15 to 20 minutes).

- 5) Turn on the ammeter and set to the proper scale. Turn on the VOM switch on the timer.
- 6) Turn on EM switch and within 3 seconds press reset button. Leds should indicate "9"s and then "0"s.
- 7) Turn on the EM switch on the timer to apply power to the test linestripe.
- 8) Verify timer operation by monitoring the green led for change in indication every six seconds. If no change is noted, turn off the EM switch and reconfirm proper experimental set up.
- 9) Set desired current stress with current adjustment potentiometers while reading current on ammeter. Start with 5K ohm potentiometer (full clockwise rotation will result in approximately 30 milliamps with a 12 volt supply voltage).

NOTE

A smaller resistance with greater accuracy can be incorporated into the experiment if needed. See Figure 69, Appendix C.

- 10) When the 5K ohm potentiometer reaches full clockwise travel, increase current slowly to desired setting with 200 ohm potentiometer.

CAUTION

Increase current in small increments when within 50 milliamps of the desired current and allow the current to stabilize from the effects of joule heating on the test stripe resistance. Current adjustment is extremely sensitive near the high end.

11) Cold Stage experiment only: Insure that the temperature remains constant and the 250 milliwatt limit is not exceeded. The refrigerator can continuously dissipate 250 milliwatts of power and still maintain the set temperature. See the Model 2105 Users Manual (20).

12) Monitor the current setting for at least 10 minutes to insure stabilization.

To Remove the Ammeter During a Stress Test:

- a) Turn off the VOM switch on the timer rear panel.
- b) Turn off ammeter.
- c) Disconnect ammeter from VOM sockets on timer rear panel.

Note

Failure to accomplish steps a through c in the proper order may cause transients that can alter the correctly displayed time as it appears on the leds.

To Accomplish a Current Reading During a Stress Test:

- a) Connect ammeter to VOM sockets on the timer rear panel.
- b) Turn on ammeter and set to appropriate scale.
- c) Turn on VOM switch on timer rear panel and take current reading.

13) Activate SEM controls and photograph the sample. See the Cwikscan users manual (64).

14) Turn off EM switch on timer rear panel after circuit failure or required elapsed time.

- 15) Record the experimental vacuum, elapsed time, and if appropriate, the experimental temperature.
- 16) If 2 or more test circuits are located on the same test vehicle, multiple runs can be performed by returning to Setup Step #3 and executing the applicable steps from that point.
- 17) Cold stage experiment only: Close the tank valve and allow the pressure to bleed out of the regulator. Turn the adjusting screw fully clockwise. Close the flow control valve.
- 18) Cold stage Experiment only: Turn off the K-77 Controller. Allow 10 minutes prior to venting the SEM to allow the refrigerator to heat up to ambient temperature.
- 19) Vent the SEM specimen chamber using procedures in the SEM Users Manual (64).
- 20) Open the chamber door and disengage the mount from the control pedestal.
- 21) Remove the bolts that secure the access port flange to the specimen chamber wall.
- 22) Carefully remove the test vehicle while it is attached to the mounting post.
- 23) Dismount the test vehicle and store it in a safe place for future reference.

The preceding experimental setup and procedure can lead to the observation of electromigration damage at controlled temperatures. For in situ crystalline structure observation, the use of a TEM is required to extract information in detail.

III-4. MARK II Holder Design

The ability to conduct electromigration studies is complicated because of the physical make up of the TEM. The electrical connections to the test vehicle must be routed from air to the inner vacuum chamber of the microscope where the test vehicle is located. The vehicle itself must be secured within the TEM and connected to an external power source, yet still be able to be inserted, oriented, and easily removed. Typical samples which are analyzed with the TEM are circular, 0.0762mm in diameter and thin enough to allow an electron beam to pass through them (less than 3000 angstroms). These samples are mounted on a stage which is only 3.937mm high and recessed within the appropriate holder. The typical electromigration test vehicle, on the other hand, is an aluminum stripe on a 0.1778mm to 0.762mm thick Silicon substrate. Silicon, like glass, is extremely difficult to dice into a circle without the use of an ultrasonic dicer, therefore the TEM sample must be square. Unique, precise engineering and routing must be incorporated in order to connect this test vehicle in the vacuum chamber of the TEM to an external current supply.

The unique external to internal routing is accomplished utilizing a Jeol EM-SHH Heating Holder shown in Figure 30.

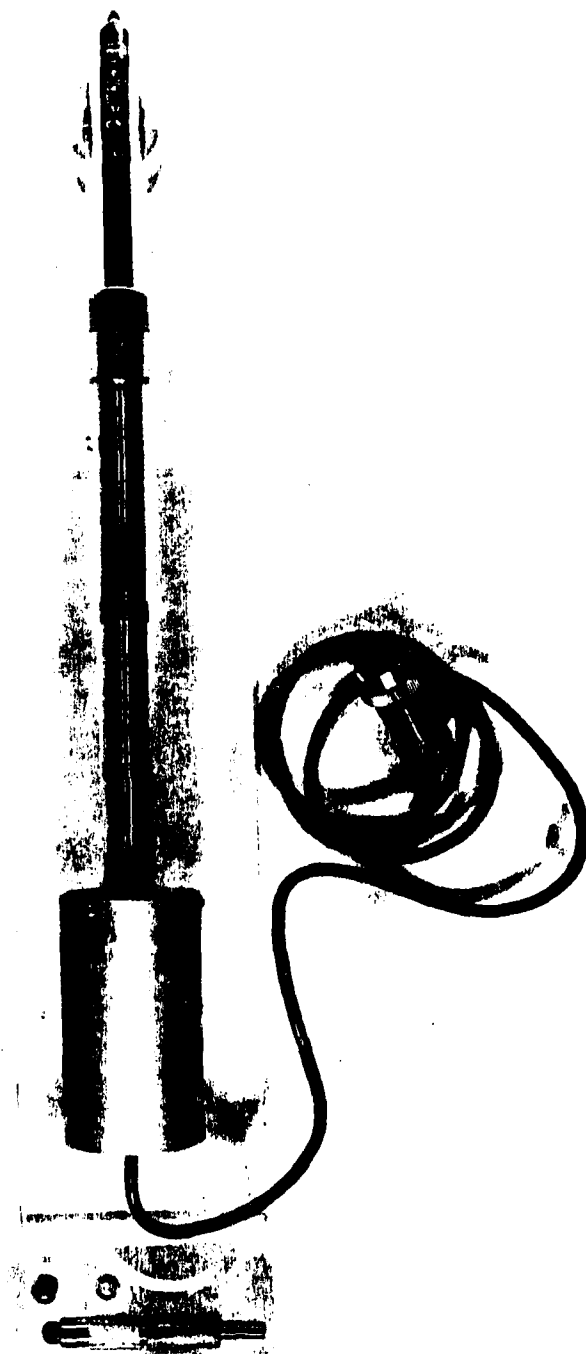


Figure 30. Jeol EM-SHH Heating Holder

The holder is specifically "designed for use in conjunction with a JEM type electron microscope side entry goniometer equipped with a Z-control in order to heat the specimen under examination." (29:1). The holder utilizes an electric furnace and a thermocouple which are connected to an external controller and monitor via four wire leads as shown in Figure 30. For this study, the holder represents an opportunity to design a new functionality for an already existent TEM interface. The ability to heat the sample is not required and the use of the thermocouple would only indicate the temperature of the cold furnace which will be a heat sink for any joule heating present on the substrate of the test vehicle resulting in inaccurate readings of test stripe joule heating. These wire leads, were utilized to provide a new and different solution to the problem of routing current to the test vehicle in situ. The four leads provide the ability to connect three different test stripes on one test vehicle. This allows up to three separate electromigration runs/observations in situ without removing the test vehicle from the TEM, thus minimizing circuit time outside of a vacuum environment. These wire leads were disconnected from the furnace and its thermocouple at the brass connection block depicted in Figure 31.

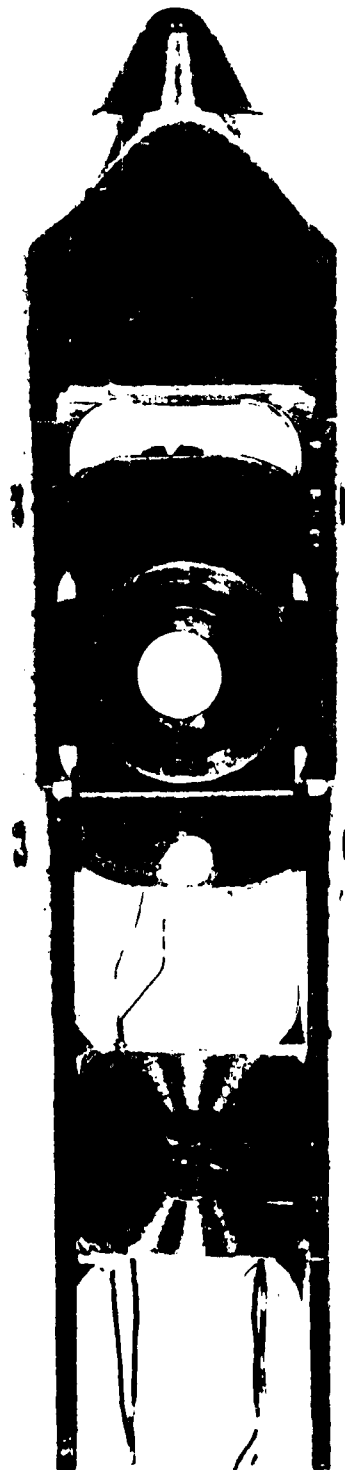
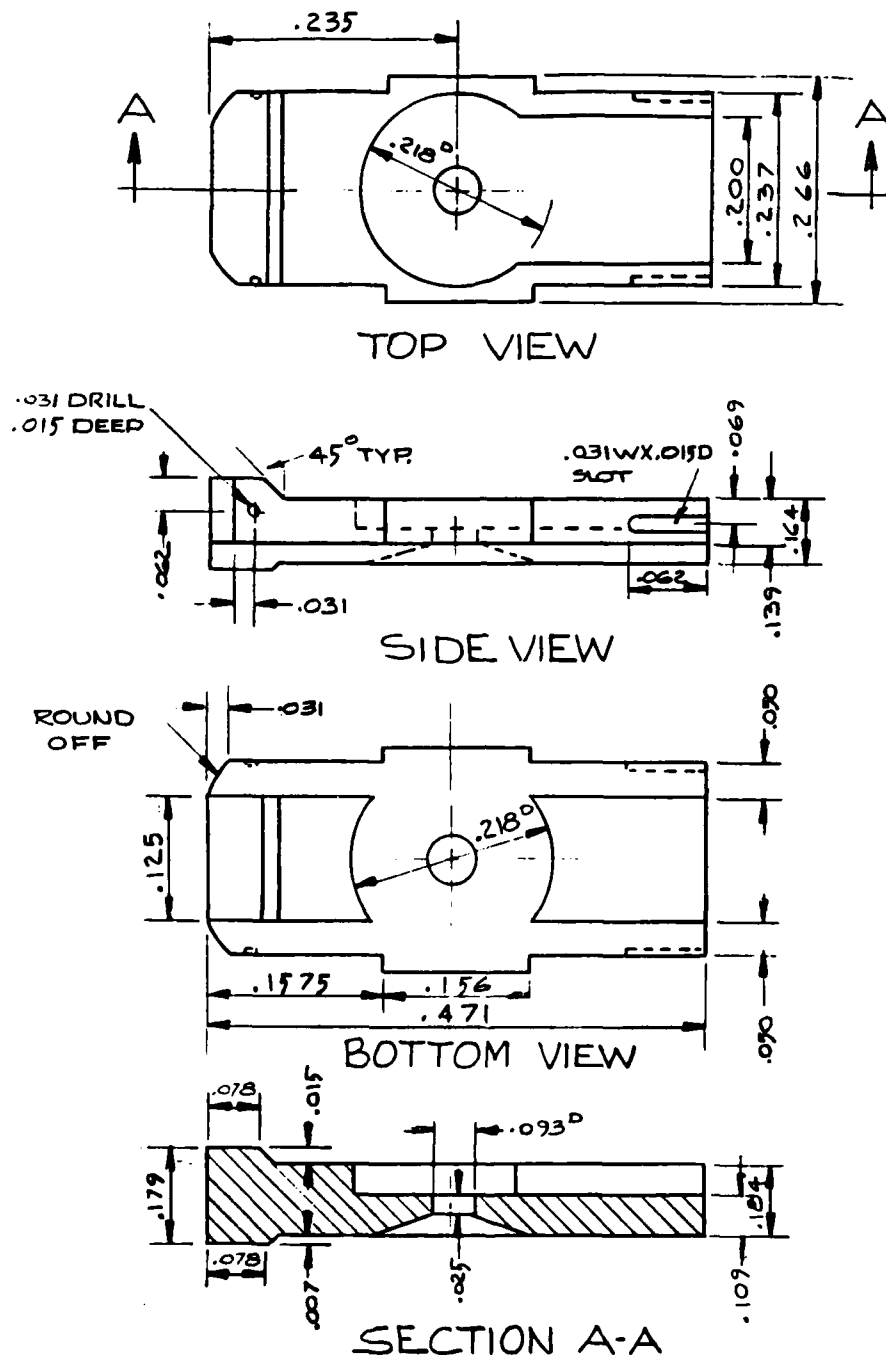


Figure 31. Jeol EM-SHH Holder Tip

New wire leads were soldered to the four wires at the brass connection block and routed up under the redesigned stage to an Alumina bonding block shown in Figure 23, which is mounted on the stage with silver paint. The wires were then soldered to the four gold stripes on the Alumina. These gold stripes serve as bonding posts for the test vehicle.

The furnace element was replaced with the newly designed stage shown in Figure 32 in order to recess the bonding block and routing wires.



ALL DIMENSIONS ARE IN INCHES
MATERIAL STAIN. STEEL

Figure 32. MARK II Holder Stage
Source: (4)

The redesigned stage was necessary due to the possible interference of the stage with the miniature door and rollers within the entry goniometer on the TEM. These rollers ride along the top and bottom surfaces of the holder as it is being inserted and removed from the goniometer. This new and different design also permits the square silicon test vehicle to be mounted on the same level with the bonding block thus facilitating bonding procedures. The prototype holder is depicted in Figure 33.

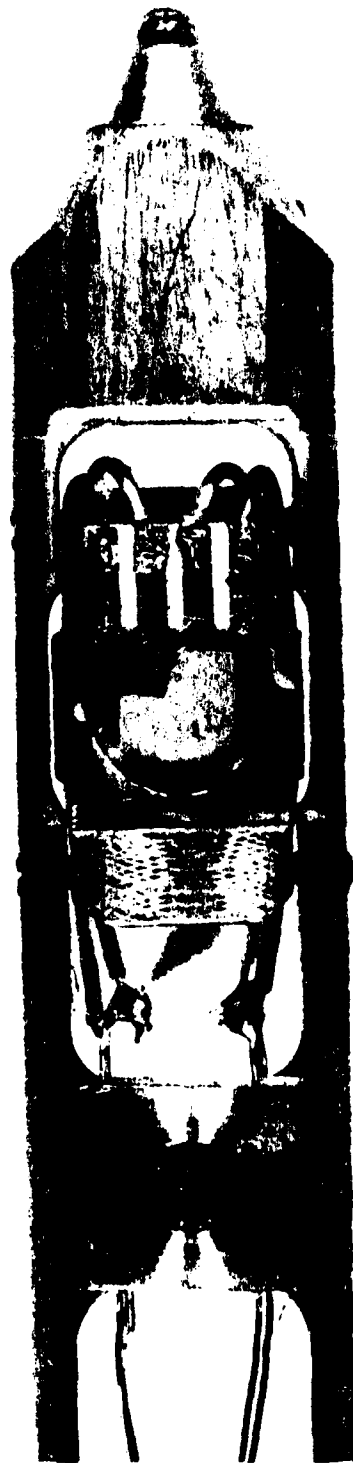


Figure 33. MARK II Holder Tip

The test vehicle is mounted in place with silver paint and then wire bonding connections are made between it and the Alumina bonding block using one mil Aluminum bonding wire. The external connector of the heating holder was replaced with color coded banana plugs to allow quick connection to the timer controller. The controller supplies current from a constant current source and is monitored by an ammeter. While current is flowing, the running time is kept by a timer circuit, which measures time by the minute (see Appendix C). When an open circuit occurs, the timer marks the elapsed time which can then be used for statistical calculations. Electromigration runs can also be accomplished outside the TEM in a specially designed transport and holding box which can contain the MARK II holder as shown in Figure 34.

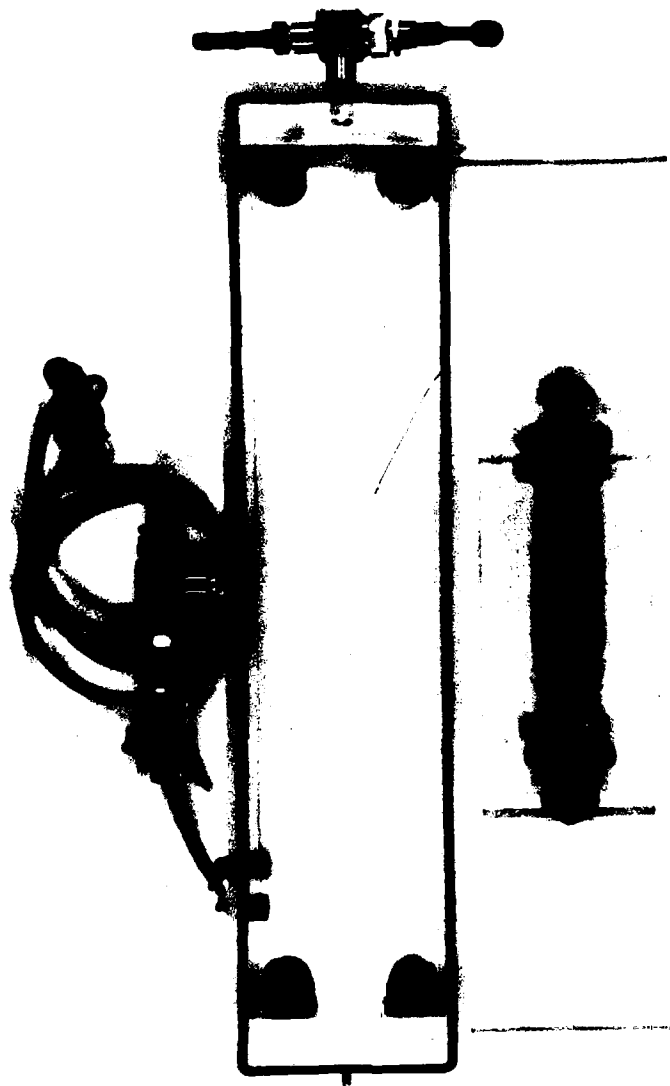


Figure 34. Transport and Holding Box

The box contains two vent valves which allow the environment within the box to be either a vacuum or Nitrogen. Feed through electrical connections provide the necessary current

for electromigration runs while maintaining the test vehicle and holder in a cleaner environment than ambient air. The vacuum box is also used to store the holder while the test vehicle is mounted on it to reduce contamination between in situ electromigration runs.

Conducting electromigration in situ provides an excellent opportunity to monitor the process through its various stages and analyzing crystalline structures without interrupting the process and reduces the possibility of outside contamination. The non-destructive redesign of the EM-SSH heating holder into the MARK II Holder facilitates this opportunity while still permitting the holder to be returned to its original configuration at a later date.

III-5. Experimental Setup and Procedure for TEM MARK II

The experimental setup and procedure of the TEM experiment is dependent on two factors; 1) Which test vehicle is being used and 2) whether the experiment is being conducted in situ or within the holding vacuum box described in section III-4.

Test vehicle selection dictates how the sample will be mounted on the holder and what bonding connections will be made to the vehicle. The test vehicles described in section III-1 vary in thickness from the 0.2286mm AFIT Test vehicle to the 0.5207mm thick MOSIS Test Vehicle. Silicon spacers, 3.3528mm square and of various thicknesses are silver painted to the underside of the thinner test vehicles to

attain, the same height on the holder as the bonding block depicted in Figure 23 thus facilitating wire bonding on the holder. Spacers for the Bridge Test Vehicle also have a hole lasered in the center which will allow the electron beam of the TEM to pass through. This setup requires the test vehicle and spacer holes be aligned and centered over the holders orifice.

Test vehicle alignment must also be considered when dicing the wafer containing the test vehicles. The die for the holder can be 3.3528mm square, however, the test vehicle must also be centered lengthwise as the side focussing of the TEM on the holder is limited to the area between the two outer edges of the innermost two gold stripes on the bonding block as shown in Figure 35.

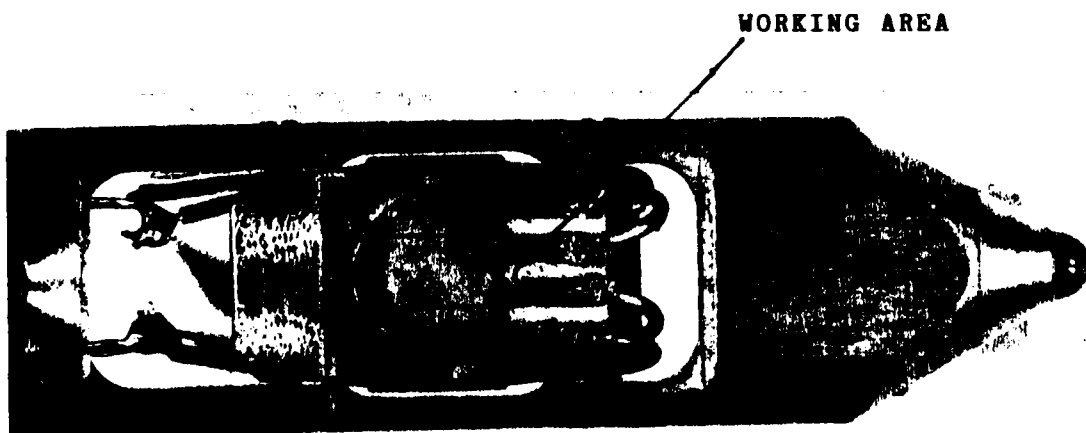


Figure 35. TEM Field of View on MARK II Holder

This restriction must be considered during test vehicle wafer dicing and wire bonding. Wire bonding is accomplished via the four gold stripes on the alumina bonding block. External holder connections are made with the four colored banana plugs which relate to the bonding block stripes as shown in Figure 36.

TEST VEHICLE

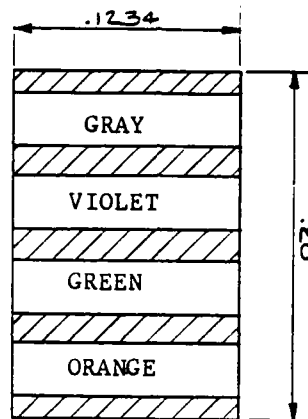


Figure 36. Banana Plug/Bonding Block Relationship

The banana plug connections are determined by the experimental run being conducted. If the holder is being used in the TEM to take pre-run or static (no current applied to the test vehicle) photographs, all four plugs are connected to case ground via a wire harness to minimize test vehicle charging.

When photographing during current stressing (dynamic) only the unused plugs are connected to the grounding wire harness.

During test sample stressing, the active plugs are connected either directly to the timer for in situ stressing, or to the connections, within the holding vacuum box which are in turn connected to the timer for external test vehicle runs.

Experimental Setup. As noted, the type of stress run being considered as well as the test vehicle in question has a direct effect of the experimental setup and procedure.

1) Set dicing saw for a 3.3528mm square die and align the test vehicle so that its thinnest dimension is centered. Set the longest dimension so the bonding pads to be utilized are as close to one edge as possible. This will facilitate later bonding.

NOTE

These alignment considerations may not be possible with the bridge test vehicle as hole centering has priority.

2) Dice test vehicle and clean in 2 minute, 80°C, ultrasonic baths of Trichloroethylene (TCE), Acetone, and finally Methyl Alcohol. Rinse in Freon.

WARNING

TCE is a known carcinogen in laboratory animals. Acetone can cause damage to the liver. Use these chemicals only under a ventilation hood.

CAUTION

Do not use ultrasonics with Bridge Test Vehicle as bridge integrity may be compromised.

- 3) Should spacers be required, clean as described above and mount to holder with silver paint. Allow to dry.
- 4) Probe test vehicle to confirm continuity.
- 5) Coat underside of test vehicle with silver paint and position test vehicle on holder stage ensuring that areas to be monitored remain within the outer edges of the inner most connection stripes as depicted in Figure 35. Butt test vehicle up against bonding block or center up hole of Bridge Test Vehicle. Allow to dry.
- 6) Accomplish bonding of test vehicle to bonding block and note connections made (recommend a microscope photograph).
- 7) Apply silver paint to perimeter surfaces of test vehicle and to vertical holder walls to reduce charging effects. Allow to dry.
- 8) Accomplish pre-stress "before" photograph mapping with all banana plugs case grounded using a wire harness which is connected to a TEM case ground.
- 9) Measure test vehicle stripe resistance across active plugs with an ohm meter.
- 10) Connect MARK II Holder to Timer.
 - a) For in situ vehicle stress:
 - 1) Connect active plugs to EM connectors on rear of timer as shown in Figure 68, Appendix C, noting polarity (red is positive, yellow is ground). Inactive plugs remain

connected to case ground wire harness.

b) For ambient vehicle stressing;

1) Connect active plugs to red (positive) and black (ground) connectors in vacuum box.

2) Connect vacuum box connector plug to EM connections on rear of timer noting polarity (ground tab side of plug to yellow)

3) Replace cover and tighten the wing nuts.

4) Either evacuate with vacuum supply valve open and purge valve closed, or apply, N_2 under positive pressure with both valves open.

11) Turn EM and VOM switches off (down) and both current setting potentiometers full counterclockwise on timer rear panel.

12) Confirm voltage source settings (+5 volts and $\leq \pm 22$ volts) with a volt meter and connect to timer as appropriate. Refer to Figure 66 and Figure 68, Appendix C. Led seven segment displays should illuminate.

CAUTION

Improper voltage or wrong polarity may damage timer circuit and/or test vehicle.

NOTE

Should current density dictate a higher voltage source than 22 volts, see Figure 70, Appendix C for alternate system hook up. Addition power supply will be required.

13) Connect Ammeter to timer noting polarity. Turn on and

set ammeter to proper scale.

Experimental Procedure. The following experimental procedure should be used.

- 1) Determine required current from target current density.
- 2) Record ambient temperature and vacuum (if utilized) surrounding test vehicle.
- 3) With system set up as described in Experimental Setup, turn on VOM switch, Ensuring ammeter is turned on and set on appropriate scale.
- 4) Turn on EM switch and within 3 seconds press reset button. Leds should indicate "9"s and then "0"s.
- 5) Verify timer operation by monitoring the green led for change in indication every six seconds. If no change is noted, turn off the EM switch and reconfirm proper experimental set up.
- 6) Set required stress current with current adjustment potentiometers while reading current on ammeter. Start with 5K ohm potentiometer (full clockwise rotation will result in approximately 30ma with a 12 volt input).
- 7) Increase current slowly to desired setting with 200 ohm potentiometer When 5k ohm potentiometer reaches full clockwise travel.

CAUTION

Current adjustment is extremely sensitive near high end. Increase current in small increments when within 50 milliamps of desired current and allow current to stabilize from the effects of joule heating on the test stripe resistance.

8) Monitor current setting for at least 10 minutes to insure stabilization.

To Remove Ammeter During Stress Run;

- a) Turn off VOM switch on timer rear panel.
- b) Turn off Ammeter
- c) Disconnect ammeter from VOM sockets on timer rear panel.

Note

Failure to accomplish steps a through c in the proper order may cause transients that can alter the correctly displayed time as it appears on the leds.

To Accomplish Current Reading During Stress Run;

- a) Connect ammeter to VOM sockets on timer rear panel.
- b) Turn on ammeter and set to appropriate scale.
- c) Turn on VOM switch on timer rear panel and take current reading.

To Interrupt/Terminate Run For Test Vehicle Photographing;

- a) Accomplish current reading as described above.
- b) Turn off EM switch.
- c) Record elapsed time in the event of power interruption during disconnection/reconnection.
- d) Set up holder in TEM.
 - 1) During in situ stress run, remove active plugs and connect them to case ground wire harness along with inactive plugs.

2) During stress runs in vacuum holding box

- A) Close vacuum/Nitrogen supply line.
- B) Open purge valve if holder is under vacuum.
- C) Remove wing nuts and cover.
- D) Disconnect active banana plugs and remove holder.
- E) Insert holder into TEM goniometer.
- F) Connect all banana plugs to case ground wire harness.

e) Photograph Test Vehicle

To Resume Stress Run

a) Set up holder

1) During in situ stress runs. Disconnect active plugs and reconnect to EM sockets on rear of timer observing proper polarity.

2) During stress runs in vacuum holding box.

- A) Disconnect all banana plugs from case ground wire harness.
- B) Remove holder from TEM goniometer and place on plexiglass stand in vacuum holding box.
- C) Reconnect active banana plugs to connections on vacuum box and timer observing proper polarity.
- D) Replace box cover and secure with wing nuts.
- E) Set purge valve;
 - 1) Open for Nitrogen.
 - 2) Closed for vacuum.

- F) Open vacuum/Nitrogen supply valve.
- G) Ensure ammeter is on and set to proper scale.
- H) Ensure VOM switch is on.
- I) Turn on EM switch and confirm operation by monitoring 6 second cycle of green Led.
- J) Adjust current as necessary.

Adherence to the above procedures should result in the acquisition of data relating to the dynamic morphology of a linestripe under current and temperature stress.

IV. Results and Discussion

This thesis research resulted in the successful design, fabrication, and testing of apparatus and associated test vehicles which permit viable research and observation of electromigration in both the SEM and TEM. The microminature refrigerator system incorporated into the SEM allows electromigration testing to be accomplished in situ while isolating a critical variable in Electromigration studies, the temperature. The modification of the Jeol heating holder and the design and testing of a test sample void of an interfering substrate yields excellent data and observation of electromigration and the study of its crystallographic composition through diffraction pattern analysis.

IV-1. SEM Technique

SEM. The SEM provided a clean vacuum for the conduct of the cold stage experiments. The vacuum was maintained at 2×10^{-6} torr with the vacuum chamber that houses the refrigerator in place. No adverse effects were noted by the integration of the refrigerator cold stage with the SEM specimen chamber.

The absence of adverse effects on the SEM vacuum environment is significant. Experimental high vacuum glues were employed in the laminar construction of the refrigerator. The glues withstood the high pressure inside of the refrigerator and maintained the seal. No leaks were noted

in the SEM specimen chamber. This result paves the way for further research on new sealants that will work at even lower pressures.

The gun electronics of the SEM showed its age as performance was marginal at best. High voltage and alignment problems kept the electron gun down throughout most of the research. For a short period of time, the gun was rendered operational, which allowed for the photograph of the test vehicle on the cold stage under powered conditions. Figure 37 shows the SEM micrograph of an NMOS test vehicle mounted on the cold stage, with power applied to a test pattern.

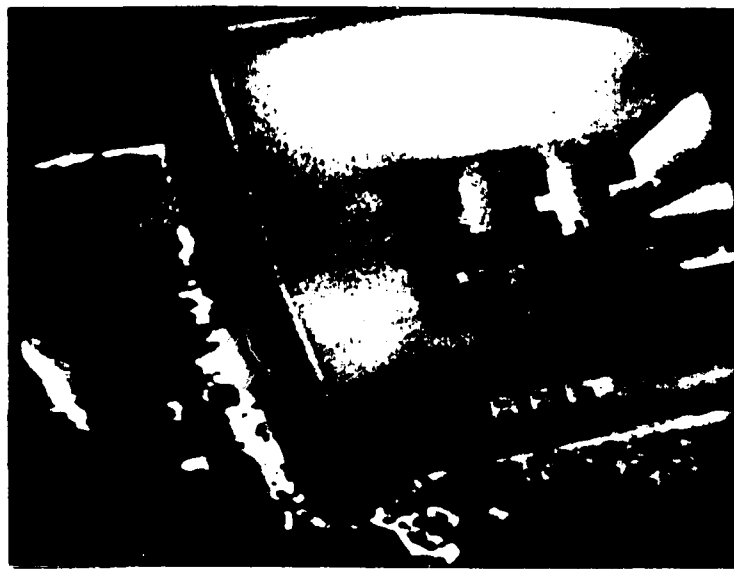


Figure 37. SEM Micrograph of In Situ Electromigration

The experimental conditions were:

Vacuum - 2×10^{-6} torr

Temperature - 223 K

Pattern - NMOS Test Vehicle, E-F Pattern

Current Density - $3.5 \times 10^6 \text{ A/cm}^2$

The SEM settings were:

Emission Current - 10 microamps

Accelerating Voltage - 20kv

Magnification - 60x

The resolution is very poor, even at this low magnification. Resolution dropped off rapidly as magnification was increased. The only picture attainable was obtained at the above SEM settings. The sample was not centered, even with full control movement of the sample stage controls. This led to a modification of the original sample mount described in chapter III, which will be described later. Although the micrograph is of poor quality, it is sufficient to demonstrate the technique of in situ viewing of electromigration on a cold stage. Better micrographs would be possible with a better SEM.

As previously mentioned, the original sample mount was modified to better position the cold stage directly under the electron beam. The modified sample mount is shown in Figure 38.

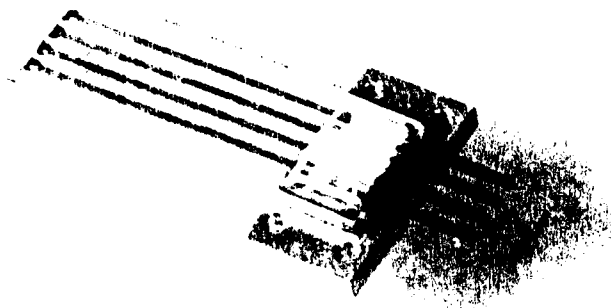
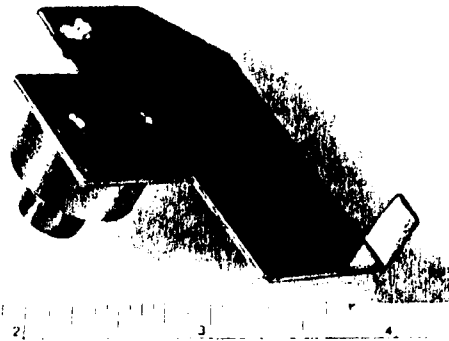
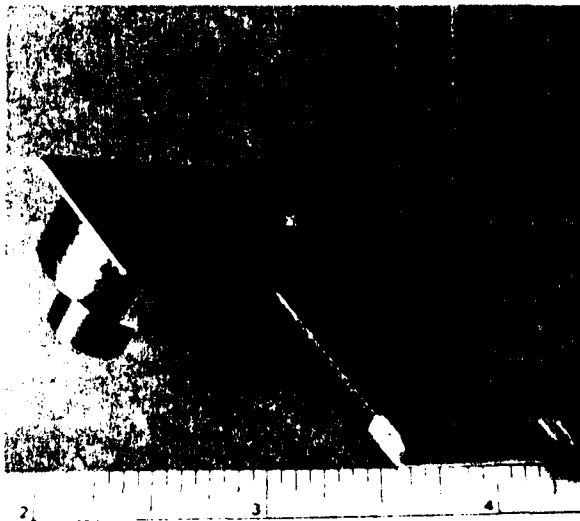


Figure 39. Quartz Refrigerator Stage

The first refrigerator experienced a failure upon initial application of Nitrogen gas pressure. The refrigerator was being leak tested with a leak detector vacuum system. Pressure increased from 5×10^{-5} torr to roughly 500 psi in less than 2 seconds, causing rupture of the cold stage and the popping out of the refrigerator cap on the end of the interface flange. Subsequent investigation of the cold stage revealed a crack in the quartz, which caused a pressure leak and eventual damage to the refrigerator.

The second refrigerator was broken during insertion into the SEM. The chamber door travel is severely limited with the refrigerator mount in place on the SEM specimen stage.



INSTITUTE OF ELECTRICAL ELECTRONICS ENGINEERS, INC

a) Original

b) Modified

Figure 38. Sample Mount

Prototype Refrigerator. Three prototype refrigerators were used in the testing phase. The quartz refrigerator stage is shown in Figure 39.

During rough out of the specimen chamber, vibrations from the roughing pump caused the specimen door to drop open. The test current input wires which curl from the Alumina bonding block underneath the cold stage and back toward the BNC connections, limited the travel of the refrigerator. The wires were stretched taut, which put a sufficient bending moment on the cold stage to break it in half. This led to a reroute of the input wires as shown in Figure 40, to preclude unnecessary torque on the cold stage.

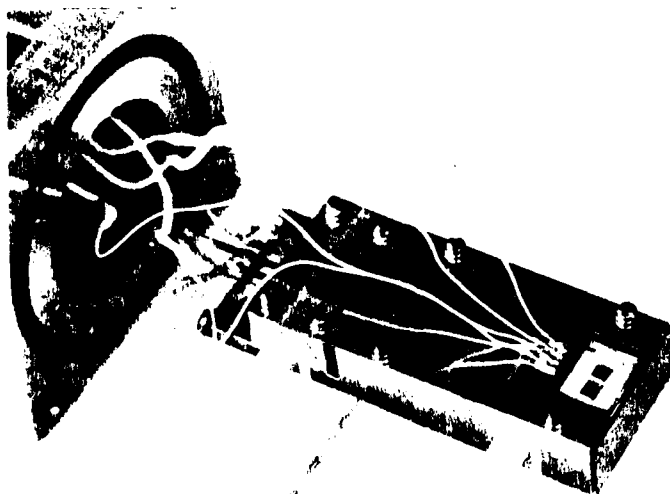
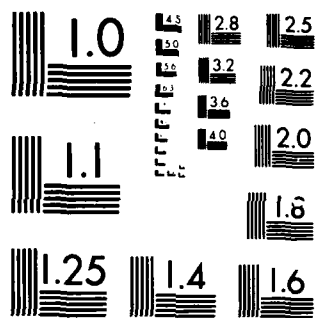


Figure 40. Modified Wiring on Cold Stage



MICROCOPY RESOLUTION TEST CHART
 NATIONAL BUREAU OF STANDARDS-1963-A

Additionally, two steel set screws were added through the floor of the refrigerator support bracket near the cold stage end. These screws are extended to contact the refrigerator during experiment preparation. They provide support for the stage to minimize the chance of accidental damage to the refrigerator. During an experimental run, the set screws must be retracted to avoid a heat leak from the support bracket to the cold stage. The extended set screws are shown in Figure 41.

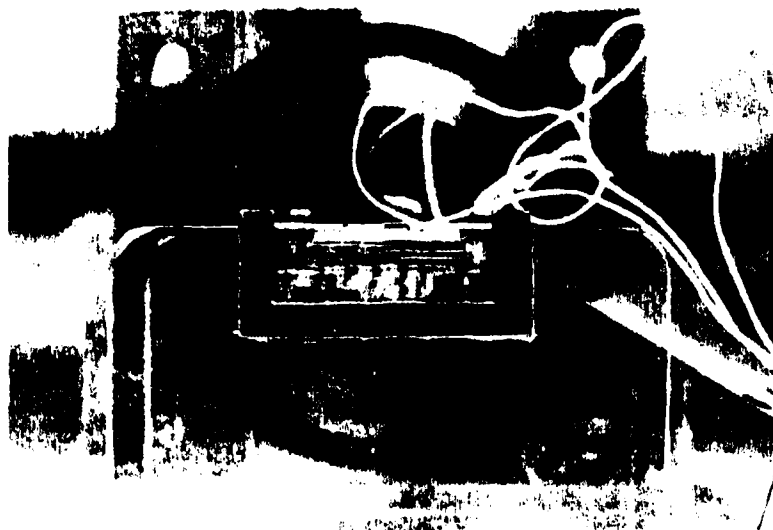


Figure 41. Refrigerator Support Set Screws

In addition to the rerouting of the input current wires, Figure 41 shows a relocation of the bonding block. Heat leaks to the cold stage (at a temperature of 76 K), at a rate of approximately 10mW/ohm for 1 mil Aluminum wires in contact with the cold stage (106). Placing the bonding block on the cold stage with four 10 mil diameter wires in contact caused a large heat leak which affected the power handling capacity of the refrigerator. In contrast to Figure 21, the original lid for the refrigerator support bracket was reinstalled. The bonding block was secured to the lid. From there, 1 mil bonding wire contacted the sample on the stage. The smaller wires, with a higher thermal resistance, reduced the heat leak through them to the cold stage.

The resistance of a linestripe can be computed using the equation

$$r = \rho l/a \quad (9)$$

where ρ , the resistivity, is a function of temperature (104:F93). By computing the resistance of the test stripe, the power dissipated across the stripe can be computed. Assuming a maximum power of 250 milliwatts, maximum current and maximum current density can be computed. For example, the MOSIS E-F pattern has a length 265 microns, and a cross sectional area of 3×10^{-6} microns. The resistivity at 300 K is 2.5×10^{-6} ohms-cm. This yields, through equation 9, a resistance of 2.2 ohms. Power is related to resistance by

the square of the current ($P = I^2R$). With a maximum power of 250 mW, a maximum current is established at 337.1 ma, which leads to a maximum current density of $1.1 \times 10^7 \text{ A/cm}^2$. This limit plotted for the operating range of the cold stage while using NMOS patterns E-F and F-I/F-C is shown in Figure 42.

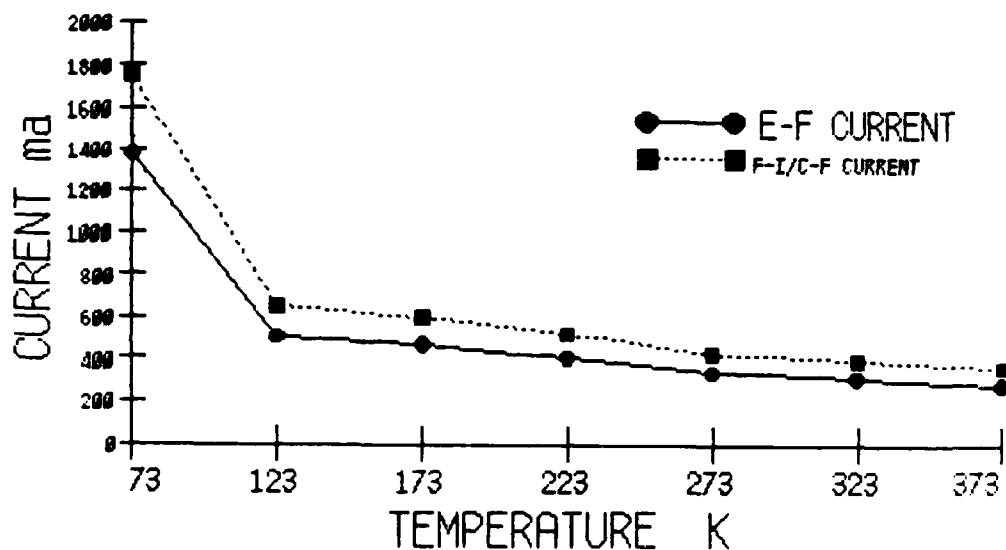


Figure 42. Operating Envelope at Maximum Power

Thermally, the refrigerator performed well. The minimum attainable temperature was a function of the individual refrigerator with the lowest observation being 86 K. The vacuum remained at 2×10^{-6} torr at all temperatures for the

cold stage. On one test at 5×10^{-5} torr, the vacuum decreased noticeably as the cold stage cooled down to below 100 K. The stage acted as a cold finger within the vacuum chamber. Our experiments show that a vacuum in the lower 10^{-6} range will minimize this effect.

A temperature instability was noted for temperatures below 223 K. The temperature deviated by as much as 10° warmer than set. At 1800 psi gas pressure, the flow rate is about 4 cubic feet per hour. The expansion reservoir under the specimen stage fills up with liquid nitrogen and overflows (106). This appears to have an effect on the temperature stability of the cold stage due to possible clogging of the heat exchanger return lines. By reducing the pressure to 1200-1500 psi, the flow rate reduces, thus preventing the reservoir from overflowing. The published temperature stability is then maintained and the visible effects of clogging (near zero flow rate and unstable temperatures), are eliminated. However, if the test sample is subject to changes in resistance over time, care must be exercised in the setting of the gas flowrate. As the stripe resistance increases, so does the heat energy that is generated. If the power generated exceeds the refrigerator capacity at some reduced flowrate, the temperature will rise unless the flowrate is increased to compensate for the additional power being generated. Most of the experimental runs were cooled using 1800 psig and then the runs were accomplished at 1200 psig.

The effects of exceeding the maximum power dissipating capacity of the refrigerator were readily apparent. With a test stripe under stress, it is reasonable to assume that joule heating will raise the temperature of the stripe. This energy is dissipated by the refrigerator cold stage. The cold stage diode will sense the temperature and maintain the preset value. By reducing the flowrate to just below the minimum required to maintain thermal equilibrium, the joule heating will exceed the refrigerator heat sink capacity. In this condition, thermal equilibrium is not maintained and the stripe temperature will rise. This temperature rise is sensed by the cold stage diode and is reflected by the K-77 controller. As soon as the flowrate is increased, the stripe temperature is rapidly reduced to the preselected value. As long as the power maximums are not exceeded by the stressed pattern, one can assume that the stripe temperature is that of the cold stage.

During an early experimental run, an electrical problem surfaced in the wiring section of the cold stage holder. The back side of the BNC connectors are not insulated, providing an opportunity for the steel gas supply tubes to contact the connectors. The proper test current could not be attained because the current was grounded into the SEM. The problem was eliminated by sheathing the gas supply tubes with a thin teflon tube. This prevented further short circuits from occurring.

Nitrogen Gas Supply. The Nitrogen gas supply provided 1800 psig gas to the refrigerator for cooling. No special handling was required for the 6000 psig tank. The regulator was easy to handle, making precise pressure control effortless. A tank containing 494 cubic feet of gas will sustain 50 to 110 hours of operation, depending on both the operating temperature and the gas flow rate used.

Constant Current Density Failure Data. The study of electromigration as a function of temperature while holding the current density constant has been accomplished before at densities greater than 10^6 A/cm^2 and at temperatures lower than 373 K (12). This data can be reduced to yield Arrhenius plots, showing a time to failure vs temperature (65-67; 73). Results of the constant current density experiments are shown in Table I.

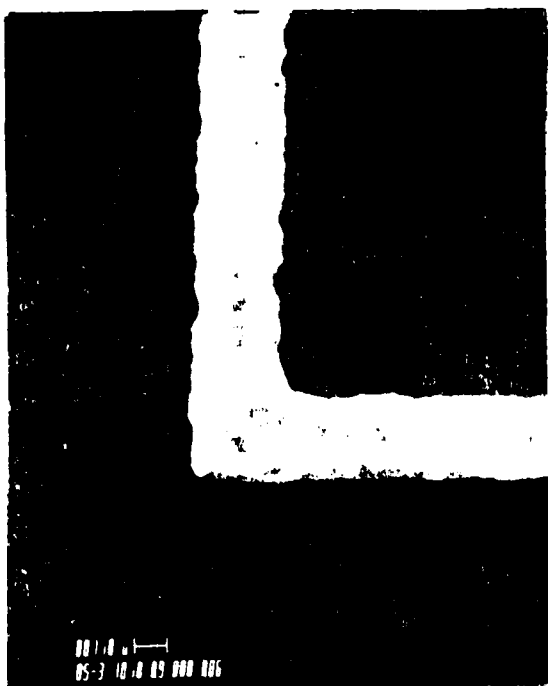
Table I.

Constant Current Density vs Temperature

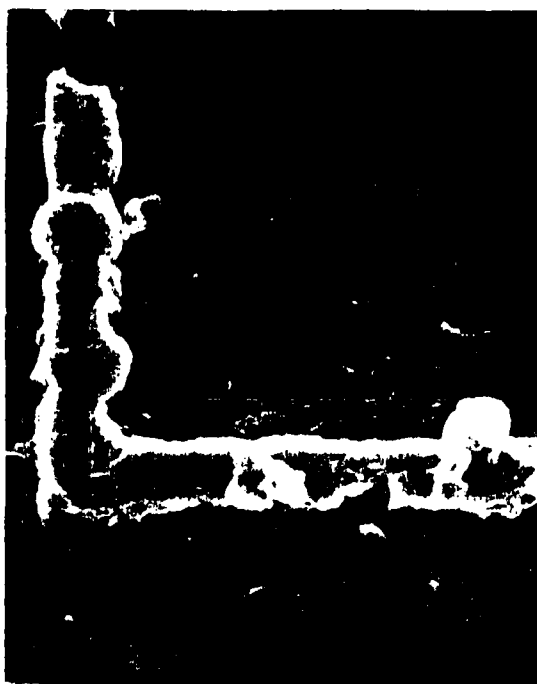
CURRENT DENSITY $4.0\text{E}+6$ A/sqcm

TEST	TEMPERATURE	TIME	
1	98 K	600 minutes	(stopped)
2	123 K	600 minutes	(stopped)
3	173 K	600 minutes	(stopped)
4	223 K	600 minutes	(stopped)
5	248 K	600 minutes	(stopped)
6	273 K	600 minutes	(stopped)
7	298 K	600 minutes	(stopped)
8	323 K	113 minutes	(failure)
9	348 K	34 minutes	(failure)

The pattern used was the NMOS F-I and C-F pattern with a thickness of 12000 angstroms with an average width of 2.5 microns (see Figure 13). Current density was set at $4 \times 10^6 \text{ A/cm}^2$. Temperature ranged from 98 K to 348 K, which remains within the operating limits of the refrigerator. In the interest of time, the test was terminated if failure was not observed by 10 hours. Failure is defined as an open circuit detectable by zero input current. The extent of electromigration damage as a function of temperature is illustrated in Figure 43, where before and after pictures are provided for various temperatures.



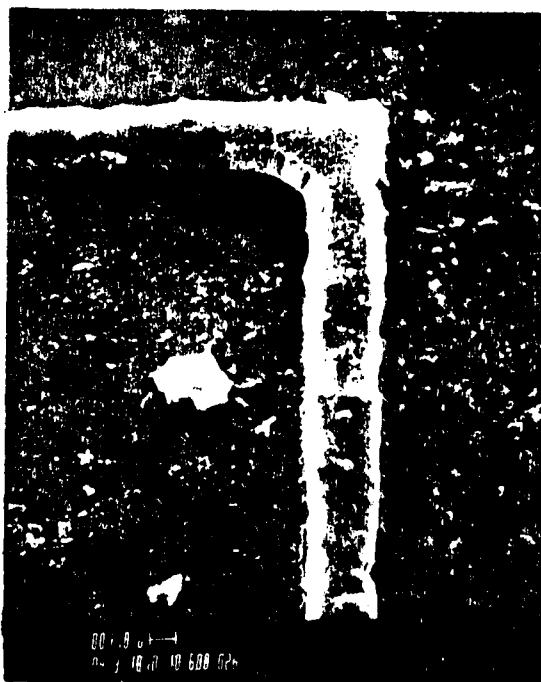
a) Before



b) 34 min at 348 K

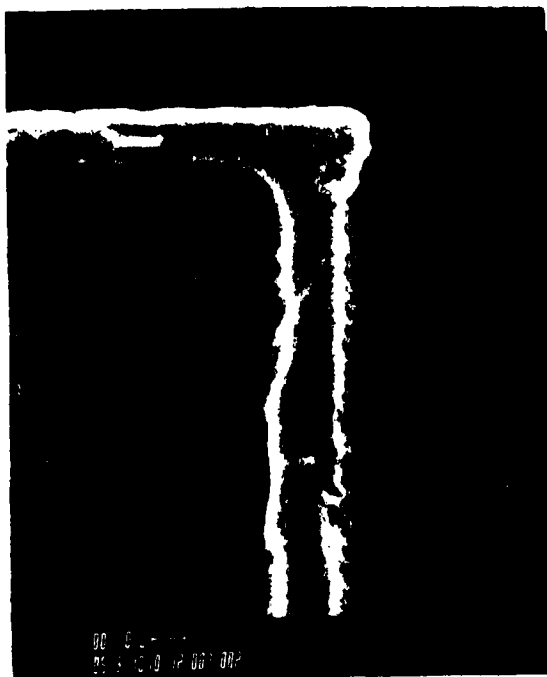


c) Before

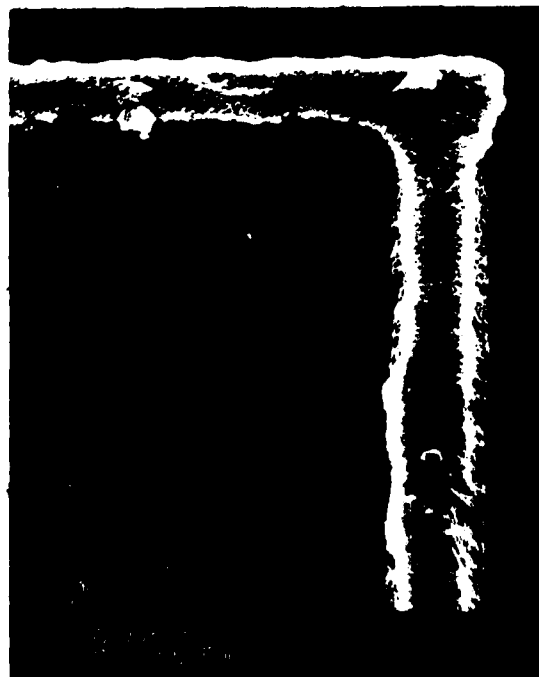


d) 600 min at 273 K

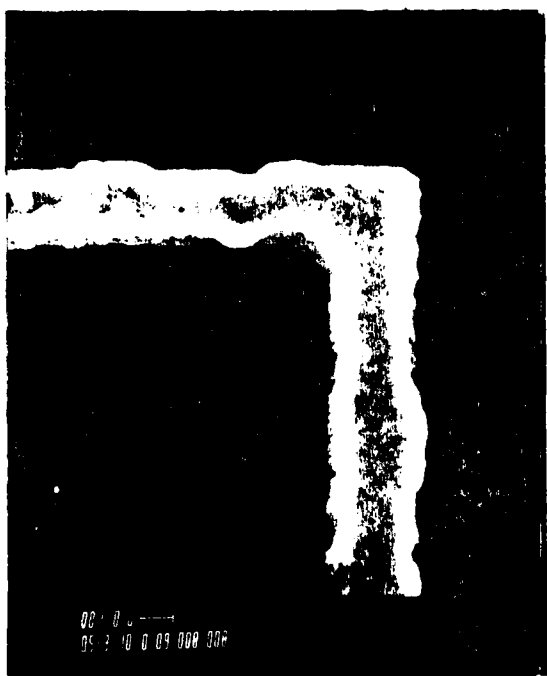
Figure 43. Constant Current Density ($4 \times 10^6 \text{ A/cm}^2$) vs Temperature



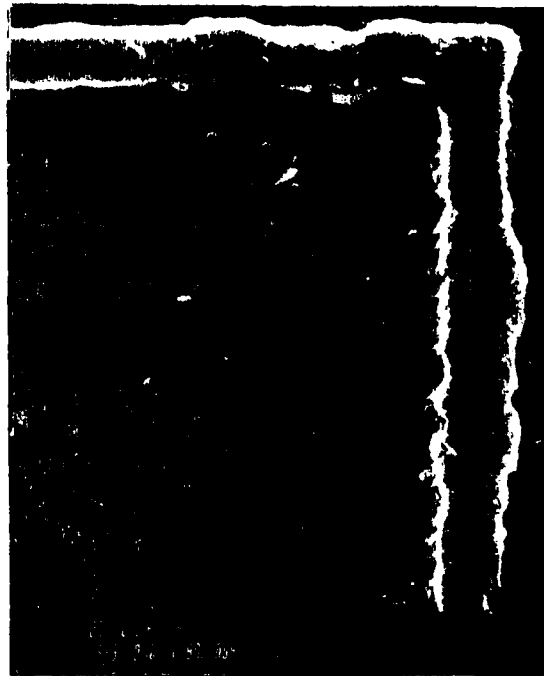
e) Before



f) 600 min at 248 K



g) Before



h) 600 min at 123 K

Figure 43 (continued). Constant Current Density
($4 \times 10^6 \text{ A/cm}^2$) vs Temperature

Through the diffusion coefficient equation,

$$D = D_0 \exp(-Q/kT) \quad (10)$$

the Einstein relationship shows a decrease in mobility as temperature decreases as shown in equation 11 (62:324).

$$u = eZ^*[D_0 \exp(-Q/kT)]/kT \quad (11)$$

The mobility of the species has a direct effect on the atomic flux. The atomic flux will decrease with decreasing mobility, and thus, decreasing temperature, as shown in equation 4 (26:1410).

$$J_a = u\bar{F} \quad (12)$$

Stress increases as a function of temperature, causing a stripe to sustain more extensive damage with higher temperature.

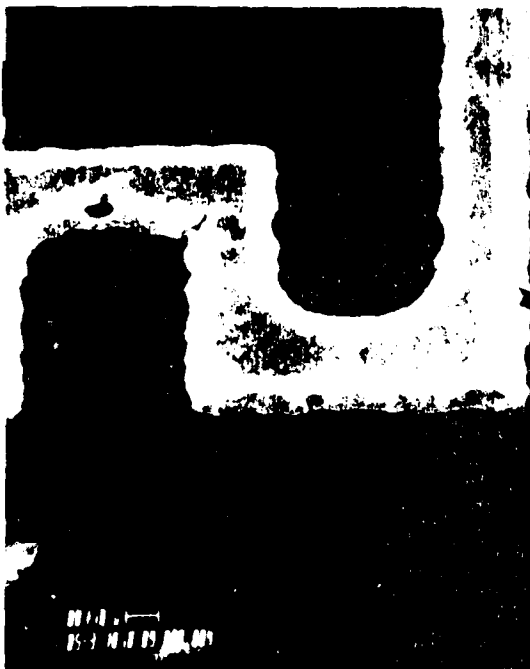
Constant Temperature Failure Data. In order to examine the effects of increasing current density at a constant temperature, experiments were run as recommended by Braun (12). An increase in current density allows for experiments to be run at cryogenic temperatures without having to wait an excessive time to see results. Constant temperature failure data is presented in Table II.

Table II.

Constant Temperature vs Current Density

TEMPERATURE 223K			
TEST	DENSITY	TIME	
1	4.5E+06 A/sqcm	600 minutes	(stopped)
2	5.0E+06 A/sqcm	326 minutes	(failure)
3	5.5E+06 A/sqcm	105 minutes	(failure)
4	6.0E+06 A/sqcm	15 minutes	(failure)

The pattern used is the MOSIS NMOS stripe E-F with a thickness of 1 micron a width of 2.5 microns. Current density ranged from $4.5 \times 10^6 \text{ A/cm}^2$ to $6 \times 10^6 \text{ A/cm}^2$. Temperature was maintained at a constant 223 K. As in the constant current density tests, run time was limited to a maximum of 10 hours with failure defined by open circuit detected by zero input current. Figure 44 shows before and after SEM micrographs of test patterns that experienced various current stress at constant temperature.



a) Before



b) 600 min at $4.5 \times 10^6 \text{ A/cm}^2$

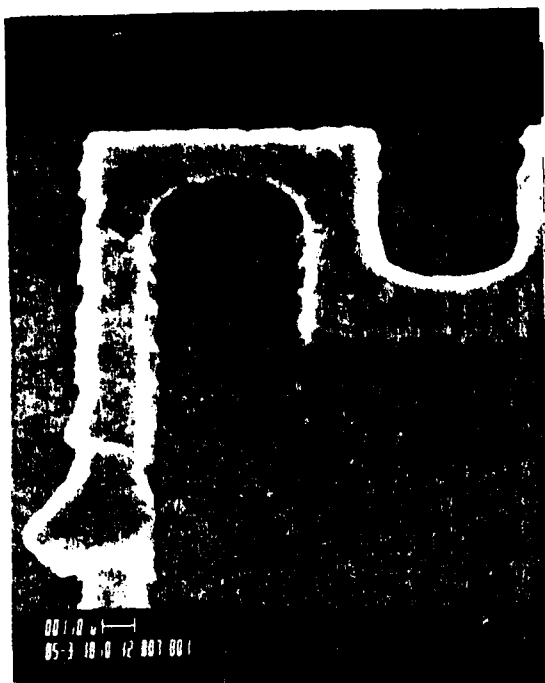


c) Before

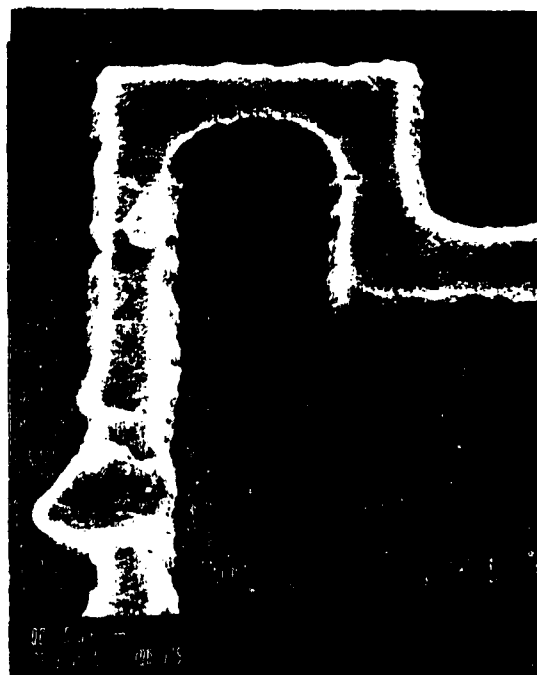


d) 526 min at $5 \times 10^6 \text{ A/cm}^2$

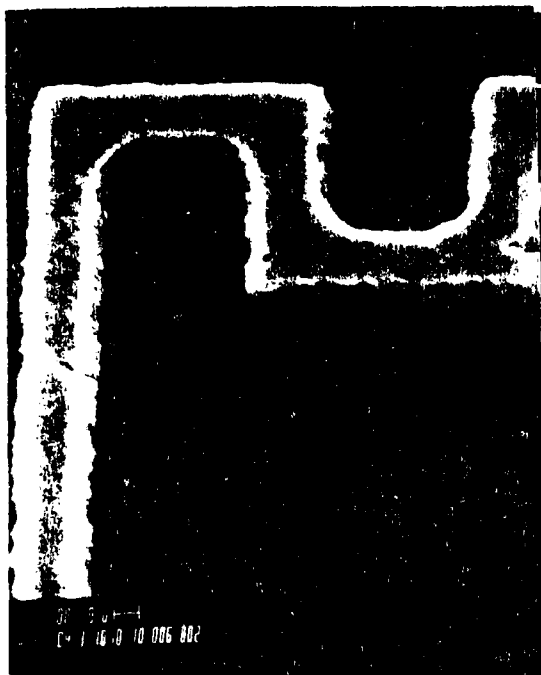
Figure 46. Constant Temperature (223 K) vs Current Density



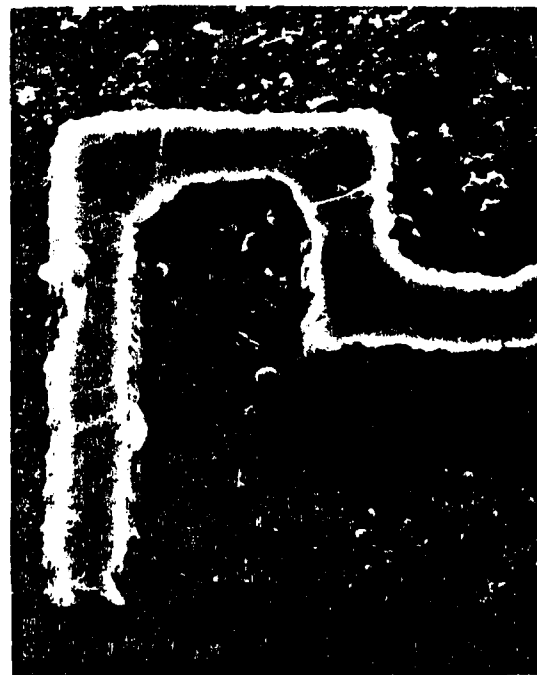
e) Before



f) 105 min at $5.5 \times 10^6 \text{ A/cm}^2$



g) Before



h) 15 min at $6 \times 10^6 \text{ A/cm}^2$

Figure 44 (continued). Constant Temperature (223 K) vs Current Density

Figure 44 illustrates the effect of increasing the current density at constant temperature. Electromigration damage is observable and evident at high current densities and low temperatures as predicted by D'Heurle (26:1412). Equation 4 can be rewritten as

$$J_a = (ND/kT)Z^*epJ \quad (13)$$

where N is the concentration of ions, D is the diffusion coefficient, Z^*e is the effective charge of the ion, p is the resistivity of the conductor and J is the current density (12:485). Equation 3 predicts that the magnitude of the atomic flux will increase with increasing current density, assuming that all other variables are held constant. As seen in chapter II, a non-zero atomic flux divergence is required to sustain electromigration damage.

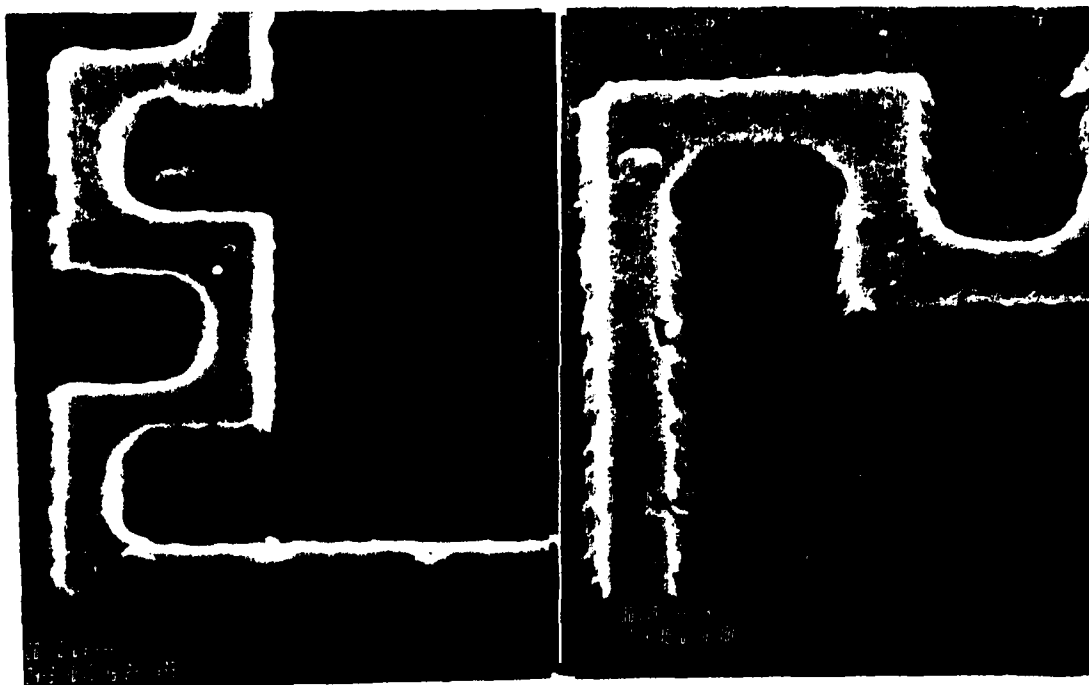
Additional Data Points. Initial experimental runs yielded data points at various points listed in Table III.

Table III.

Additional Data Points

TEST	CIRCUIT	TEMPERATURE	DENSITY	TIME
1	E-F	175 K	3.5E+06 A/sqcm	1500 minutes (stopped)
2	F-I	98 K	6.0E+06 A/sqcm	600 minutes (stopped)
3	E-F	92 K	8.0E+06 A/sqcm	3 minutes (failure)

Some early runs produced interesting results. One test run at 135 K shows little or no electromigration damage after 26 hours at a current density of $3 \times 10^6 \text{ A/cm}^2$. Figure 45 shows the before and after condition of the test stripe.



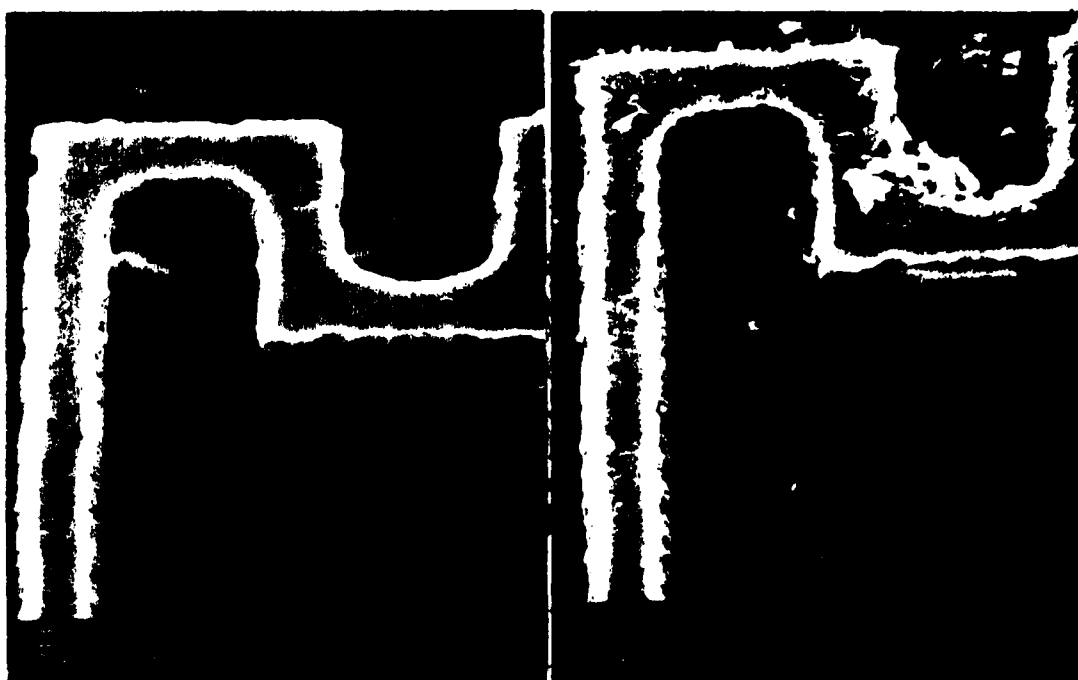
a) Before

b) 1560 min at $3 \times 10^6 \text{ A/cm}^2$

Figure 45. Test Stripe at 135 K.

Another run at an even lower temperature, 100 K, produced different results. Under a stress of $8 \times 10^6 \text{ A/cm}^2$, this cir-

cuit lasted only three minutes. Electromigration damage is seen to occur at cryogenic temperatures, as depicted in Figure 46, provided the current density is high enough.



a) Before

b) 3 min at $8 \times 10^6 \text{ A/cm}^2$

Figure 46. Test Stripe at 100 K

Gradient T and Structure. Equation 5 presented the derivative of the atomic concentration at any point as the gradient of the atomic flux, rewritten here (18:8).

$$dc/dt = -\text{del} \cdot (\bar{J}_a) \quad (14)$$

Assuming that J_a is a function of both composition and temperature, then the one dimension case can be written as

$$dc_x/dt = -\{(dJ_a/ds)(ds/dx) + (dJ_a/dt)(dt/dx)\} \quad (15)$$

which is equation 5 rewritten (18:8). Equation 7 shows that for a non zero flux divergence to exist, either a structural irregularity or a temperature gradient must exist. Huntington and others observed that for properly heat sunk stripes, voids and hillocks formed at random, their position being determined by structural changes, such as grain boundaries (43:276; 33:52). The lack of a temperature gradient from pad to pad drives the $(dJ_a/dt)(dt/dx)$ term of equation 7 to zero, leaving the structural term. The randomness of the void and hillock formations for both Figures 45 and 46 tends to confirm the lack of a significant temperature gradient. Even without the temperature gradient, the structural term contributes to a non-zero flux divergence. With a polycrystalline linestripe, a flux divergence should occur at any temperature when J_a is non-zero. The time required to failure will be a function of the temperature and the current density. Further data collection and statistical analysis should determine the relative magnitude of these two contributions toward a failure time while an investigation of the stripe morphology will lead toward a better understanding of flux divergence.

IV-2. TEM Technique

Design of The MARK II Holder The design and fabrication of the MARK II Holder presented some initial problems which were eventually solved. The initial attempt consisted of mounting the test vehicle and Gold on Alumina bonding block on the existing furnace stage as shown in Figure 47.

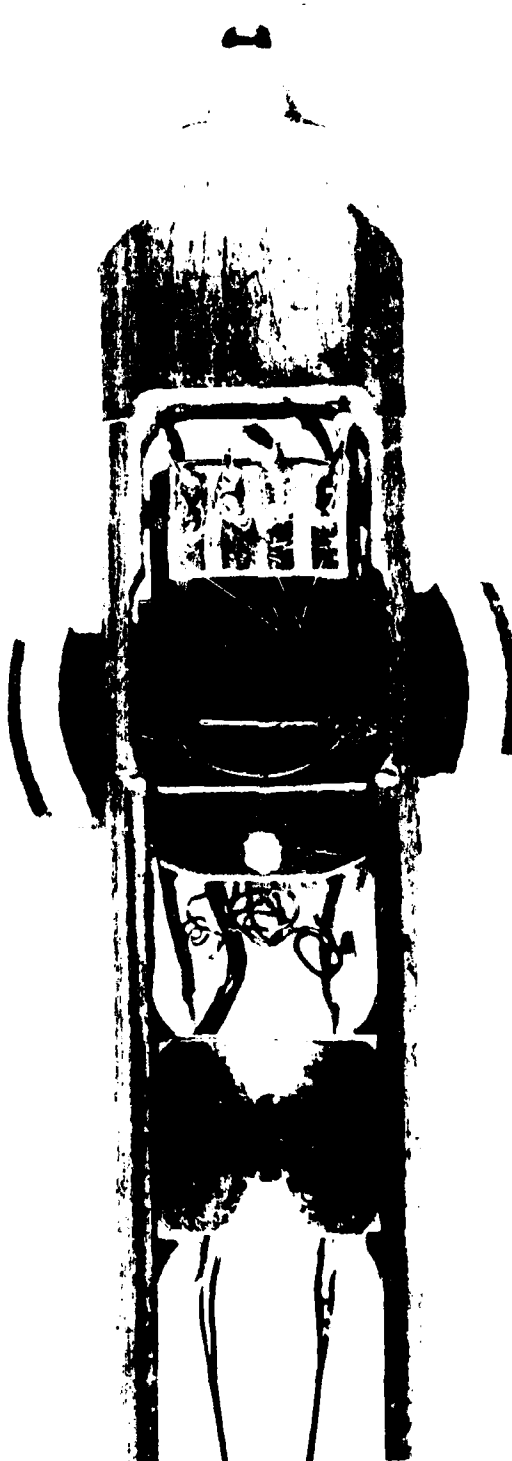


Figure 47. First Attempt at Holder Design

The wires were disconnected from the furnace and the temperature sensing diode and rerouted from the holder's connecting block to the Alumina bonding block on top of the furnace. Initial insertion into the TEM resulted in the removal of both the sample and bonding block from atop the furnace stage during extraction from the TEM. Internal examination of the specimen port on the TEM revealed the existence of an access door which rides on rollers across the upper and lower surfaces of the heating holder furnace stage. The test vehicle, routing wires, and bonding block all had to be recessed beneath the upper and lower surfaces of the furnace stage in order to allow proper insertion and removal of the test vehicle. This was accomplished through a new and unique redesign of the entire stage area of the heating holder as shown in Figure 32, page III-22. A MOSIS NMOS test vehicle was utilized for the initial testing of the redesigned holder which is shown mounted in Figure 48.



Figure 48. MOSIS Test Vehicle Mounted on MARK II Holder

Wire bonding the test stripe to the Alumina bonding block required fabrication of a plexiglass holder designed to secure the holder and support its weight while being bonded. Bonding was then easily accomplished after some unique settings were made on the bonding machine for depth and draw of the bonding wire. The holder was operationally tested by inserting it into the TEM to take before run test stripe pictures in the SEM mode of the TEM. Some electron charging was noted which required the fabrication of a grounding harness which connects the four banana plugs of the MARK II to case ground of the TEM. Additionally, it was found that silver painting all surfaces of the test vehicle not associated with the stripe under test greatly reduced the charging interference. During the photographing of the test vehicle, it was noted that the field of vision of the TEM in higher magnifications is restricted laterally to the area between the outer edges of the two inside gold stripes on the Alumina bonding block (see Figure 35). This first NMOS test vehicle was mounted half outside this area and thus only half the stripe was able to be photographed above 500x. Subsequent test vehicles were placed within the high magnification field of vision. After the test stripe was mapped in the SEM mode, the holder was removed and placed in the vacuum holding box shown in Figure 34 to accomplish the electromigration run verification.

The experimental conditions were:

Experiment #1 Initial Holder Acceptability Test

Test vehicle used - MOSIS NMOS pattern Q-R (see Figure 13).

Line Width - 3 micron

Line Thickness - 1.38 micron (Dektak measurement)

Cross sectional area (Determined by SEM) - $6.9 \times 10^{-9} \text{ cm}^2$

Current Density - $3 \times 10^6 \text{ A/cm}^2$

Required Current - 93.15 ma

Test Situation - Conducted in vacuum Holding Box

Ambient Temperature - 21.11°C

Vacuum (box) - 1.5×10^{-3} torr

Resistance - 6.0 ohms

Current Density - $3.5 \times 10^6 \text{ A/cm}^2$

Applied Current - 93.8 amps

The TEM settings were:

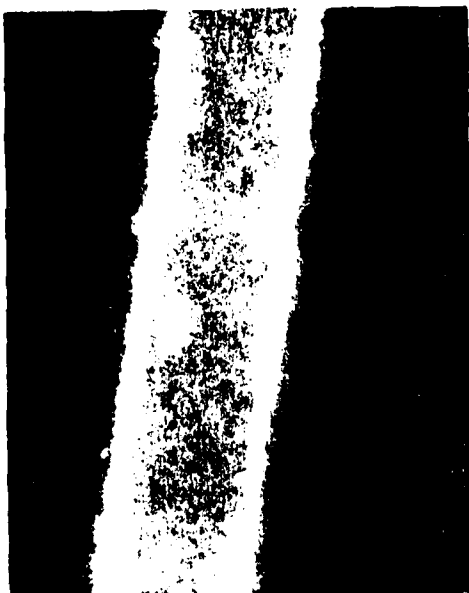
Vacuum - 6.0×10^{-8} torr

Emission Current - 95-100 microamps

Accelerating Voltage - 100 kv

The initial evacuation of the vacuum box holder indicated a need to add a spacer block to the lid to prevent the sides from caving in under low pressure. The electromigration run was interrupted several times for progress observation and photograph mapping of the stripe.

The electromigration test run terminated due to open circuit failure after 76059 minutes. Figure 49 shows SEM mode photographs taken in the TEM of a section of the stripe before, during and after the test run.



a) Before Stress, 5000X



b) after 12688 Minutes, 10000X



c) After 36644 Minutes, 10000X



d) Failure, 10000x

Figure 49. Electromigration Effects on Test Vehicle

In all cases above, the electron flow is up. As shown, the hillocks have formed "down stream" of the voids. This is in agreement with published information on electromigration (8:142; 25:234, 26:1413). With this confirmation that the MARK II holder can be used for electromigration studies, the Bridge Test Vehicle was designed and fabricated for TEM related studies.

Aluminum Bridge Test Vehicle. The design and fabrication of a test vehicle in which the underlying Silicon substrate is completely removed from the Aluminum stripe proved to be a formidable task. Initial attempts were made to both mechanical drill and laser drill holes in the Silicon wafers then back fill with photoresist or mounting wax. A diamond tipped dentist burr was used to successfully drill holes in the wafer. This proved unacceptable in that the perimeter of the hole was cracked and chipped. Additionally, the minimum size hole realizable was ≥ 300 microns. The drilled holes could not be arrayed on the wafer to any extent because the wafer would not stand up to the stress of multiple drilling. The lasered holes on the other hand were successfully arrayed to a 3x3 pattern on a 3.81cm wafer. These holes, however, were also very rough around the perimeter and although smaller than the drilled holes, they were still over 250 microns in diameter. An Aluminum linestripe 2000 angstroms thick and less than 10 microns wide would have difficulty supporting itself across a void that size.

The process which proved most promising with respect to the hole size and array capability was the KOH directed etch technique. A major portion of the thesis research period was devoted to developing this technique of etching an array of holes from the back side of <110> wafers. Experimentation included determination of the proper oxide thickness to protect and mask the 13 mil wafer during etching, and determining the required etch time versus temperature to use. An Array of holes, masked with the CTV Source/Drain mask etched in a trapezoidal shape, measuring only 9 microns wide. Subsequent attempts at filling the holes with photoresist or mounting wax proved unacceptable. The photoresist repeatedly shrank into the hole during bakeout while the wax went into partial melt during Aluminum evaporation due to radiated heat in the metal evaporation system. The Picolastic D100 mounting wax, however, was crucial in the successful solution to the Bridge Test Vehicle design problem when it was used to form an etchant mask.

The Bridge Test Vehicle was successfully designed using the Bell Labs test vehicle, and manually painting on a wax mask on the back side of the pattern prior to back side etching of the wafer. Details of this technique are presented in Appendix A. This technique results in a hole etched thru the Silicon, as shown in Figure 19, section III, where 1 or more stripes are either freely suspended or supported by the underlying oxide window, depending on the amount of etching time provided. The following observations

were obtained from inspection of several test vehicles during etching.

Table IV.

Effects of Etching Time of Bridge Test Vehicle

Wafer: 9 mil <111> Boron Doped 1.5>"

Oxide: 3000 angstroms Wet Thermally Grown

<u>Etching Time (Minutes)</u>	<u>Results</u>
25	No light visible from underside
30	Light Barely Visible from underside
32	Patterns exposed with oxide windows
34	Oxide etched away
36	Aluminum Stripes Destroyed

The light source was directed upward from beneath the microscope through the sapphire disk on which the test vehicle was mounted. The Picolastic D100 wax is clear and observations were made at 400x. The ideal case is that in which the oxide is thinned as much as possible without being completely removed. Figure 50 shows the test stripe of a BTV taken in the STEM mode of the TEM.

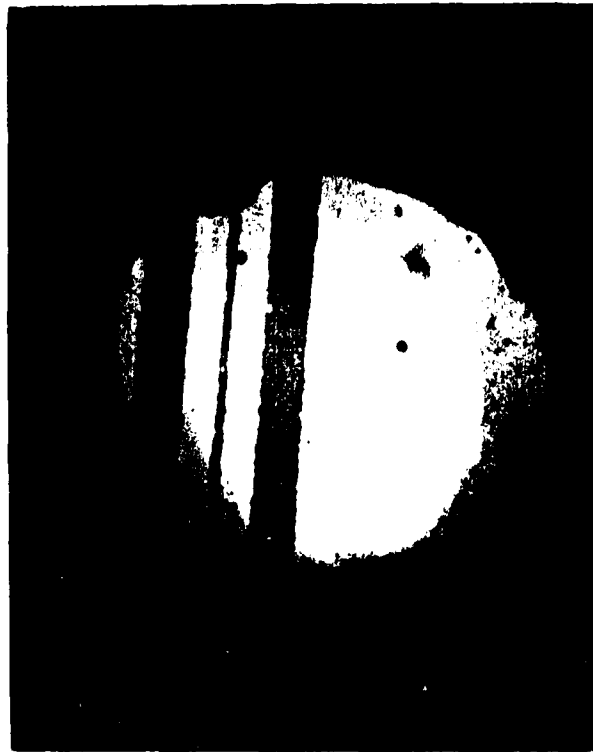


Figure 50. STEM Photograph of Bridge Test Vehicle, 800x

The thinning oxide is clearly visible toward the center of the etched out hole. The thinner the oxide, the less interference there will be in the diffraction patterns of the test stripe. A diffraction pattern of the oxide window is shown in Figure 51.



a) STEM of SiO₂ Window
8300x

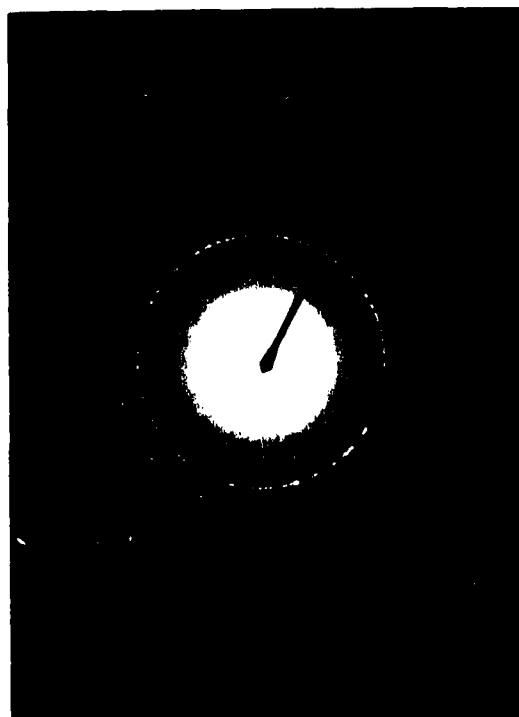
b) SiO₂ Diffraction Pattern

Figure 51. Diffraction Pattern of Underlying SiO₂

This pattern must be considered when analyzing the diffraction patterns obtained during the electromigration stress testing in the TEM.

Electromigration Diffraction Patterns The main objective of designing TEM apparatus and test vehicles with which to conduct electromigration in situ is to be able to analyze grain structure and crystallographic changes which may occur as a result of electromigration. Grain structure

analysis can be obtained with photographs of the Bridge Test Vehicle taken in the STEM mode as shown in Figure 50 above. Crystallographic analysis is obtained from bright field illumination and diffraction patterns taken in the TEM mode as shown above in Figure 51 and in Figure 52.



a) Bright Field STEM of Al Stripe
8300x

b) Diffraction Pattern

Figure 52. Diffraction Pattern of Aluminum Stripe

Figures 51 and 52 are the prestress pictures of the Bridge Test Vehicle which was mounted and bonded in the MARK II holder as shown in Figure 53.

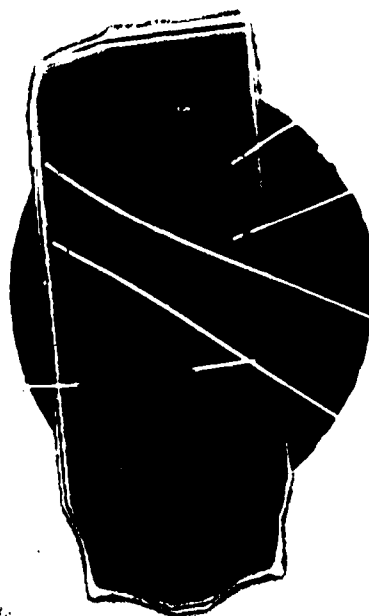
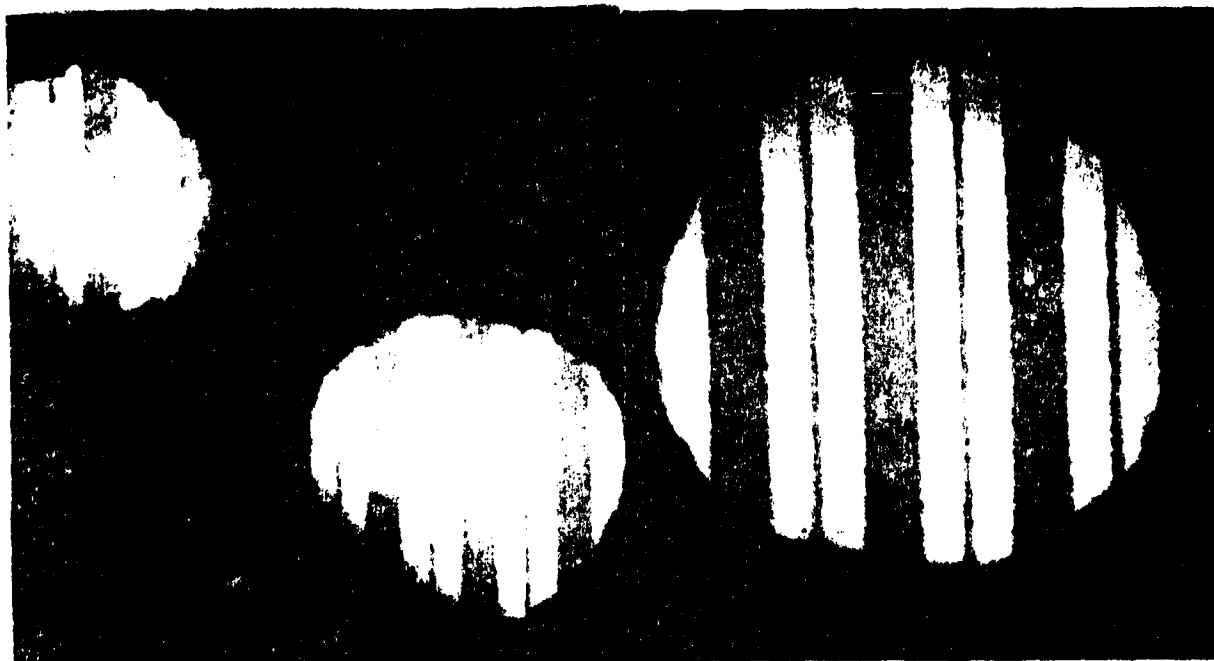


Figure 53. SEM of BTV in Place on MARK II Holder, 20x

The etched holes in the BTV are clearly visible and are depicted at increased magnifications in Figure 54.



a) Oxide Window Holes
in BTv, 500x

b) Larger Hole, 800x

Figure 54. Bright Field STEM of Etched Holes in BTv

The center stripe across the thinnest region of the oxide over the larger of the two holes was photo-mapped in the STEM mode and is depicted as a mosaic reconstruction of the stripe in Figure 55.

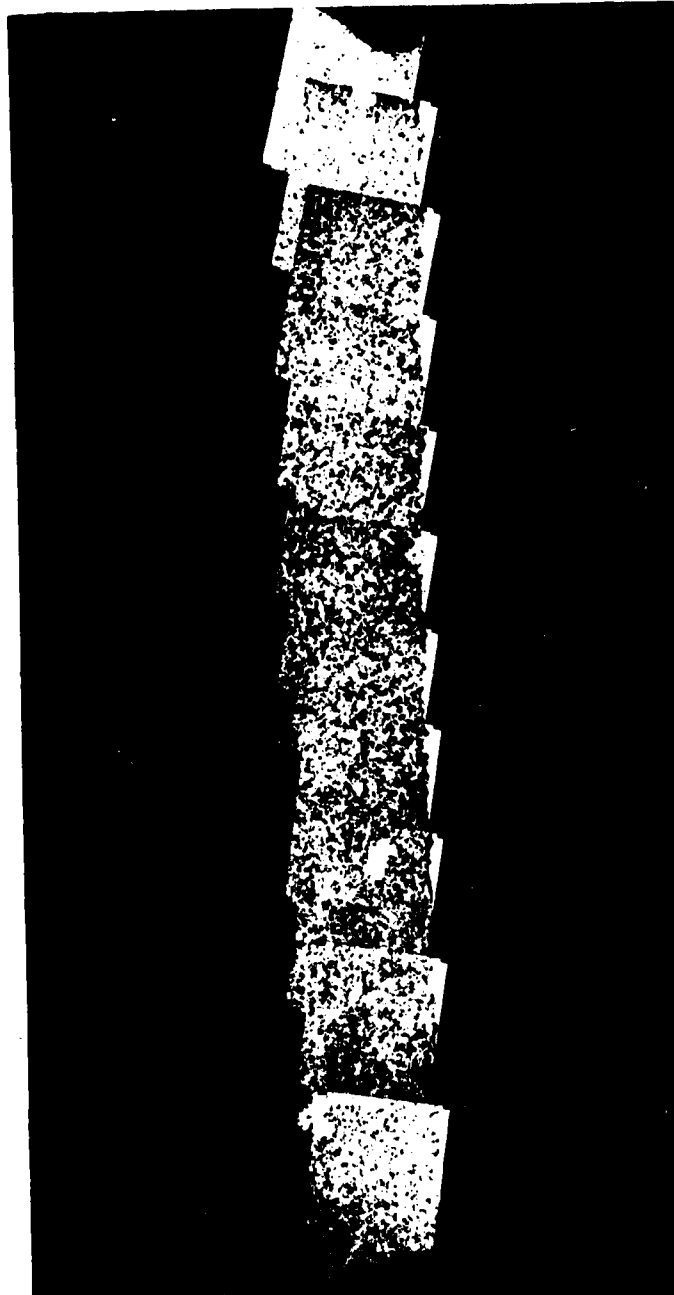


Figure 55. Mosaic Mapping of BTV Stripe

The experimental conditions were:

Equipment #2 - In Situ Stress Run For Crystallographic Analysis.

Test Vehicle Used - Aluminum Bridge Test Vehicle.

Line Width - 9.24 microns

Line Thickness - 1900 Angstroms (Dektak measurement)

Cross Sectional Area (Determined by SEM) - $1.76 \times 10^{-10} \text{ cm}^2$

Current Density - $2 \times 10^6 \text{ A/cm}^2$ for 3 minutes then
 $1.5 \times 10^6 \text{ A/cm}^2$

Required Current - 35.1ma and 26.33ma

Actual Current - 35.1ma and 26.33ma

Test Situation - Conducted in situ under 6×10^{-8} torr

Ambient temperature - 21.11°C

Vacuum - 6.0×10^{-8} torr

Resistance - 285 ohms

The TEM settings were:

Vacuum - 6.0×10^{-8} torr

Emission Current - 95-100 microamps

Accelerating Voltage - 100 kv

Aperture - Third, Field Limiting, 200um

Length - 76cm

The test vehicle was then powered in situ. Examination of the test stripe after 3 minutes at $2 \times 10^6 \text{ A/cm}^2$ revealed that massive voiding and accumulation was occurring. Current density was then reduced to $1.5 \times 10^6 \text{ A/cm}^2$ to prevent failure. After 16 minutes total stress time, the stripe was again

photo-mapped and the changes in the stripe can be seen by comparing the mosaic reconstruction of the stripe in Figure 56 with the prestress mosaic in Figure 55.

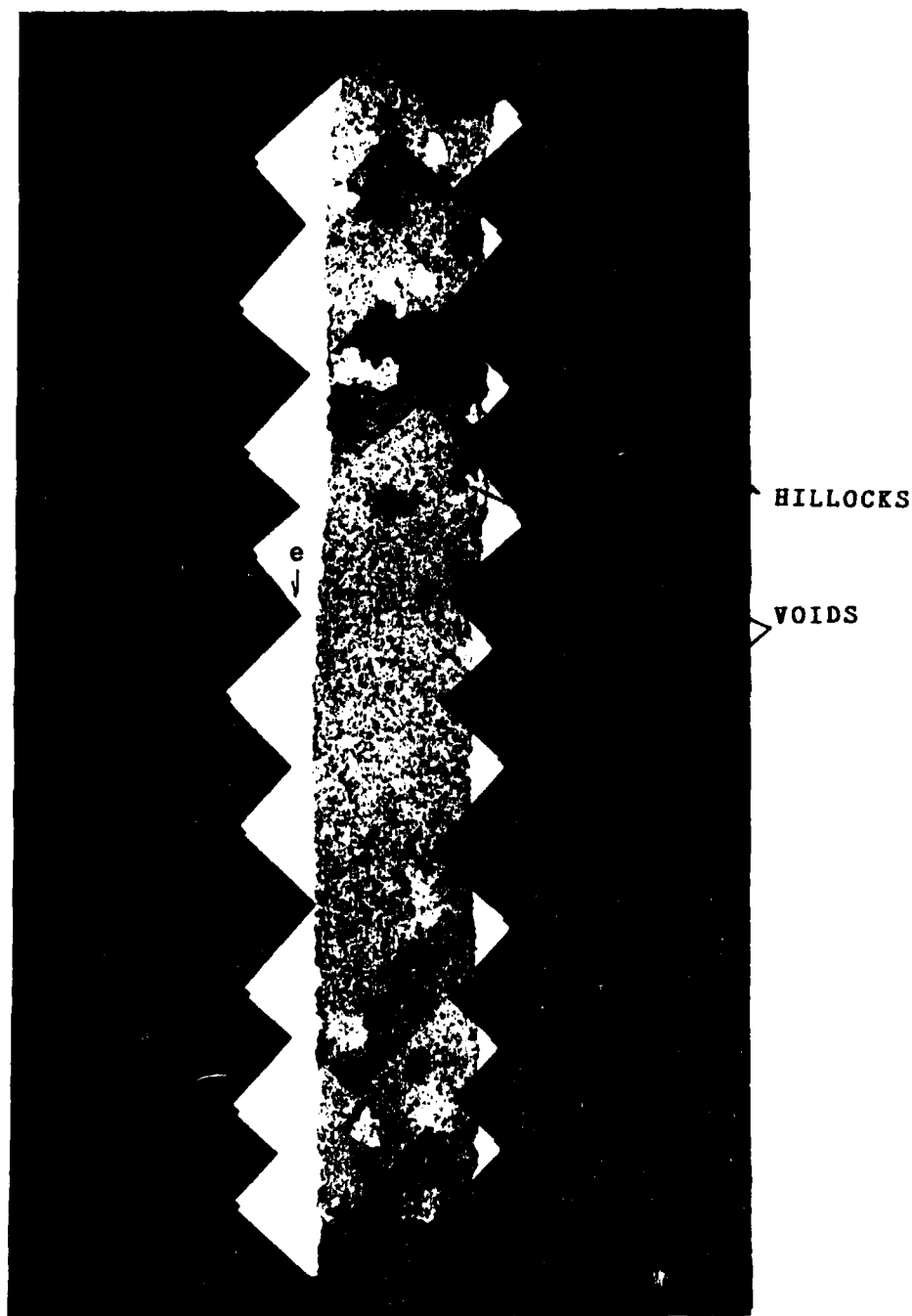
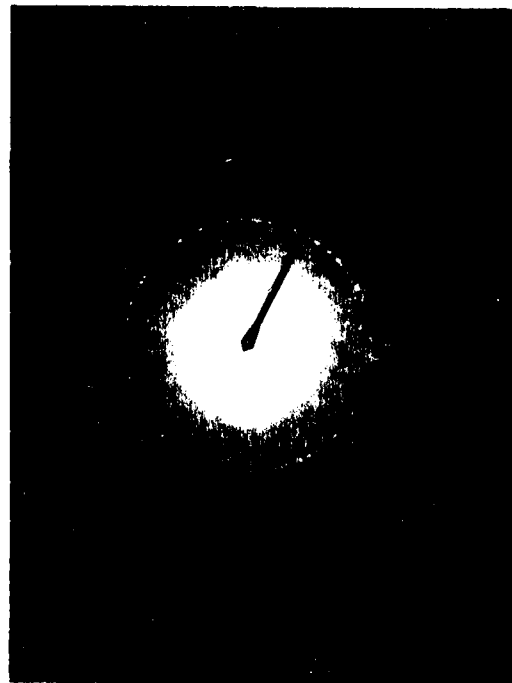


Figure 56. Post Stress Mosaic of BTV Stripe

Electron flow or "electron wind" in Figure 56 is from top to bottom. The accumulations have occurred at the anode and voiding at the cathode, which is in agreement with published findings (12:485; 75:263; 77:201). The diffraction pattern of a voided area is shown in Figure 57.



a) STEM of Voided Area, 6600x

b) Diffraction Pattern

Figure 57. Crystallographic Micrographs of Voided Stripe

Comparison of Figure 57b with Figure 52 shows a less intense pattern in the voided area indicating that the area is indeed thinning but is still crystalline in structure.

Dramatic changes in crystal structure is evident in the
linestripe when the experiment is permitted to progress to
failure. This was the case with experiment # 3. The BTV
was mounted and bonded as shown in Figure 58.

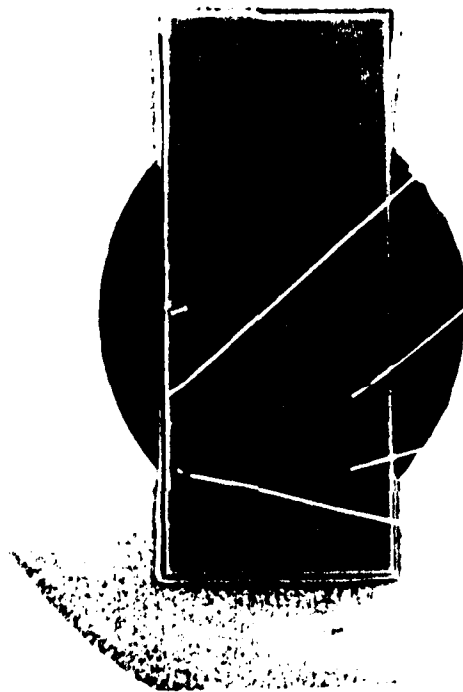


Figure 58. BTV Mounted in MARK II Holder, 20x

The processing of this BTV yielded two holes over two sepa-
rate patterns as shown in Figure 59.

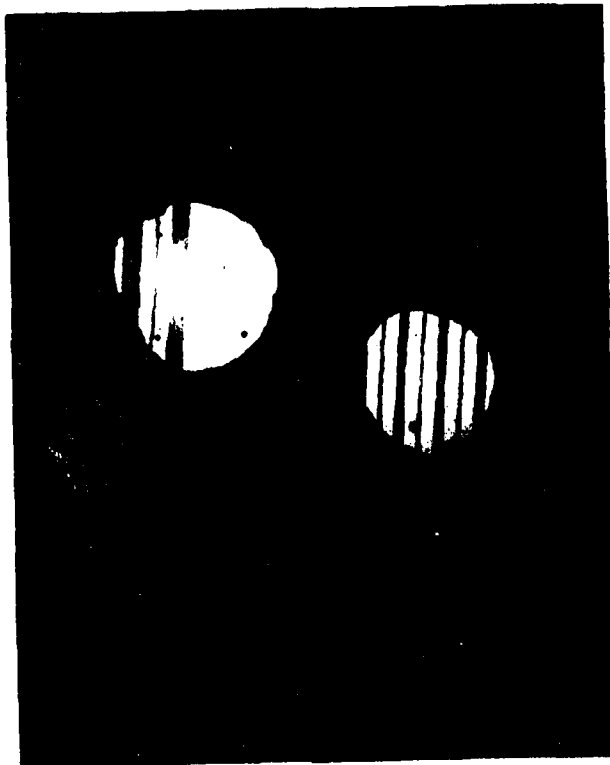


Figure 59. Dual Etched holes in BTV of Experiment #3, 300x

The hole over the pattern stressed in experiment #3 is depicted in Figure 50. The experimental conditions were:

Experiment #3 - In Situ Stress Run to Failure

Test Vehicle Used - Aluminum Bridge Test Vehicle.

Line Width - 6.75 microns

Line Thickness - 1900 Angstroms (Dektak measurement)

Cross Sectional Area (Determined by SEM) - $1.76 \times 10^{-8} \text{ cm}^2$

Current Density - $1.0 \times 10^6 \text{ A/cm}^2$ and
 $2 \times 10^6 \text{ A/cm}^2$

Required Current - 11.6ma and 25.65ma

Actual Current - 11.6ma and 25.7ma

Test Situation - Conducted in situ under 6×10^{-8} torr

Ambient temperature - 21.11°C

Vacuum - 6.0×10^{-8} torr

Resistance - 480 ohms

The TEM settings were:

Vacuum - 6.0×10^{-8} torr

Emission Current - 95-100 microamps

Accelerating Voltage - 100 kv

Aperture - Third, Field Limiting, 200um

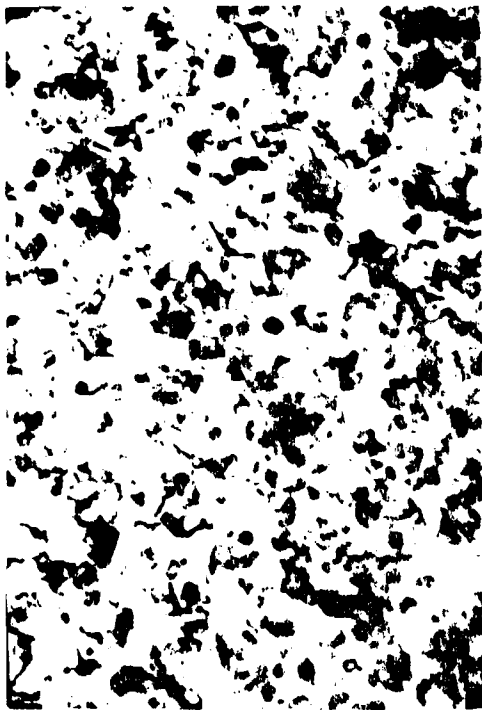
Length 76cm

The stripe was stressed for 4098 minutes at $1 \times 10^6 \text{ A/cm}^2$ then increased to $2 \times 10^6 \text{ A/cm}^2$ to accelerate the electromigration process. Failure occurred at 4203 minutes. The point of failure is depicted in Figure 60.



Figure 60. Bright Field TEM of Failure Point, 26000x

Figure 61 depicts the grain structure change of the stripe.



a) Prestress

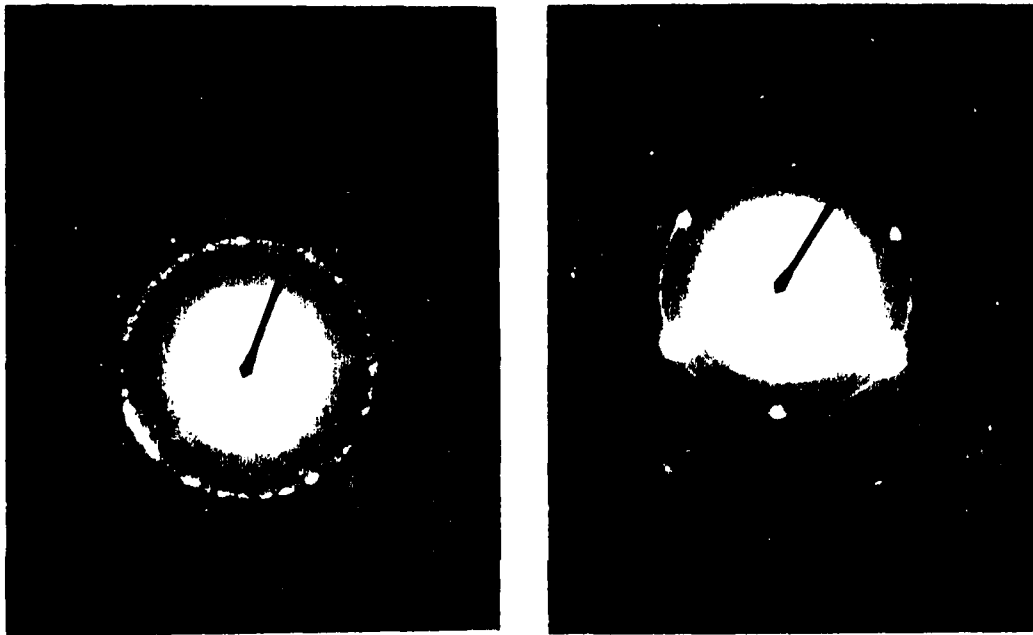


b) Post Failure

Figure 61. Bright Field TEM of Linestripe, 25000x

Comparison of Figures 61a and b indicate that the crystalline grain structure of the test stripe after being stressed tended increase in size. Indications are that this is due in part to the annealing affects of the joule heating present during the failure of the line stripe. A video taken during an electromigration run clearly shows the wave of heat emanating from the failure point shown in Figure 60 and the immediate change in the grain structure of the linestripe.

The change in diffraction patterns can be seen in Figure 62 with the oxide window diffraction pattern depicted in Figure 63.



a) Prestress

b) Post Failure

Figure 62. Diffraction Patterns of BTV Experiment #3

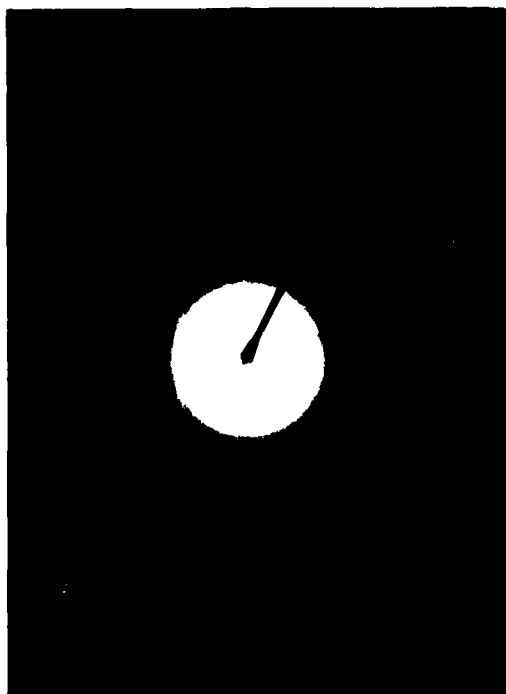


Figure 63. Diffraction Pattern of Oxide Window,

Figure 62 shows the change in crystalline structure from a polycrystalline structure to one which has two phases: single crystal and many fine grains which can be attributed to the annealing effects of the joule heating (34:12; 35:75).

The results and discussion of this effort clearly show progress in the technique of electromigration analysis. The mating of the SEM with a prototype microminiature Joule-Thompson refrigerator provides the capacity to view in situ, the effects of electromigration in the high current density, low temperature range. Electromigration damage has been

observed at cryogenic temperatures. The refrigerator provides the opportunity to precisely control the temperature variable and temperature gradients across the test pattern. This precision will lead to more consistent statistical analysis of reliability data derived from electromigration studies.

The technique for the in situ observation of electromigration damage in the TEM has been demonstrated. The incorporation of the bridge test circuit afforded the chance to examine the changing morphology of a polycrystalline line-stripe through the use of the STEM mode of operation and the TEM diffraction patterns. With this technique, the effects of a failure on the morphology of the linestripe has been observed and documented.

V. Conclusions and Recommendations

The research effort accomplished to date has established a baseline for future research. With equipment already available at the institute, techniques for the investigation of electromigration and device reliability have been demonstrated. By interfacing the SEM with a prototype cold stage, electromigration was observed in situ. New data points were collected from previously untouched temperature and current density regimes. Electromigration was shown to occur at cryogenic temperatures. A technique for the in situ observation of electromigration damage in a TEM was demonstrated. The bridge test vehicle was developed to allow for the unique TEM monitoring of crystallographic and grain boundary changes due to current stress. Changes in the crystallographic structure of a stripe under stress was observed using TEM diffraction patterns. These two related efforts open up new opportunities for the institute to conduct research on Reliability Physics.

Recommendations

The results of this work lead the way to numerous follow on investigations. The collection of data is but a small part of the overall research effort. Many new ideas and techniques are ready for investigation. The expansion of laboratory facilities would provide nearly unbounded growth in many research directions. This work is a start toward a continuing effort in Reliability Physics research.

The following recommendations would enhance this effort;

1. Acquire a SEM. To be a viable research effort, a SEM is needed with sufficient growth potential to keep up with future research efforts.
2. Fabricate, through the MOSIS system, test vehicles that include planar diodes under the test stripe, as described in chapter II. This would offer a better understanding of the temperature profile of the test stripe.
3. Perform electromigration experiments, holding T constant while varying J. More data points are needed for a thorough statistical analysis of the data base.
4. Perform electromigration experiments, holding J constant while varying T. A statistical analysis of the data is the objective.
5. Perform electromigration experiments, varying either J or T while operating in a controlled atmosphere ranging from hydrogen to methane.
6. Seal the microminiature refrigerator while it is not in use to prevent moisture from entering the system and causing subsequent clogs.
7. A redesign of the timer circuit is required to handle the high power requirements. Minimum potentiometer rating should be 5 watts. Move the readouts and 6 second light so that they are easily visible at eye level. Replace the 6 second 555 timer with either a crystal oscillator or a 60hz monitor to increase the accuracy of the timer.

8. Perform comparison experiments for electromigration damage between glassivated and non-glassivated line stripes. The test vehicles are currently available at the institute.
9. Acquire strip recorders for the continuous monitoring of test current, stripe temperature and gas flowrate. This will help validate results of test runs by insuring that the set parameters were maintained for the duration of the experimental run.
10. Acquire a programmable temperature controller that will control the temperature of the microminiature refrigerator. Coupled with the Z-100, programs can be created that allow for the investigation of electromigration using the TRACE technique (82; 83).
11. Mount the bridge test vehicle on the cold stage of the microminiature refrigerator. The suspended stripe, with no contact with the cold stage, should heat up above the temperature of the rest of the stripe. This will increase the probability of EMD in the bridge area. EMD can then be studied in a preselected area with a reasonable probability of localizing the damage to the area of interest.
12. Build bridge circuit test vehicles on <110> silicon wafers. After dicing, the test vehicle is then prepared for etching as per chapter III. A KOH directed etch is then used which should offer better control of the hole geometry.
13. Fabricate a pattern and hole mask set which will allow for easy alignment from opposite sides of the wafer. Hole mask should be narrow lines which will line up perpendicular

to the test stripes on the test pattern mask.

14. Modify redesign of EM-SHH holder with spring contacts to both hold down the sample and facilitate electrical contacting of the test vehicle.

15. Design a new MOSIS NMOS pattern with thick leadouts from the bonding pads (pads 1/4" apart) to a short electro-migration teststripe (\leq 200 microns long). This will facilitate massive etching techniques from the back side and limit the required observation area under the SEM/TEM.

APPENDIX A
ALUMINUM BRIDGE TEST VEHICLE

ALUMINUM BRIDGE TEST VEHICLE

The fabrication of the aluminum bridge test vehicle, (BTV), for use in the crystallographic studies of electro-migration involves several photolithographic processes, some common, while others quite unique.

It is most important to start with a clean wafer of known orientation. The wafers used are 7 mil thick boron doped silicon wafers. The diameter of the wafer is 1.5 inches with a resistivity of 10-20 ohm-cm. The crystallographic orientation is $\langle 111 \rangle$. To obtain a bridge test vehicle, proceed as follows;

1. Clean the wafer using the following solution and times:

3:2 $\text{H}_2\text{SO}_4:\text{H}_2\text{O}_2$ 10 minutes (Sulfuric Acid:Hydrogen Peroxide).

DIW 5 minutes (Deionized Water)

10:1 DIW:HF 5 minutes (DIW:Hydrofluoric Acid)

spin dry as required

2. Grow an oxide on the surface of the wafer. The oxide will insulate the linestripe from the substrate, help support the linestripe during subsequent etching, and protect the pattern from the etchant. At 1050°C , a wet oxide should be grown to a thickness of 3000 angstroms. The approximate time will be 60 minutes in steam.

3. Deposit Aluminum on the surface of the wafer. A maximum of 2000 angstroms should be evaporated on the surface. A minimal thickness is required for TEM beam penetration. The

evaporation pressure used was 2×10^{-6} torr at ambient temperature.

4. Spin on waycoat 43 cps negative resist at a rate of 5000 rpm for 20 seconds.
5. Prebake wafer at 70°C for 20 minutes.
6. Expose the resist using a mask aligner loaded with the Bell Labs pattern. Exposure is for 7 seconds.
7. Postbake the wafer at 150°C for 30 minutes.
8. Develop the resist. Mount the wafer on a spinner and spin at a rate of approximately 1000 rpm. Develop using the following sequence:

Predeveloper	20 seconds
Xylene	30 seconds
Butyl Acetate	25 seconds
N ₂ Dry off	40 seconds

9. Etch the wafer by immersion in a solution heated to 50°C that is composed of:

120 ml	H ₃ PO ₄	(Phosphoric Acid)
120 ml	DIW	
7 ml	HNO ₃	(Nitric Acid)
7 ml	CH ₃ COOH	(Acetic Acid)

Etch the wafer until the pattern emerges. The time required for a 2000 angstrom thick deposit is approximately 2 minutes.

10. Rinse the wafer in DIW to remove all traces of the etchant.
11. Dry with a N₂ blowoff.
12. Remove negative photoresist from the pattern in a

plasma asher.

13. Mount the wafer on a dicing saw and dice the patterns.

Separate the individual test vehicles.

14. Clean the test vehicle by ultrasonic bath in the following sequence:

$C_2H_3Cl_3$	10 minutes	(Trichloroethylene)
CH_3COCH_3	10 minutes	(Acetone)
CH_3OH	10 minutes	(Methyl Alcohol)
DIW	10 minutes	
Spin Dry	10 minutes	

15. Probe the four meanders on the pattern for continuity.

16. Optically inspect meanders for good definition.

17. Melt a drop of clear Picolastic D100 mounting wax on to the surface of a clean sapphire disk which is heated to 95°C.

18. Press the test vehicle into the wax with the pattern side down.

19. Melt wax onto the perimeter of the test vehicle, leaving only center third of the vehicle exposed.

20. Draw strands of wax across the exposed area to form two exposure windows which will center between two meander patterns on the reverse. Each etched hole will clear Silicon from beneath the center few lines of the two side by side patterns. Allow the structure to cool.

21. Immerse the sapphire disk with the test pattern for 10 seconds in a solution of 10:1 DIW:HF to remove the oxide over the remaining exposed substrate.

22. Etch the test vehicle substrate mounted on the sapphire disk by immersion in a solution of 10:6:6 Acetic Acid:HF Acid:Nitric Acid. The approximate etching time is 35 minutes total. Initial immersion should not exceed 25 minutes. Inspect for light shining through and reimmerse for two minute intervals until light is observed through the etched hole.

23. Continue etching for one minute intervals and check for oxide thinning by removing the disk from the etchant, rinsing with DIW, drying with N₂ blowoff, and inspecting under the microscope.

CAUTION

Additional etch time will expand the hole through the substrate. Eventually, the etchant will break through the oxide layer directly under the test pattern, which will result in damage to the test circuit.

24. Remove the oxide with repeated 10 second dips in 10:1 DIW:HF Acid.

25. Soak pattern in Acetone overnight to facilitate removal of the test vehicle from the sapphire disk.

26. Rinse off remaining wax under gentle Acetone spray.

27. Remove the Acetone by dipping the test vehicle in Methyl Alcohol.

28. Rinse the test vehicle with Freon and dry with a gentle N₂ blowoff.

29. Probe the test pattern to determine electrical continuity.

30. Mount the test vehicle on the MARK II Holder as per chapter III.

31. Wire bond to the appropriate bonding pads required for testing.

APPENDIX B
MICROMINIATURE REFRIGERATOR SYSTEM

MICROMINIATURE REFRIGERATOR SYSTEM

An essential part of this thesis is the ability to monitor test vehicle temperature and maintain the vehicle at a low temperature while running an experiment. This capacity is provided by the use of a prototype microminiature refrigerator system, manufactured by MMR Technologies Inc.. The system consists of an experimental cold stage connected through a feedback loop to a temperature controller. Some support equipment is required and there are limitations on the cooling capacity of the system. The refrigerator operates on the Joule-Thompson effect of capillary cooling (23:164; 47:337; 56:662; 59:13). Extensive information can be found in the users manuals for both the cold stage and the temperature controller (20; 44).

The basic refrigerator is the Model K2205, shown in Figure 64.

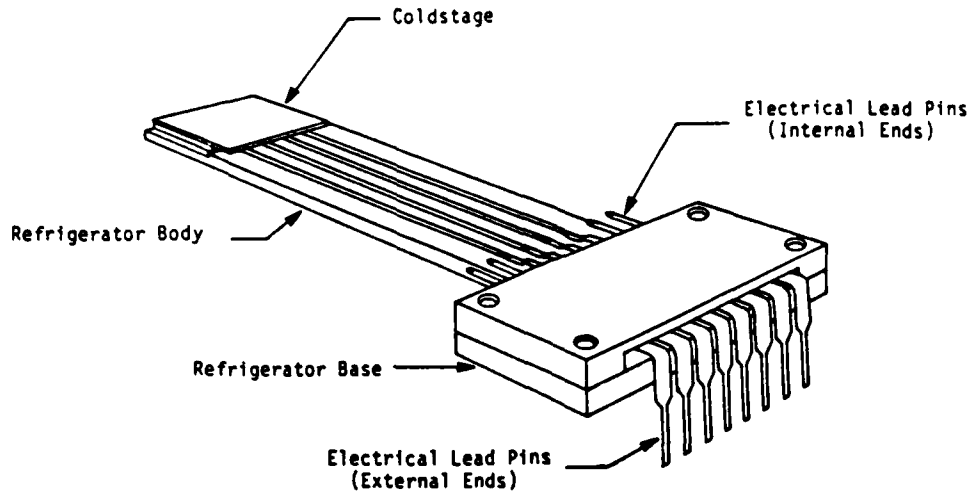


Figure 64. Standard Refrigerator
Source:(20:5)

The heart of the refrigerator assembly is a thin quartz slide that has capillary tubes that meander through the slide body. These capillaries provide a means of removing heat from the cold stage by cycling high pressure Nitrogen gas through the refrigerator. The tubes are connected at one end to an outside gas supply and run under the cold stage end of the refrigerator, where the sample is mounted. Once the gas cycles through the refrigerator, it is exhausted to the atmosphere.

The sample is mounted on the cold stage end of the refrigerator by silver paint. The thermal resistance between the device and the mounting pad is about 60mK/mW (20:13). Good thermal contact is essential for proper operation of

the cold stage. The temperature is monitored by a cold stage diode under the mounting pad on the refrigerator.

Electrical power is provided to the cold stage diode and the refrigerator heater element through a wiring harness that connects to the refrigerator through a pin socket. Power to the sample is provided by connecting wires to the lead pin ends that protrude from the base of the refrigerator. The smallest possible wires should be used to minimize the heat leakage from the wires into the sample (20:5). With the refrigerator connected to electricity and gas, the assembly is now ready for a controlled environment.

The refrigerator will slide in through the end of the vacuum chamber jacket and be sealed inside by the refrigerator base. Once sealed, the atmosphere seen by the sample can be changed, monitored, or pumped out. Observation of the sample takes place through a window on the vacuum chamber jacket. Once in the desired atmosphere, the refrigerator assembly is connected to the K-77 Temperature Controller and the required temperature can be set.

The K-77 Temperature Controller, shown in Figure 65, controls the temperature of the cold stage through a temperature range of 373 K to 76 K (20:1).

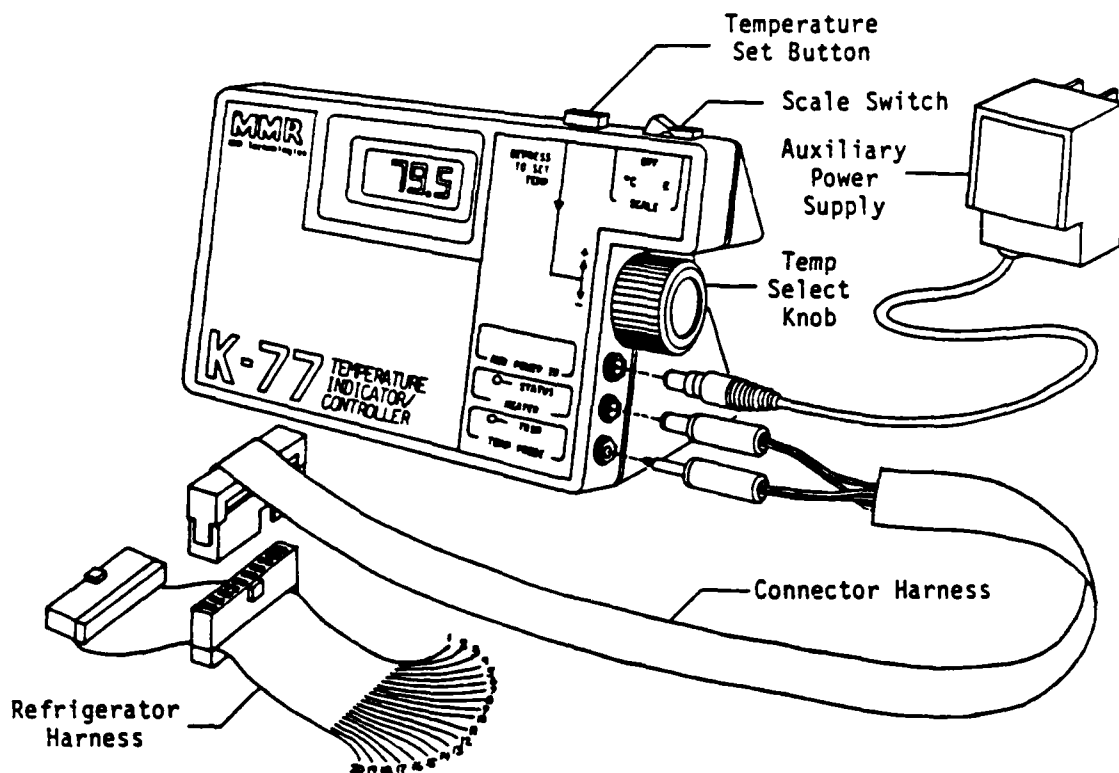


Figure 65. K-77 Controller Diagram
Source:(44:6)

The controller senses the temperature from the diode located under the mounting pad and adjusts the temperature to above minimum with the resistor heater also located under the mounting pad. The controller rapidly changes the temperature toward the desired setting, and then maintains it to within 2° throughout the range of 76 K to 323 K. The system displays temperature in either Kelvin or Centigrade and can be operated up to 373 K with a loss of the 2° accuracy. The

temperature accuracy at 373 K is about $\pm 6/-0$ K (44:2). Accuracy is limited by the non-linearity of the diode over a wide temperature range (44:2). Temperatures below 80 K require a vacuum assist (44:1). The rate of temperature change usually exceeds $1^\circ/\text{sec}$. To reach the full potential of the refrigerator, some support equipment is required.

Besides electrical sources to power the diode and heater elements, another source will be required to power the test vehicle on the cold stage. The specifications are determined by the experiment at hand. A Nitrogen gas supply is required for cooling. A maximum pressure of 1800 psi is allowed. The system will run on less pressure, but the heat dissipation capacity of the refrigerator will diminish. In addition, to reach the lowest temperatures, a vacuum assist is required on the Nitrogen exhaust port. The vacuum system should be capable of maintaining 5 millitorr or better (20:14). At full capacity, there are limits on refrigerator operation.

Limitations on the refrigerator must be observed to avoid undesired effects. At 76 K, the refrigerator is capable of dissipating 250mW of power from the test vehicle on the cold stage (20:1). This places limits on the power that can be placed on the test vehicle without affecting the refrigerator operation. Gas pressure must not exceed 1800 psi to avoid damage to the capillary tubes. The introduction of high pressure gas lines into a vacuum environment can be hazardous to equipment. The refrigerator system is

not compatible with a vacuum of 10^{-6} torr or better due to the possibility of nitrogen out-gas contamination of the vacuum system (106). Observance of these limitations will lead to the attainment of published performance for the refrigerator system.

The Model K2205 with the K-77 Temperature Controller allows for the unique temperature control of a test vehicle under powered conditions in a controlled environment. Detailed discussions of the design and operation of the temperature control system and refrigerator can be found in references 44 and 20 from MMR Technologies Inc..

APPENDIX C
ELAPSED MINUTE TIMER

TIMER CIRCUIT

The electromigration process may take a long time. By incorporating a timing device which operates as long as a closed circuit is detected in the electromigration circuit the elapsed time from power application and/or time to failure can be accurately measured by electrical means. The electromigration test circuit and timer interface are shown in Figure 66.

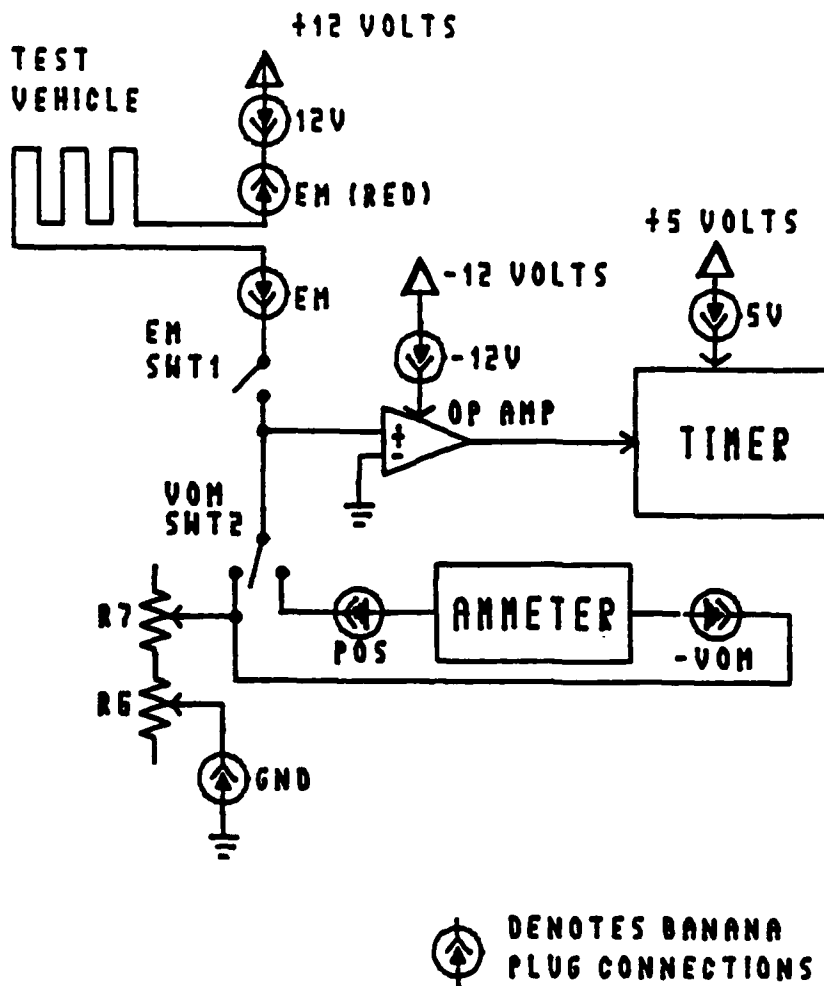


Figure 66. Electromigration Circuit with Timer Interface

The test circuit current and hence current density are controlled with the variable resistors (R6 and R7) and monitored by the ammeter. The ammeter need not be on continuously and is isolated from the circuit except during current readings. By switching off the VOM switch (swt2),

the ammeter is bypassed. The circuit is constructed such that the current density everywhere outside of the test pattern is inconsequential, compared with that required for accelerated electromigration. The test circuit is monitored on the power supply side of the test stripe. At this location, either a failed test stripe or open EM switch (swt 1) will result in a positive voltage being present. A closed test circuit (swt 1 closed and current flow through the test stripe) results in an essentially 0 voltage reading at the monitoring point in the test circuit. The timer circuit utilizes an op amp to detect the voltage at the monitoring point. The op amp has a high input impedance which results in a negligible current flow from the test circuit into the timer circuit. Op amp output is used to enable a 6 second timer via a 5 volt zener diode (D1) as shown in the schematic diagram in Figure 67.

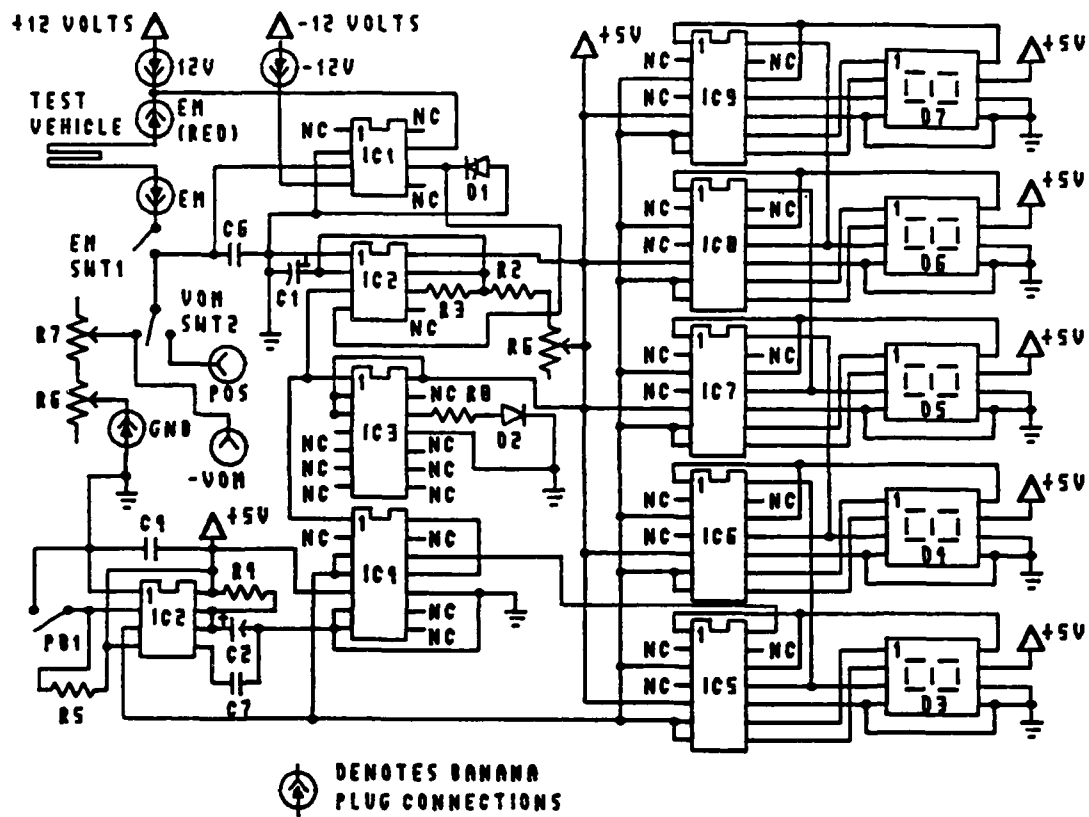


Figure 67. Timer Schematic Diagram

The associated parts list for the schematic diagram is given in Table V.

Table V.

Timer Parts List and Description

DIAGRAM #	PART #	TIMER USE
D1	1N914	5 VOLT ZENER DIODE
D2	4-382B	MONITORING GREEN LED
D3-D7	HP7340	5 HEX DISPLAYS
IC1	741	DETECTOR OP AMP
IC2	555	6 SECOND TIMER CHIP
IC3	7473	JK MONITORING FLIP FLOP
IC4	7490	DIVIDE BY 10 COUNTER
IC5-IC9	7490	5 HEX DISPLAY DRIVERS
IC10	555	RESET TIMER CHIP
C1-C2	10 uF	TIMING CAPACITORS
C3-C5	.1 uF	NOISE SUPPRESSION CAPACITORS
C6-C7	.01 uF	NOISE SUPPRESSION CAPACITORS
R1	20K Ohm	TIMING POTENTIOMETER
R2	1.1K Ohm	TIMING RESISTOR
R3	1K Ohm	TIMER THRESHOLD RESISTOR
R4	100K Ohm	RESET TIMER RESISTOR
R5	330 Ohm	RESET TIMER RESISTOR
R6	5K Ohm	EM CURRENT ADJUSTMENT POT
R7	200 Ohm	EM CURRENT ADJUSTMENT POT
R8	30 Ohm	DIODE RESISTOR
SWT1	SPST	EM ACTIVATION SWITCH
SWT2	DPST	VOM SWITCH
PB1	SPST	RESET PUSHBUTTON

The 6 second timer is constructed from a 555 timer chip and adjusted through variable resistor R1 to provide a pulse every 6 seconds as long as its reset pin (pin 4 which is connected to the op amp output) is maintained at 5 volts. The op amp enables the timer by providing this 5 volt signal as long as it detects 0 voltage at the monitoring point in the test circuit. The zener diode prevents the op amp from sending anything larger than 5 volts to the timer. The

timer will provide a pulse every 6 seconds to the rest of the timer circuit as long as the test circuit remains a closed circuit. This pulse is monitored by the JK flip flop (IC3) which cycles the associated LED (D2) on and off every 6 seconds, allowing the timer to be calibrated using the adjustable resistor connected to the 6 second timer (R1).

The 555 output pulse is also fed into a TI7490 decade counter chip (IC4). This integrated circuit serves as a divide-by-10 counter and provides a signal once for every 10 signals it receives from the 6 second timer thus providing a minute count of elapsed time. This minute count is sent to a second decade counter (IC5) which drives its corresponding hex display (D3). The hex display is an HP7340 chip. There is one decade counter for each of 5 hex displays. The displays are cascaded so that the next display is incremented after the previous display transitions from a 9 to a 0. With five displays, a running time of up to 69.4 days (99999 minutes) can be recorded. When the 6 second 555 chip is disabled by the op amp, the hex displays freeze the elapsed time until timing is resumed or reset for another run by the reset timer (IC10) via its corresponding reset push button (PB1).

The timer circuit is encapsulated in a transparent plexiglass box which provides protection for the circuit while allowing observation of the hex displays. The timer /test circuit controls and interconnecting plugs are mounted on the removable rear panel of the box as shown in Figure 68.

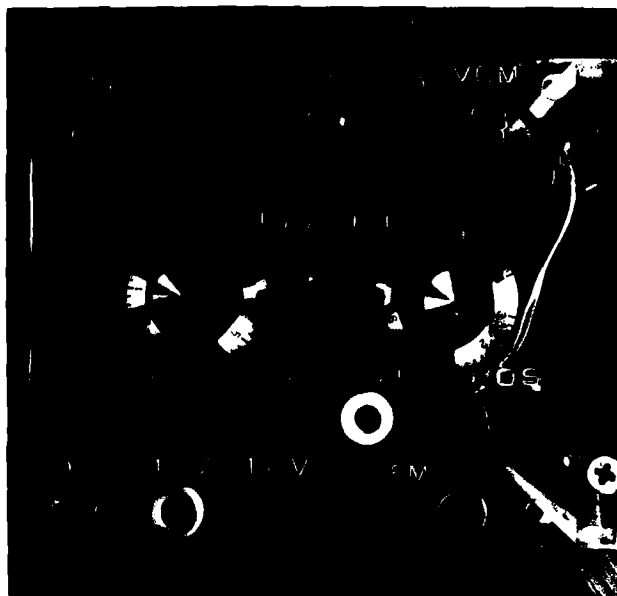


Figure 68. Timer Rear Panel Diagram

Banana plugs are used to connect the timer/test circuit to its power supply, the ammeter, and the electromigration test sample.

These banana plug connections on the rear of the timer allow for simple modifications to the basic electromigration circuit setup. By making the connection changes shown in Figure 69 (as compared with Figure 66), the timer device can be modified to incorporate an external adjustable high power rated resistor for unique electromigration studies.

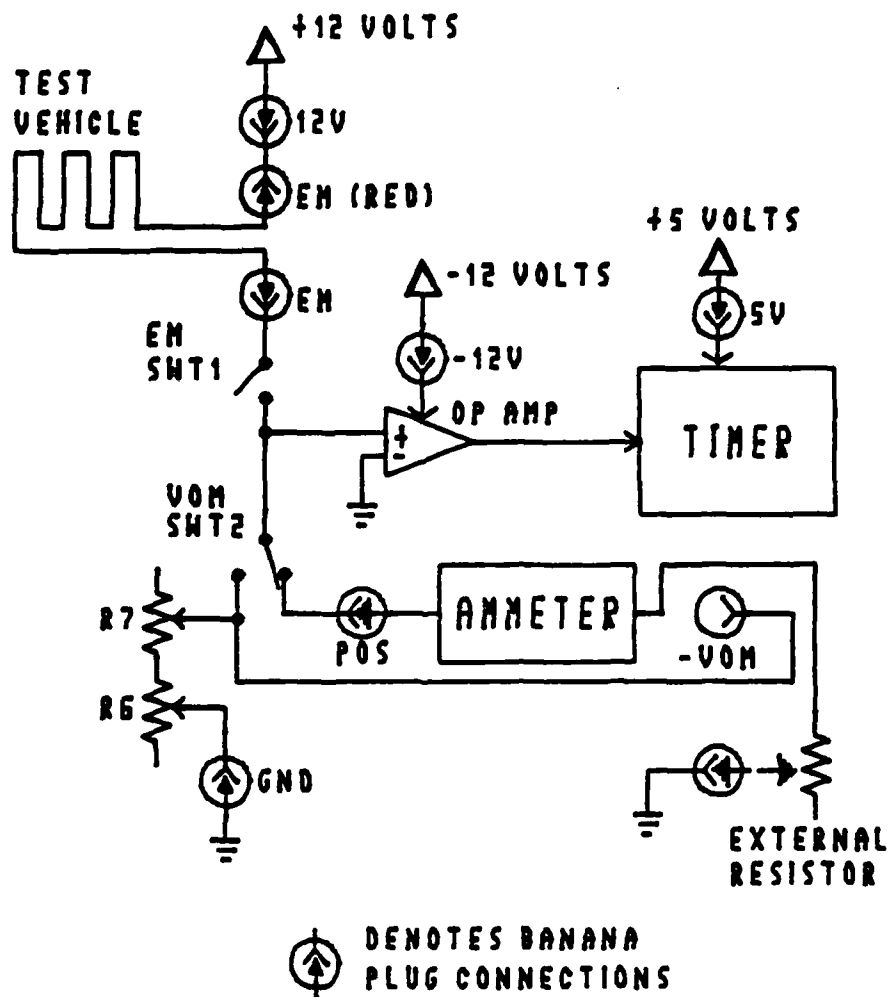


Figure 69. Modified Timer Setup for External Resistor

In the same manner, the connections can also be changed to accept a larger, external power supply (external in that it is in addition to the ± 12 volt supply which is normally used to power the electromigration circuit as well as the op amp monitor). These changes are depicted in Figure 70 (as compared with Figure 66).

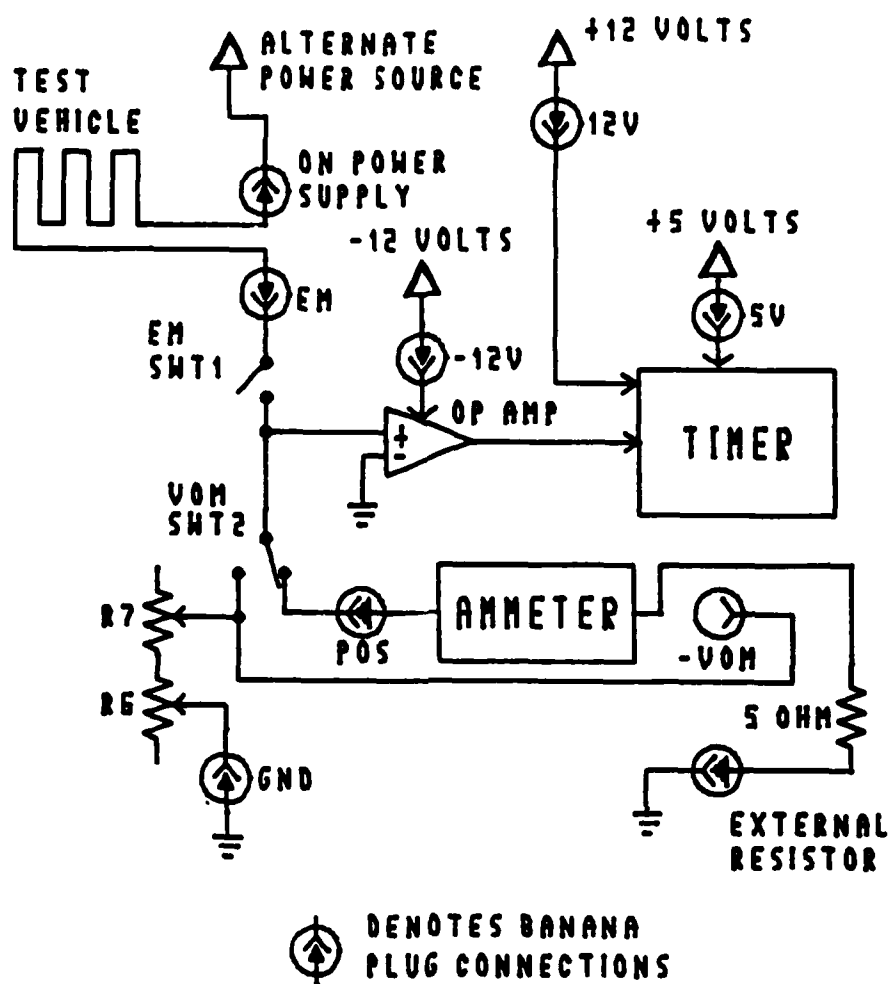


Figure 70. Modified Timer Setup for External Power Supply

The timer device described generates an accurate measurement of elapsed time of current application without interfering with the electromigration process and provides an easy method of interconnecting the components of the entire system.

Bibliography

1. Agarwala, B. N. et al. "Dependence of Electromigration-Induced Failure Time on Length and Width of Aluminum Thin-Film Conductors," Journal of Applied Physics, 41 (10): 3954-3960 (1970).
2. Attardo, M. J. and R. Rosenberg "Electromigration Damage in Aluminum Film Conductors," Journal of Applied Physics, 41 (6): 2381-2386 (May 1970).
3. Balluffi, R. W. and J. M. Blakely "Special Aspects of Diffusion in Thin Films," Thin Solid Films, 25: 363-392 (1975).
4. Balog, Alexander G. Project Designer. Personal Correspondence. Design and Construction Department, Rutgers University, New Jersey, September '985.
5. Berenbaum, L. "Electromigration Damage of Grain Boundary Triple Points in Aluminum Thin Films," Journal of Applied Physics, 42 (1): 880-882 (August 1970).
6. Black, J. R. "Electromigration of Al-Si Alloy Films," Proceedings of the IEEE 16th Annual Symposium on Reliability Physics. 233-240. IEEE Press, New York, 1978.
7. -----. Reliability Study of Doped Aluminum Conductor Films. RADC-TR-77-410. Rome Air Development Center, Griffiss AFB, N.Y., December 1977.
8. -----. "Physics Of Electromigration," Proceedings of the IEEE 12th Annual Symposium on Reliability Physics. 142-147 IEEE Press, New York, 1974.
9. -----. "Electromigration - A Brief Survey and Some Recent Results," IEEE Transactions on Electron Devices, ED-16 (4): 338-347 (April 1969).
10. -----. "Electromigration Failure Modes in Aluminum Metallization for Semiconductor Devices," Proceedings of the IEEE, 5: 1587-1594 (September 1969).
11. Blech, I. A. "Direct Transmission Electron Microscope Observation of Electrotransport in Aluminum Thin Films," Applied Physics Letters, 11 (8): 263-266 (15 October 1967).

12. -----, and E. S. Meieran. "Electromigration in Thin Al Films," Journal of Applied Physics, 40 (2): 485-491 (February 1969).
13. Braun, Leonard. "Electromigration Testing - A Current Problem," Microelectronics and Reliability, 13: 215-228 (1974).
14. Brusis, P. G. Fine Line Electromigration, The Effect of Crossed Thermal Gradients. RADC-TR-83-224. Rome Air Development Center, Griffiss AFB, N.Y., September 1983.
15. Burns, J. M. et al. 2-3 GHz Digital GaAs LSI. AFWAL-TR-81-1083. Avionics Lab, Air Force Wright Aeronautical Lab, Wright-Patterson AFB, OH, June 1981.
16. Chaudhari, P. "Hillock Growth in Thin Films," Journal of Applied Physics, 45 (10): 4339-4346 (October 1974).
17. Chen, T. M. and T. P. Djeu. "Electromigration and 1/f Noise of Aluminum Thin Films," Proceedings of the 23rd IEEE Symposium on Reliability Physics. 87-92 (1985).
18. Christou, A. et al. Metal Migration in Thin Film Aluminum/Silicon. NWL-TR-2762. Naval Weapons Lab, Dahlgren, Virginia, June 1972.
19. Colbourne, E. D. et al. "Reliability of MOS LSI Circuits," Proceedings of the IEEE, 62 (2): 185-211 (February 1974).
20. Cryogenic Microminiature Refrigeration System IIB. User's Manual. MMR Technologies Inc., Mountain View, Ca.: October 1984.
21. Das, A.K. and Sir Rudolf Peierls. "The Force In Electromigration," Journal of Applied Physics: Solid State Physics, 8: 3348-3352 (1975).
22. Davis, T. L. "Nucleation Rate of Vacancy Clusters in Aluminum," Journal of Applied Physics, 38 (9): 3756-3760 (August 1967).
23. Deslogue, E. A. Thermal Physics. New York: Holt Rinehart and Winston, Inc., 1968.
24. d'Huerle, F. M. and R. Rosenberg. "Electromigration in Thin Films," Physics of Thin Films, Advances in Research and Development. Vol 7, Edited by G. Hass et al. New York: Academic Press, 1973.
25. d'Heurle, F. M. and P.S. Ho. Electromigration in Thin Films. New York: John Wiley and Sons, 1978.

26. d'Heurle, Francois M. "Electromigration and Failure in Electronics: An Introduction," Proceedings of the IEEE, 59: 1409-1418 (October 1971).
27. d'Heurle, F. M. and I. Ames. "Electromigration in Single-Crystal Aluminum Films," Applied Physics Letters, 16 (2): 80-81 (January 1970).
28. d'Heurle, Francois M. "On the Structure of Aluminum Films," Transactions of the Metallurgical Society, 242: 502-511 (1968).
29. EM-SHH Heating Holder. User's Manual. Jeol USA Inc., Boston, Ma., 15 September 1981.
30. Eshelby, J. D. "A Tentative Theory of Metallic Whisker Growth," Physics Review, 91: 755-756 (1953).
31. Fu, C. Y. and T. Van Duzer. "Hillock Growth on Pb Films Upon Cycling to Cryogenic Temperatures," Journal of Vacuum Science Technology, 17 (3): 752-754 (May 1980).
32. Ghatge, P. B. "Some Observations on the Electromigration in Al Films," Applied Physics Letters, 11: 14-16 (1967).
33. Ghatge, P.B. "Electromigration-Induced Failures in VLSI Interconnects," Solid State Technology, 26: 113-120 (March 1983).
34. Ghatge, P.B. "Electromigration Testing of Aluminum Alloy Films," 25 Sept 1978-30 June 1980. RADC-TR-80-328. Griffis AFB, New York: RADC, October 1980.
35. Ghatge, P.B. et al. "Metallization In Microelectronics," Thin Solid Films, 45: 69-84 (1977).
36. Glaser, A.B. and Gerald E. Subak-Sharpe. Integrated Circuit Engineering. Reading, Ma: Addison Wesley, 1977.
37. Goldstein, J. I. et al. Practical Scanning Electron Microscopy. New York: Plenum Press, 1975.
38. Gupta, D. "On the Direct Measurement of Diffusion at Temperatures Less Than 0.5 T_m," Thin Solid Films, 25: 231-244 (1975).
39. Hardy, H. K. "The Filamentary Growth of Metals," Progress in Metal Physics, Edited by B. Chalmers, and R. King New York: Pergamon Press Ltd., 1956.

40. Hong, Charles C. and Dwight L. Crook. "A New Technique for Monitoring Metallization Reliability at Wafer Level," Proceedings of the 23rd IEEE Symposium on Reliability Physics, 108-114 (1985).
41. Hummel, R. E. et al. "Activation Energy for Electrotransport in Thin Aluminum Films by Resistance Measurements," Journal of Physics and Chemistry of Solids, 37: 73-80 (1976).
42. Huntington, H. B., and A. R. Grone. "Current Induced Marker Motion in Gold Wires," Journal of Physics and Chemistry of Solids, 20: 76-87 (1961).
43. Huntington, H. B. "Effect of Driving Forces on Atom Motion," Thin Solid Films, 25: 265-286 (1975).
44. K-77 User's Manual. MMR Technologies Inc., Mountain View, Ca.: October 1984.
45. Kaba, 1st Lt. Ali. Improving the Efficiency of Vertical Junction Silicon Solar Cells. MS Thesis GE/EE/85J-2. School of Engineering, Air Force Institute of Technology (AU), Wright-Patterson AFB OH, June 1985.
46. Kinsbron, E. "A Model for the Width Dependence of Electromigration Lifetimes in Aluminum Thin Film Stripes," Applied Physics Letters, 36 (12): 968-970 (15 June 1980).
47. Kittel, C. and H. Kroemer. Thermal Physics, Second Edition. San Francisco: W. H. Freeman and Company, 1980.
48. Koonce, S.E. and S. M. Arnold. "Growth of Metal Whiskers," Journal of Applied Physics, 24: 365 (1953).
49. Kreyszig, E. Advanced Engineering Mathematics, 5th ed. New York: Wiley and Sons, 1983.
50. Kumar, P. and R.S. Sorbello. "Linear Response Theory of the Driving Forces for Electromigration," Thin Solid Films, 25: 25-35 (1975).
51. LaCombe, Donald J. and Earl Parks. "A Study of Resistance Variations During Electromigration," Proceedings of the 23rd IEEE Symposium on Reliability Physics, 74-80 (1985).
52. Lahir, S. K. and O. C. Wells. "Reversible Hillock Growth in Thin films," Applied Physics Letters, 15 (7): 234-235 (October 1969).

53. Lane, Clyde H. Practical Problems in the Application of Aluminum Electromigration Failure Studies, GOMAC Digest of Papers, 18-21 (1976).
54. Learn, A. J. "Effect Of Structure and Processing on Electromigration-Induced Failure in Anodized Aluminum," Journal of Applied Physics, 44 (3): 1252-1259 (March 1973).
55. Learn, A. J. and W. H. Shepherd. "Reduction of Electromigration Induced Failure in Aluminum Metallization Through Anodization," IEEE Ninth Annual Proceedings on Reliability Physics, 129-134 (1971).
56. Little, W. A. "Microminiature Refrigeration," Review of Scientific Instrumentation, 55 (5): 661-680 (May 1984).
57. Lloyd, J. R. "Electromigration-Induced Extrusions in Multi-Level Technologies," 21st Annual IEEE International Reliability Physics Symposium, 208-210 (1983).
58. Lloyd, J. R. and S. Nakahara. "Grain Boundary and Vacancy Diffusion Model for Electromigration Damage in Thin Film Conductors," Thin Solid Films, 72: 451-456 (1980).
59. Mackinnon, L. Experimental Physics at Low Temperature. Detroit: Wayne State University Press, 1966.
60. Mano, M. Digital Logic and Computer Design. Englewood Cliffs, New Jersey: Prentice Hall Inc., 1979.
61. Mead, Carver and Lynn Conway. Introduction to VLSI Systems. Reading, MA: Addison-Wesley Publishing Company, 1980.
62. McKelvey, J. P. Solid State and Semiconductor Physics. New York: Harper and Row, 1966.
63. MG-98 Operating Manual for Gas Regulator. Matheson Gas Products, Inc., Dayton, Ohio 1982.
64. Model 100-2 102 And 102A. Operation and Maintenance Manual. Coates And Welter Instrument Corp., Sunnyvale, Ca., 1 April, 1975.
65. Nelson, W. "Analysis of Accelerated Life Test Data - Part 1: The Arrhenius Model and Graphical Methods," Transactions on Electrical Insulation, EI-6: 165-181 (December 1971).

66. Nelson, W. "Analysis of Accelerated Life Test Data - Part 2: Numerical Methods And Test Planning," IEEE Transactions on Electrical Insulation, EI-7 (1): 36-55 (March 1972).
67. Nelson, W. "Analysis of Accelerated Life Test Data - Part 3: Product Comparisons and Checks on the Validity of the Model and Data," IEEE Transactions on Electrical Insulation, EI-7 (2): 99-119 (June 1972).
68. Oliver, C. B. and D. E. Bower. "Theory of the Failure of Semiconductor Contacts by Electromigration," IEEE Eighth Annual Proceedings on Reliability Physics. 116-120 (1970).
69. Partridge, J. and G. Littlefield. "Aluminum Electromigration Parameters," Proceedings of the 23rd IEEE Symposium on Reliability Physics. 119-125 (1985).
70. Peattie, C. G. et al. "Elements of Semiconductor-Device Reliability," Proceedings of the IEEE, 62 (2): 149-168 (February 1974).
71. Pierce, J. M. and M. E. Thomas. "Electromigration in Aluminum Conductors Which are Chains of Single Crystals," Applied Physics Letters, 39 (2): 165-168 (15 July 1981).
72. Ralston, Anthony Ed., Encyclopedia of Computer Science and Engineering, Second Edition. New York: Van Nostrand Reinhold Co. Inc., 1983.
73. Reynolds, F. H. "Thermally Accelerated Aging of Semiconductor Components," Proceedings of the IEEE, 62 (2): 212-222 (February 1974).
74. Root Bryan J. and Tim Turner. "Wafer Level Electromigration Tests for Production Monitoring," Proceedings of the 23rd IEEE Symposium on Reliability Physics, 100-107 1985.
75. Rosenberg, R. "Inhibition of Electromigration Damage in Thin films," Journal of Vacuum Science and Technology, 9: 263-270 (July 1971).
76. Rosenberg, R. and M. J. Attardo. "Electromigration Damage in Aluminum Film Conductors," Journal of Applied Physics, 41 (96): 2381-2386 (May 1970).

77. Rosenberg, R. and L. Berenbaum. "Resistance Monitoring and Effects of Non-Adhesion During Electromigration in Al Films," Journal of Applied Physics Letters, 12 (5): 201-204 (1 March 1968).
78. Sahni, R. J. "Use of Test Patterns In Evaluating The Reliability Of Integrated Circuits," Proceedings of the Eighth Annual Reliability Physics Symposium, 121-126 (1970).
79. Schafft, Harry A. and Tammy C. Grant. "Electromigration and the Current Density Dependence," Proceedings of the 23rd IEEE Symposium on Reliability Physics, 93-99 (1985).
80. Schoen, J. M. "Monte Carlo Calculations of Structure-Induced Electromigration Failure," Journal of Applied Physics, 51 (1): 513-521 (January 1980).
81. Schwartz, K. E. Elektrolytische Wanderung in Flussigen Und Festen Metallen. Berlin: Leipzig, 1940.
82. Schwarz, J. A. and L. E. Felton. "Compensating Effects in Electromigration Kinetics," Solid State Electronics, 28 (7): 669-675 (1985).
83. Schwarz, J. A. "Determining Electromigration Kinetics of Thin Film Interconnects," Semiconductor International, 8 (3): 96-103 (March 1985).
84. Shung, C. and H. L. Huang. "Temperature Distribution on Thin Film Metallizations," Journal of Applied Physics, 47 (5): 1775-1779 (May 1976).
85. Sigsbee, R. A. "Electromigration and Metallization Lifetimes," Journal of Applied Physics, 44 (6): 2533-2540 (June 1973).
86. Smooha, Y. and Y. Komen. "The Growth of Whiskers in Gold Films Due to High Current Densities," Journal of Crystal Growth, 38: 149-154 (1977).
87. Sorbello, R. S. "Atomic Configuration Effects in Electromigration," Journal of Physics and Chemistry of Solids, 42: 309-316 (1981).
88. ----- "Basic Concepts of Electro- and Thermomigration; Driving Forces," Electro- and Thermo-Transport in Metals and Alloys. New York: The American Institute of Mining, Metallurgical, and Petroleum Engineers, 2-19 (1977).

89. Sorbello, R. S. and B. Dasgupta. "Local Fields in Electron Transport: Application to Electromigration," Physical Review, 16 (12): 5193-5205 (15 December 1977).
90. Sorbello, R. S. and P. Kumar. "Linear Response Theory of the Driving Forces for Electromigration," Thin Solid Films, 25: 25-35 (1975).
91. ----- "A Pseudopotential Based Theory of the Driving Forces for Electromigration in Metals," Journal of Physics and Chemistry of Solids, 34: 937-950 (1973).
92. Stewart, R. G. "A Causal Redefinition of Failure Rate Theorems, Stress Dependence, and Applications to Devices and Distributions," IEEE Transactions on Reliability, R-15 (3): 95-114 (December 1966).
93. Sze, S. M. VLSI Technology. New York: McGraw-Hill, 1983.
94. Tai, K. L. and M. Ohring. "Grain-Boundary Electromigration in Thin Films 1. Low Temperature Theory," Journal of Applied Physics, 48 (1): 28-35 (January 1977).
95. Tai, K. L. et al. "Lateral Self-Diffusion and Electromigration in Thin Metal Films," Thin Solid Films, 25: 343-352 (1975).
96. Thomas, Dr R. W., Chief Product Evaluation Section. Personal interview. RBRE/Rome Air Development Center, Griffiss AFB, NY, 31 January 1985.
97. Thomas, R. W. and D. W. Calabrese. "Phenomenological Observations on Electromigration," 21st Annual IEEE Proceedings on Reliability Physics, 1-9 (1983).
98. Thornton, P. R. et al. "Scanning Electron Microscopy in Device Diagnostics and Reliability Physics," IEEE Transactions on Electron Devices, ED-16 (4): 360-371 (April 1971).
99. Towner, Janet M. "Electromigration-Induced Short Circuit Failure," Proceedings of the 23rd IEEE Symposium on Reliability Physics, 81-86 (1985).
100. Vaidya, S. et al. "Electromigration Resistance of Fine-Line Al for VLSI Applications," 18th Annual IEEE Proceedings on Reliability Physics, 165-170 1980.

101. Venables, J. D. and R. G. Lye. "A Statistical Model for Electromigration Induced Failure in Thin Film Conductors," 10th Annual IEEE Proceedings on Reliability Physics, 159-164 (1972).
102. Von Staszewski, G. M. and N. E. Walsoe De Reca. "Electromigration Mechanism in Aluminum Conductors," Solid State Electronics, 23: 481-485 (1980).
103. Wada, T. et al. "Electromigration in Double-Layer Metallization," IEEE Transactions on Reliability, R-34 (1): 2-7 (1 April 1985).
104. Weast, R. C. Ed., Handbook of Chemistry and Physics. Cleveland, Ohio: The Chemical Rubber Company. 1970.
105. Weste, N. and K. Eshraghian. Principles of CMOS Design, A Systems Perspective. New York: Addison-Wesley Co. 1985.
106. Wolfe, Dr. C. Robert, Senior Engineer, Staff Scientist. Telephone Interview. MMR Technologies Inc., Mountain View, California, 21 Sept 1985.
107. Wu, C. J. and M. J. McNutt. "Effects of Substrate Thermal Characteristics on the Electromigration Behavior of Al Thin Film Conductors," 21st Annual IEEE Proceedings on Reliability Physics, 24-36 1983.
108. Yau, L. et al. "Passivation Material and Thickness Effects on the MTTF of Al-Si Metallization," Proceedings of the 23rd IEEE Symposium on Reliability Physics, 115-118 (1985).
109. Yi-Shung Chaug, Huel Li Huang. "Temperature Distribution On Thin Film Metalizations," Journal Of Applied Physics, 47 (5): 1775-1779 (May 1976).
110. Yue, J. T. et al. "Stress Induced Voids in Aluminum Interconnects During IC Processing," Proceedings of the 23rd IEEE Symposium on Reliability Physics, 126-137 (1985).

VITAE

Captain James V. Maskowitz was born on 26 March, 1955 in Perth Amboy, New Jersey. He served as senior class president and graduated from Perth Amboy High School in June 1973, and attended the United States Air Force Academy from which he received his regular commission and the degree of Bachelor of Science in Electrical Engineering in June 1977. Upon graduation he entered undergraduate pilot training at Vance Air Force Base, Oklahoma. He completed pilot training and received his wings in October 1978. He remained in Air Training Command serving as a T-38 Instructor pilot and the Wing Scheduler in the 14th Flying Training Wing, Columbus Air Force Base, Mississippi until January 1982. He then served as a C-141 aircraft commander and pilot scheduler in the 18th Military Airlift Squadron, McGuire Air Force Base, New Jersey. During this tour, he attended Squadron Officer School and was selected as a Distinguished Graduate. He entered the School of Engineering, Air Force Institute of Technology, in May 1984.

Permanent address: 741 Columbus Drive

Perth Amboy, New Jersey 08861

Captain William E. Rhoden was born on 26 February, 1955 in New Orleans, Louisiana. After graduating from high school in New Orleans in 1973, he attended the USAF Air Force Academy where he received a degree of Bachelor of Science in Electrical Engineering in June 1977. Upon graduation, he received a commission in the USAF and an assignment to Undergraduate Pilot Training at Columbus AFB, Mississippi, where he received his wings in July 1978. He served as a T-38 instructor pilot from July, 1978 until his assignment to Randolph AFB, Texas, in August 1981. He served as a T-38 instructor pilot until his assignment to Edwards AFB, California in August 1982. At Edwards, he served as Chief of Operations and Training, Scheduling Section for the USAF Test Pilot School, T-38 Flight Examiner, Scheduler, and O-2 instructor pilot until entering the School of Engineering, Air Force Institute of Technology, in May 1984.

Permanent address: 16731 Chadsford Avenue
Baton Rouge, Louisiana 70816

REPORT DOCUMENTATION PAGE

1a. REPORT SECURITY CLASSIFICATION UNCLASSIFIED			1b. RESTRICTIVE MARKINGS		
2a. SECURITY CLASSIFICATION AUTHORITY			3. DISTRIBUTION/AVAILABILITY OF REPORT APPROVED FOR PUBLIC RELEASE; DISTRIBUTION UNLIMITED		
2b. DECLASSIFICATION/DOWNGRADING SCHEDULE					
4. PERFORMING ORGANIZATION REPORT NUMBER(S) AFIT/GE/ENG/85D-25			5. MONITORING ORGANIZATION REPORT NUMBER(S)		
6a. NAME OF PERFORMING ORGANIZATION SCHOOL OF ENGINEERING/AIR FORCE INSTITUTE OF TECHNOLOGY		6b. OFFICE SYMBOL (If applicable) AFIT/ENG	7a. NAME OF MONITORING ORGANIZATION		
6c. ADDRESS (City, State and ZIP Code) WRIGHT PATTERSON AFB, OHIO 45433			7b. ADDRESS (City, State and ZIP Code)		
8a. NAME OF FUNDING/SPONSORING ORGANIZATION RADC		8b. OFFICE SYMBOL (If applicable) RADC/RBE	9. PROCUREMENT INSTRUMENT IDENTIFICATION NUMBER		
8c. ADDRESS (City, State and ZIP Code) GRIFFISS AFB, NEW YORK 13441			10. SOURCE OF FUNDING NOS.		
11. TITLE (Include Security Classification) SEE REVERSE			PROGRAM ELEMENT NO.	PROJECT NO.	TASK NO.
12. PERSONAL AUTHOR(S) JAMES V. MASKOWITZ CAPTAIN, USAF WILLIAM E. RHODEN CAPTAIN, USAF			WORK UNIT NO.		
13a. TYPE OF REPORT MS THESIS		13b. TIME COVERED FROM _____ TO _____	14. DATE OF REPORT (Yr., Mo., Day) 85/DECEMBER/13		15. PAGE COUNT 180
16. SUPPLEMENTARY NOTATION					
17. COSATI CODES			18. SUBJECT TERMS (Continue on reverse if necessary and identify by block number)		
FIELD	GROUP	SUB. GR.	ELECTROMIGRATION SEM TEM METAL FILMS THERMAL RESISTANCE		
09	01				
11	06				
19. ABSTRACT (Continue on reverse if necessary and identify by block number) SEE REVERSE					
20. DISTRIBUTION/AVAILABILITY OF ABSTRACT UNCLASSIFIED/UNLIMITED <input checked="" type="checkbox"/> SAME AS RPT. <input type="checkbox"/> DTIC USERS <input type="checkbox"/>					
21. ABSTRACT SECURITY CLASSIFICATION UNCLASSIFIED					
22a. NAME OF RESPONSIBLE INDIVIDUAL DONALD R. KITCHEN, INSTRUCTOR OF ELECTRICAL ENGINEERING			22b. TELEPHONE NUMBER (Include Area Code) (513) 255-4960		22c. OFFICE SYMBOL AFIT/ENG

Approved for public release; LAW AFB 190-17
BY: [Signature] 16 JAN 86
BY: E. WOLAVEN
Dean for Research and Professional Development
Air Force Institute of Technology (AFIT)
Wright-Patterson AFB OH 45433

11. ELECTRON MICROSCOPY OBSERVATION OF ELECTROTRANSPORT

THESIS CHAIRMAN

MAJOR DONALD R. KITCHEN

INSTRUCTOR OF ELECTRICAL ENGINEERING

19. An investigation of electromigration has resulted in the development of apparatus and test vehicles for use in conducting research in situ both in the scanning and transmission electron microscopes (SEM and TEM) respectively. The unique design of test vehicles and modification of equipment allows for the experimental use of a prototype Joule-Thompson microminiature refrigerator. The refrigerator inside the SEM allows for the direct observation of electromigration experiments while controlling the temperature of the test vehicle. Research was performed in a temperature range lower than any previous effort, (93K to 373K). Results agree with published literature.

The patent-pending design and fabrication of the TEM specimen probe and its associated test vehicles provides the means for conducting in situ research into the crystalline structures and crystallographic changes associated with electromigration. The design provides the previously unattainable ability to monitor structure changes during the electromigration process in a non-contaminating environment which exists in the TEM. Results agree with published literature. (Doc.)

END

FILMED

3-86

DTIC